ASSESSMENT OF A NEXT GENERATION GRAVITY MISSION FOR MONITORING THE VARIATIONS OF EARTH'S GRAVITY FIELD

WP2420 Mission Architecture Definition/Supervision

Written by	***Responsibility***
T. Reubelt	Author
N. Sneeuw	Author
Verified by	
Approved by	
Documentation Manager	
N. Sneeuw	

CHANGE RECORDS

ISSUE	DATE	§ CHANGE RECORDS	AUTHOR
draft	July 30	Draft including figures, but large part of text missing	TR, NS
draft	August 10	Draft with full text	TR, NS
final	November 10	Final version including the supplements 1,2	TR, NS

TABLE OF CONTENTS

1. INTRODUCTION

In this document the sensitivity of future mission options is investigated. For the sensitivity analysis quick-look tools as described in section 3 were used with which the sensitivity of a mission option can be investigated and represented in terms of different error measures. The quick look tools are based purely on error propagation and thus can not be used for the analysis of (temporal and spatial) aliasing effects of time variable gravity field sources as e.g. ocean tides, short periodic atmospheric and ocean circulation signals and so on. Aliasing has be proven to be a serious error source for GRACE, and for a future mission it will be even more serious since the metrology device and the mission design will be sophisticated compared to GRACE. But it has to be considered that also the time-variable models used for de-aliasing will improve in future so that aliasing effects will be reduced compared to state-of the art investigations. Furthermore the measurements of a future mission might be of such a high quality that they can be used to improve the background models. This means that the sensor noise and the impact of basic mission parameters still are very important future mission drivers. For this reason the impact of basic mission design parameters and the sensor noise is investigated in this document. As soon as the result of the full-scale retrievals computed by DEOS are published the influence of aliasing for the different simulation scenarios defined at the Progress Meeting 2 held at TU Delft at 24 March 2010 are investigated in order to find out which formation or combination of formations shows the least aliasing.

2. DOCUMENTS

2.1 Applicable Documents

-

2.2 ESA Reference Documents

[RD-1] T. van Dam et al., Monitoring and Modelling Individual Sources of Mass Distribution and Transport in the Earth System by Means of Satellites, Final Report, ESA Contract No. 20403, November 2008

[RD-2] Anselmi, A (2010) TN6: Mission Architecture outlines. Technical Note of the ESA-Contract 22643/09/NL/AF "Assessment of a Next Generation Gravity Mission for Monitoring the Variations of Earth's Gravity Field".

[RD-3] Visser PNAM, Ditmar PG, Teixeira da Encarnacao (2010) WP2330 Backward Module. Technical Note of the ESA-Contract 22643/09/NL/AF "Assessment of a Next Generation Gravity Mission for Monitoring the Variations of Earth's Gravity Field".

[RD-4] Cossu F, Anselmi A, Cavaglia R (2010) TN5: Multi-Satellite Simulation Tool for SST Mission. Technical Note of the ESA-Contract 22643/09/NL/AF "Assessment of a Next Generation Gravity Mission for Monitoring the Variations of Earth's Gravity Field".

[RD-5] van Dam T, Visser PNAM (2010) WP3200 Scientific Assessment of the Baseline Mission. Technical Note of the ESA-Contract 22643/09/NL/AF "Assessment of a Next Generation Gravity Mission for Monitoring the Variations of Earth's Gravity Field".

[RD-6] Final Report (2010) Final Report of the ESA-Contract 22643/09/NL/AF "Assessment of a Next Generation Gravity Mission for Monitoring the Variations of Earth's Gravity Field".

2.3 Further Reference Documents

[RD-7] N. Sneeuw, A Semi-Analytical Approach to Gravity Field Analysis from Satellite Observations, DGK, Reihe C, Dissertationen, Heft Nr. 527, Verlag der Bayerischen Akademie der Wissenschaften, München

3. QUICK-LOOK-TOOLS

The semi-analytic quick-look tool (QLT) [RD-7] is an efficient and fast tool for the investigation of the influence of basic parameters on the gravity field accuracy. The influence of the following parameters can be studied:

- measurement type (potential V, gravitational acceleration (along-track, cross-track, radial), gravitational gradient (SGG, all tensor elements), orbit disturbances (along-track, cross-track, radial), low-low-satellite-tracking (range, range-rate, range-acceleration, only for inline-formations))
- measurement accuracy (as psd (power spectral density))
- orbit height
- inclination
- mission duration (or period)
- maximum spherical harmonic resolution (maximum degree L)
- intersatellite distance (for low-low-SST)

Under the assumption of a nominal orbit ($I = I_0$, $r = r_0$) a block-diagonal error propagation (order wise with even/odd degree separation) from the observational and stochastic model to gravity field errors can be performed. The following representations of error estimates are used in this study:

- degree-RMS-curves
- triangle plots of the formal errors of the spherical harmonic (SH) coefficients
- geoid error per latitude
- covariance functions (at the equator)

Although the semi-analytic tool offers an efficient tool for sensitivity analysis of a satellite mission, it has to be mentioned that aliasing errors can not be simulated and investigated with this quick-look tool. Therefore full-scale simulations are necessary. Another problem is that only inline low-low-SST missions can be studied with this quick-look tool since no transfer coefficient could be derived for the other formations so far. For the error-propagation of other formation types, another tool was implemented, which will be described later on.

The theory behind the quick-look tool is briefly described in the following passage, for a detailed derivation see [RD-7].

First, the gravitational signal has to be represented along the orbit in Kepler elements. For example, the (complex) Kaula representation of the potential V along the orbit reads

$$V(r,u,I,\Lambda) = \frac{GM}{R} \sum_l \sum_m \sum_k \left(\frac{R}{r}\right)^{l+1} \overline{F}_{lmk}(I) K_{lm} e^{i(ku+m\Lambda)}$$

with the inclination function $\bar{F}_{lmk}(I)$ and the complex SH coefficients K_{lm}. This formula can be expressed as a lumped coefficient representation:

$$V(r,uI,\Lambda)=\sum_m\sum_k A_{mk}^V(r,I)e^{i(ku+m\Lambda)}$$

$$A_{mk}^V(r,I)=\sum_l \underbrace{\frac{GM}{R}\left(\frac{R}{r}\right)^{l+1}\bar{F}_{lmk}(I)}_{H_{lmk}^V(r,I)}K_{lm}$$

For a nominal circular ($r = r_0$) orbit with constant inclination ($I = I_0$) the transfer coefficient $H_{lmk}^V(r,I)$ and the lumped coefficient $A_{lmk}^V(r,I)$ become constant and the normal equation gets a orderwise blockdiagonal structure (with an additional separation for even and odd degrees), which can be solved fast and easy by blockwise least squares. The lumped coefficients $A_{lmk}^V(r,I)$ can be obtained by means of a 2D-Fourier transformation from grid-values of the potential $V(r = r_0,u,I = I_0,\Lambda)$ on the torus-domain (u,Λ) or from a 1D-Fourier transformation of the potential V along the (repeat) orbit. Analogously to the potential V an arbitrary generic gravitational functional can be represented along the orbit as

$$f(t)=f(u(t),\Lambda(t),r(t),I(t))=\sum_l\sum_m\sum_k H_{lmk}^f K_{lm}e^{i\dot{\psi}_{mk}(t-t_0)}$$

with the frequency $\dot{\psi}_{mk}=k\dot{u}+m\dot{\Lambda}$ and the corresponding transfer coefficient H_{lmk}^f. Again the lumped coefficient representation reads for a nominal orbit

$$f(t)=\sum_m\sum_k A_{mk}^f e^{i\dot{\psi}_{mk}(t-t_0)}$$

$$A_{mk}^f=\sum_l H_{lmk}^f K_{lm}$$

In our case, we are not interested in the solution for the SH coefficients but in their accuracy (variance-covariance matrix $\mathbf{Q}_{\hat{x}}$), which can be estimated by means of blockwise (per order m, even/odd degree separation) variance-covariance propagation $\mathbf{Q}_{\hat{x}}=\left(\sum_i \mathbf{A}_i^T\mathbf{Q}_{y_i}^{-1}\mathbf{A}_i\right)^{-1}$ from the variance-covariance matrix $\mathbf{Q}_{y_i}$ of the observations. The design matrix **A** is composed by the transfer coefficients H_{lmk}^f and the variance-covariance matrix $\mathbf{Q}_{y_i}$ of the corresponding block can easily be derived as a diagonal matrix from the *psd* of the functional *f*. Here the psd-value belonging to the frequency $\dot{\psi}_{mk}=k\dot{u}+m\dot{\Lambda}$ of the lumped coefficient A_{mk}^f has to be inserted. From the estimated variance-covariance matrix the error measures used for visualisation are derived. From the diagonal of $\mathbf{Q}_{\hat{x}}$, $diag(\mathbf{Q}_{\hat{x}})$, directly the variances σ_{lm}^2 of the SH coefficients are obtained, which can be transformed in degree-RMS representation by

$$RMS_l=\sqrt{\frac{\sum_m c_{lm}^2+s_{lm}^2}{2l+1}}$$

By means of error propagation $\mathbf{Q}_{\hat{x}}=\mathbf{B}\mathbf{Q}_x\mathbf{B}^T$ further error measures, e.g. spatial covariance functions $\sigma_N(\theta)$ or $C_{\Delta g}(\theta_1,\theta_2,\Delta\Lambda)$ can be derived.

The transfer coefficient H^{ρ}_{lmk} of low-low-SST for an inline-formation (leader-follower) can be computed from the transfer coefficients of the along-track orbit perturbations

$$H^{\Delta x}_{lmk} = R\left(\frac{R}{r}\right)^{l-1}\left[i\frac{2(l+1)\beta_{mk} - k(\beta^2_{mk}+3)}{\beta^2_{mk}(\beta^2_{mk}-1)}\right]\overline{F}_{lmk}(I)$$

as $H^{\rho}_{lmk} \approx 2i\sin(\eta\beta_{mk})H^{\Delta x}_{lmk}$ with $\sin\eta = 0.5\rho_0/r$. The set of transfer coefficients for range, range-rate and range-acceleration is obtained by differentation :

$$\begin{array}{ccccc} \rho(t) & \rightarrow & \dot{\rho}(t) & \rightarrow & \ddot{\rho}(t) \\ H^{\rho}_{lmk} & \rightarrow & H^{\dot{\rho}}_{lmk} = in\beta_{mk}H^{\rho}_{lmk} & \rightarrow & H^{\ddot{\rho}}_{lmk} = -n^2\beta^2_{mk}H^{\rho}_{lmk} \end{array}$$

Since low-low SST can also be interpreted as line-of-sight grsdiometry, a relation between the transfer coefficients for range-acceleration and for the along-track SSG-component can be found :

$$\lim_{\rho_0\to 0}\frac{H^{\ddot{\rho}}_{lmk}}{\rho_0} \approx H^{xx}_{lmk}$$

Since up to now no (time invariant) low-low SST transfer coefficient for the other formations could be found, another strategy was used for the formal error simulation of the formations. This formation-quick-look-tool can be regarded as some kind of pseudo-quick-look-tool and is based on the formulation of the equation for range-accelerations :

$$\ddot{\rho}(t) - \frac{1}{\rho(t)}\left(\left(\Delta\dot{\mathrm{X}}^2_1(t)\right)^2 - \dot{\rho}^2(t)\right) = \mathbf{e}^2_1\left(\mathrm{grad}V\left(\mathbf{X}_2(t)\right) - \mathrm{grad}V\left(\mathbf{X}_1(t)\right)\right)$$

The designmatrix is composed from the right hand side of this equation. The needed positions of the two satelites $\mathbf{X}_2(t)$, $\mathbf{X}_1(t)$ are computed by

1) computation of circular (β/α)-repeat orbits ($I = I_0$, $r = r_0$) for the center $(\mathbf{X}_2+\mathbf{X}_1)/2$ of both satellites
2) computation of the relative movement of the two satellites by means of the homogeneous solution of the Hill-equations:

$$x(t) = -2A\sin(nt+\alpha) - \frac{3}{2}ntz_{\mathrm{off}} + x_{\mathrm{off}}$$

$$y(t) = B\cos(nt+\beta)$$

$$z(t) = A\cos(nt+\alpha) + z_{\mathrm{off}}$$

with the initial conditions

$$A = \frac{1}{n}\sqrt{\dot{z}_0^2 + (2\dot{x}_0 + 3nz_0)^2} \qquad \tan\alpha = \frac{\dot{z}_0}{2\dot{x}_0 + 3nz_0} \qquad x_{\mathrm{off}} = x_0 - \frac{2}{n}\dot{z}_0$$

$$B = \frac{1}{n}\sqrt{\dot{y}_0^2 + (ny_0)^2} \qquad \tan\beta = \frac{\dot{y}_0}{ny_0} \qquad z_{\mathrm{off}} = \frac{2}{n}(\dot{x}_0 + 2nz_0)$$

The following initial elements have to be chosen for the formations (start point at t_0 is over the equator):

- inline (leader-follower, GRACE-like): $x_0 = \rho$

- Pendulum: $x_0 = \rho_x$, $y_0 = \rho_y$ (along-track distance ρ_x, maximum cross-track-distance over equator ρ_y)
- Cartwheel: $x_0 = -2\rho_r \sin(\alpha_{CW})$, $z_0 = \rho_r \cos(\alpha_{CW})$, $\dot{x}_0 = -2n\rho_r \cos(\alpha_{CW})$, $\dot{y}_0 = -n\rho_r \sin(\alpha_{CW})$ (maximum radial distance: ρ_r, latitude where low-low-SST is purely in radial direction: α_{CW})

The angular velocity of the reference orbit is n, here also secular effects caused by J_2 on the angular velocity are considered ($n = \dot{u}$).

4. SIMULATIONS (SENSITIVITY ANALYSIS)

A series of simulations for sensitivity analysis of future mission/formation options and basic mission parameters based on the quick look tools has been done. These simulations contain the following investigations:

- investigation of basic mission parameters (for inline-formation): sensor noise, intersatellite distance, orbit height, observation interval, inclination
- tests of refined noise cases for laser/accelerometer
- investigation of the new reference for sensor noise
- tests for laser-noise-only for higher orbits
- sensitivity analysis of different formations (only with formation quick look tool): inline, PENDULUM, CARTWHEEL
- sensitivity analysis for combinations of formations (inline and mixed) with different inclinations (BENDER-design)

4.1 Investigation of basic parameters

First the influence of basic mission parameters is studied, which have been suggested by Alenia at the Requirements Review Meeting (RRM) in Torino at 19th November 2009. The investigations have been done for a single satellite pair in an inline-formation (GRACE-like tandem) by means of the QLT. The following basic limits and parameters have been studied:

- upper (pessimistic) and lower (optimistic) boundaries for sensor noise (laser, accelerometer).
- different intersatellite distances ρ; the realistic boundaries are ρ = 10 km/100 km. Tested values are ρ = 1/10/25/50/75/100/200 km.
- upper (h = 400 km) and lower boundaries (h = 300 km) for the orbit height h as well as an intermediate case h = 350 km; the lower boundary for the orbit height together with the lower boundaries for sensor noise are called the "optimistic case", the combined upper boundaries for orbit height and sensor noise are called "pessimistic case".
- shorter against longer observation period (for individual solutions) T
- near polar (I = 89°) against sun synchronous orbit (SSO, I ≈ 97°)

The simplified noise functions for the two main sensors, laser and accelerometer, are given by Alenia in terms of Power Spectral Densities (PSD) as:

PSD of laser range error

$$\delta\tilde{d}(f, L_0, \mathrm{n_{rel}}) = L_0 \times \begin{cases} \mathrm{n_{rel}} & \text{for } f \geq 0.01\,\mathrm{Hz} \\ \mathrm{n_{rel}} \cdot \left(\dfrac{0.01}{f}\right) & \text{for } f < 0.01\,\mathrm{Hz} \end{cases} \quad \frac{\mathrm{m}}{\sqrt{\mathrm{Hz}}}$$

PSD of accelerometer error

$$\delta\tilde{\ddot{d}}_D(f, n_{floor}) = \begin{cases} n_{floor} & \text{for } f \geq 0.001 \text{ and } f \leq 0.1\,\text{Hz} \\ n_{floor} \cdot \left(\dfrac{0.001}{f}\right)^3 & \text{for } f < 0.001\,\text{Hz} \\ n_{floor} \cdot \left(\dfrac{f}{0.1}\right)^2 & \text{for } f > 0.1\,\text{Hz} \end{cases} \quad \frac{\text{m}}{\text{s}^2\sqrt{\text{Hz}}}$$

The noise of the laser is range-dependent (L_0) and consists of a flat (relative) white noise part (n_{rel}) for frequencies larger than the corner frequency (0.01 Hz) and an increase of noise for the lower frequencies with 1/f. The accelerometer noise consists of a flat white noise part (n_{floor}) for frequencies between the upper and lower corner frequencies and an increase of noise outside this area with $(1/f)^3$ towards the lower frequencies and $(1/f)^2$ towards the higher frequencies. The upper/lower limits for the flat noise parts of the laser and accelerometer are given as

	optimistic noise	pessimistic noise
n_{rel}	$5 \cdot 10^{-13}\ [1/\sqrt{\text{Hz}}]$	$5 \cdot 10^{-12}\ [1/\sqrt{\text{Hz}}]$
n_{floor}	$1 \cdot 10^{-11}\ [\text{m/s}/\sqrt{\text{Hz}}]$	$1 \cdot 10^{-10}\ [\text{m/s}/\sqrt{\text{Hz}}]$

A spherical harmonic coefficient of degree l produces as a rule of thumb a signal on the frequency $f = f_{rev} * l$ (where f_{rev} is the orbit frequency $f_{rev} = 1/T_{rev}$). This means the measurement bandwidth is mainly driven by the revolution time and the maximum degree L_{max} as $[1/T_{rev}, L_{max}/T_{rev}]$, which is for a LEO and $L_{max} = 200$ approximately $[2\cdot10^{-4}$ Hz, 0.04 Hz]. **Figure 4-1** shows the PSDs for the pessimistic and optimistic noise cases (laser, accelerometer and combined) for the two extremal intersatellite distances $\rho = 1$ km and $\rho = 200$ km in the unit $[\text{m/s}^2/\sqrt{\text{Hz}}]$ within the frequencies of interest. The following important characteristics can be captured:

- the improvement of factor 10 of the optimistic noise case compared to the pessimistic noise
- while the noise on the lower frequencies is mainly driven by the accelerometer, it is mainly determined by the laser on the higher frequencies
- the longer the intersatellite distance, the larger is the impact of the laser noise. For a distance of $\rho = 200$ km the total noise is driven by the laser noise for frequencies > 10^{-3} Hz. This means, for an intermediate distance the total noise will be more balanced.

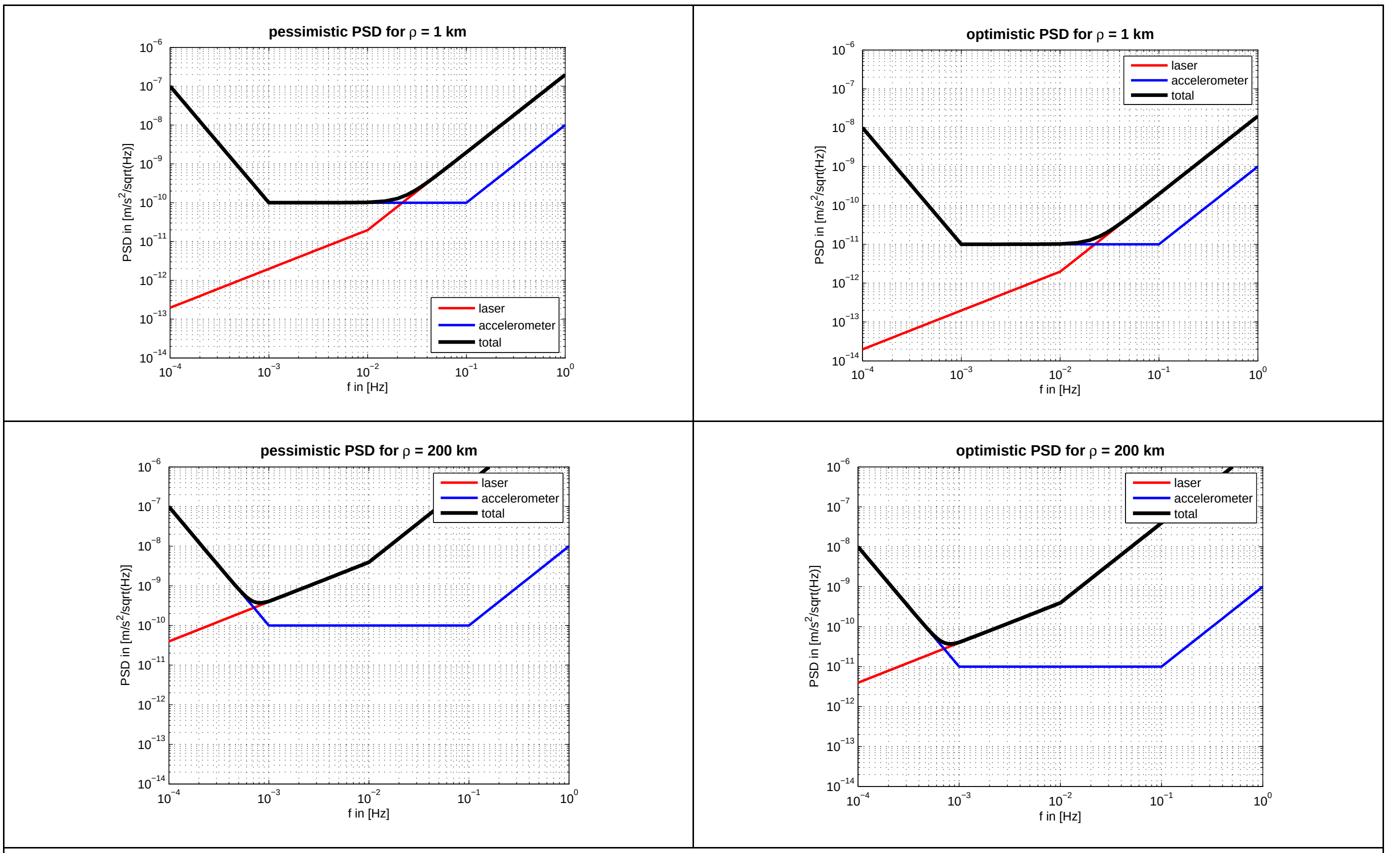

Figure 4-1: PSDs for optimistic and pessimistic noise cases (for extreme boundaries of intersatellite distances ρ = 1 km/200 km)

Figure 4-2 shows the formal errors for the pessimistic and optimistic noise cases, both considered for the mission parameters h = 300 km, ρ = 100 km, I = 89°, T = 15 d. Clearly visible is the improvement of factor 10 over all coefficients for the optimistic noise case compared to the pessimistic noise case. Due to the anisotropy of the low-low-SST of an inline-formation (see covariance-functions later on) the coefficients of lower order m have a higher accuracy than those of higher order. If the upper limit for the orbit height, h = 400 km, is taken into account together with the pessimistic noise level, which represents the pessimistic case, the differences grow larger than a factor of 10 compared to the optimistic case (optimistic noise, lower limit for orbit height h = 300 km), especially for higher degrees l. The reason for this is the signal attenuation for higher orbits with the factor $(R/(R+h))^{l+1}$. This effect of signal attenuation can easily be seen in the degree-RMS and geoid errors per latitude in **Figure 4-4** and in the formal errors in **Figure 4-5**. Especially the degree-RMS error-curve exhibits a steeper rise for larger degrees l if the orbit gets higher. Thus, for instance, the degree-RMS for h = 300 km intersects the hydrology signal curve (mean variation) at degree l ≈ 95 while the intersection is shifted to l = 75 km for h = 400 km.
In summary a big gain in accuracy can be expected if the lower boundaries for orbit height and sensor noise can be met.

pessimistic noise | optimistic noise

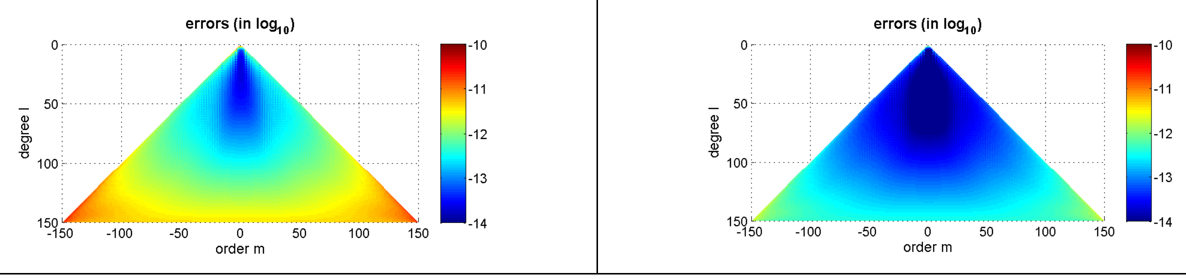

Figure 4-2: pessimistic noise vs. optimistic noise (for h = 300 km); ρ = 100 km, I = 89°, T = 15 d

pessimistic case (pessimistic noise, h = 400 km) | optimistic case (optimistic noise, h = 300 km)

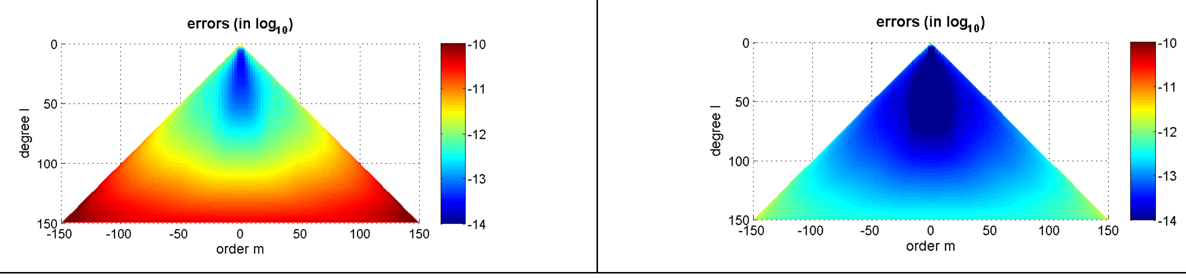

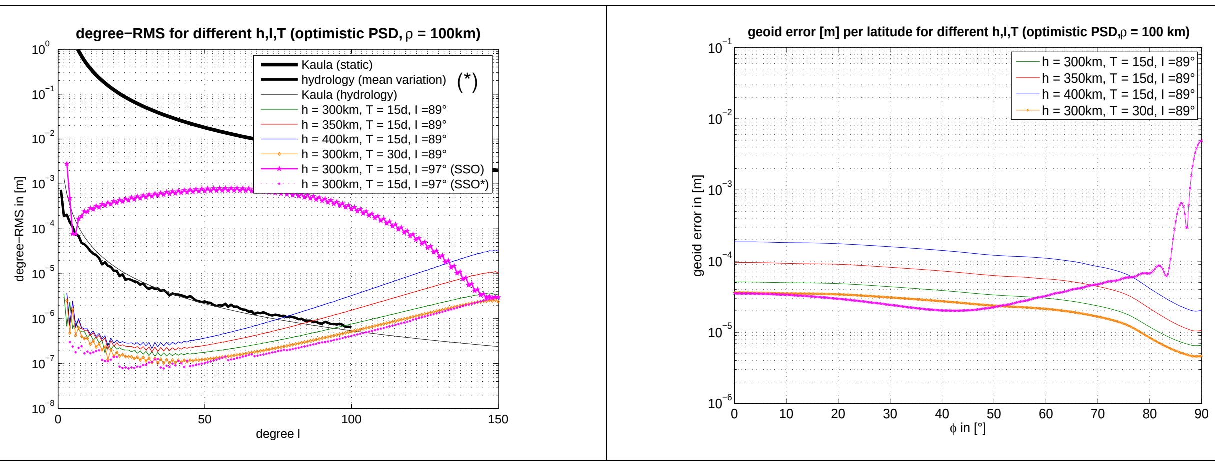

Figure 4-4: influence of the parameters orbit height h, inclination I and time interval T (for optimistic noise and ρ = 100 km).

(*) "Kaula (static)" represents the static gravity signal-RMS curve, "hydrology (mean variation)" the hydrology mean variation signal-RMS curve and "Kaula (hydrology)" a fitted Kaula-curve for hydrology mean variation.

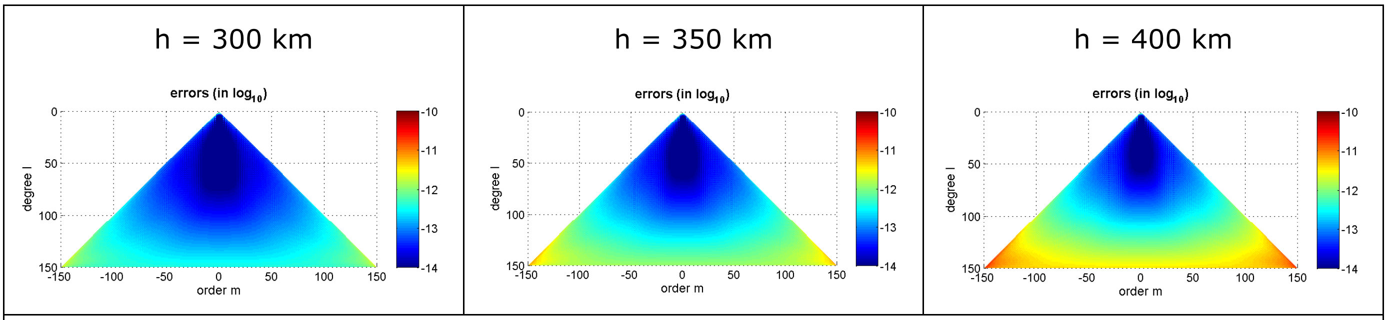

Figure 4-5: influence of orbit height (for optimistic noise); ρ = 100 km, I = 89°, T = 15 d

Figure 4-6 shows the influence of different time intervals T in terms of formal errors for the two cases T = 15 d and T = 30 d (the results in terms of degree-RMS and geoid errors per latitude are displayed in **Figure 4-4**). The influence of the time interval T is $\sqrt{T}$ for all coefficients. So an improvement of a factor $\sqrt{2}$ for the case T = 30 d compared to T = 15 is visible in all Figures. This means a shorter time interval which might lead to a higher temporal resolution produces larger errors.

Figure 4-7 (and also **Figure 4-4**) display the errors caused by different inclinations, here for the two cases (near) polar orbit (I ≈ 90°) and sun-synchronous orbit (I ≈ 97°). The influence of the polar gap produced by the inclined orbit is clearly visible in the geoid errors per latitude, which are very large at the polar gap and similar or even better compared to the near polar orbit at areas which are covered well with measurements. Furthermore the formal errors in **Figure 4-7** show that the accuracy of the zonal and low order coefficients is reduced dramatically while the accuracy of higher order coefficients is improved slightly (the reason for the latter might be due to the enhanced isotropy caused by the larger intersection angle of ascending/descending arcs). Of course the bad accuracy of the low order coefficients contaminates the degree-RMS of inclined orbits, but if the low order coefficients are removed the degree-RMS show a similar (or even slightly better) accuracy than for polar orbits. All the mentioned effects grow larger if the inclination deviates more from I = 90° (See also section 4.6). Although an inclined single formation mission might be problematic due to the mentioned problems and the data gap, an inclined formation might be advantageous in a multi-formation mission (section 4.6). The influence of the inclination is investigated in more details in section 4.6.

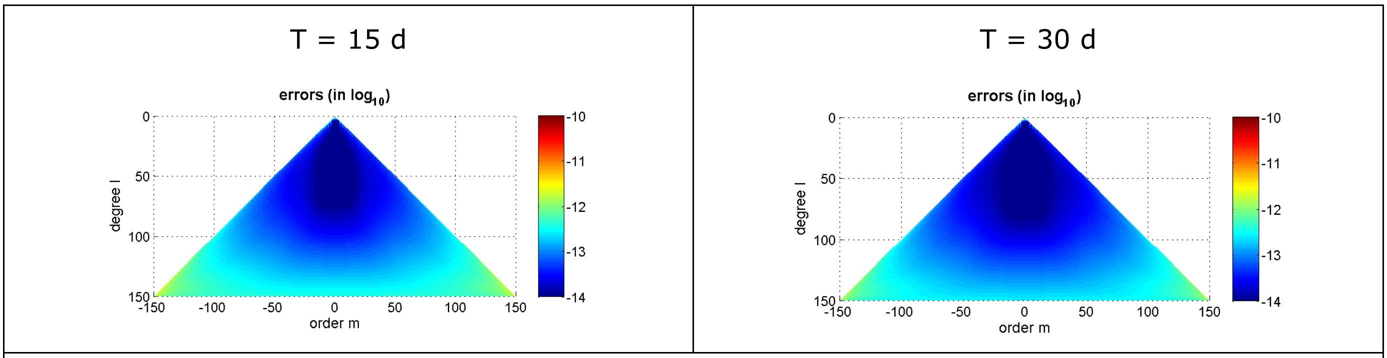

Figure 4-6: influence of time interval (for optimistic noise); ρ = 100 km, h = 300 km, I = 89°

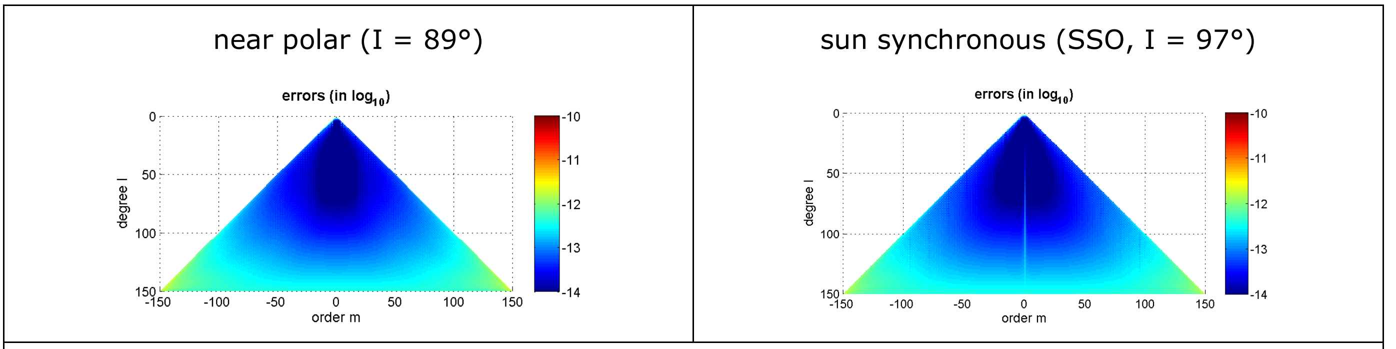

Figure 4-7: influence of inclination (for optimistic noise); ρ = 100 km, h = 300 km, T = 15 d

On of the major aspects to be addressed in a future mission design is the influence of the intersatellite distance ρ (or L_0). From technological view a short distance as ρ = 1 km or ρ = 10 km is desired. In contrast, from geodetic side a long distance as ρ = 100 km of ρ = 200 km is aimed at due to higher sensitivity, even if the laser noise decreases directly with a factor of L_0. The only margin from geodetic side is the avoidance of common mode effects, which occur if the satellite distance is larger than the highest gravity field resolution λ = 2πR/l. **Figure 4-8**, **Figure 4-9** and **Figure 4-10** show the results obtained for different intersatellite distances ρ for the optimistic and pessimistic cases. From ρ = 1 km to ρ = 10 km there is an improvement of one order of magnitude over all degrees. From ρ = 10 km to ρ = 100 km the improvement is already less than one order of magnitude, especially for the higher degrees, which is due to the rising influence of the range-dependent laser noise. The improvement from ρ = 100 km to ρ = 200 km is already marginal. As the formal errors show, the coefficients of higher orders benefit more form the larger distance ρ, which leads to a more homogenous error distribution (improvement of isotropy?) in the formal error plots for larger satellite distances. The reason might be, that the higher order coefficients are determined from the signals on the lower frequencies, whose accuracy is mainly determined by the range-independent accelerometer noise.
It can be captured from **Figure 4-8** to **Figure 4-10** that between ρ = 75 km and ρ = 200 km there isn't a big improvement any more. Thus, a intersatellite distance of ρ = 75 km is regarded as a good compromise between geodetic sensitivity and technical feasibility and is chosen as baseline value.

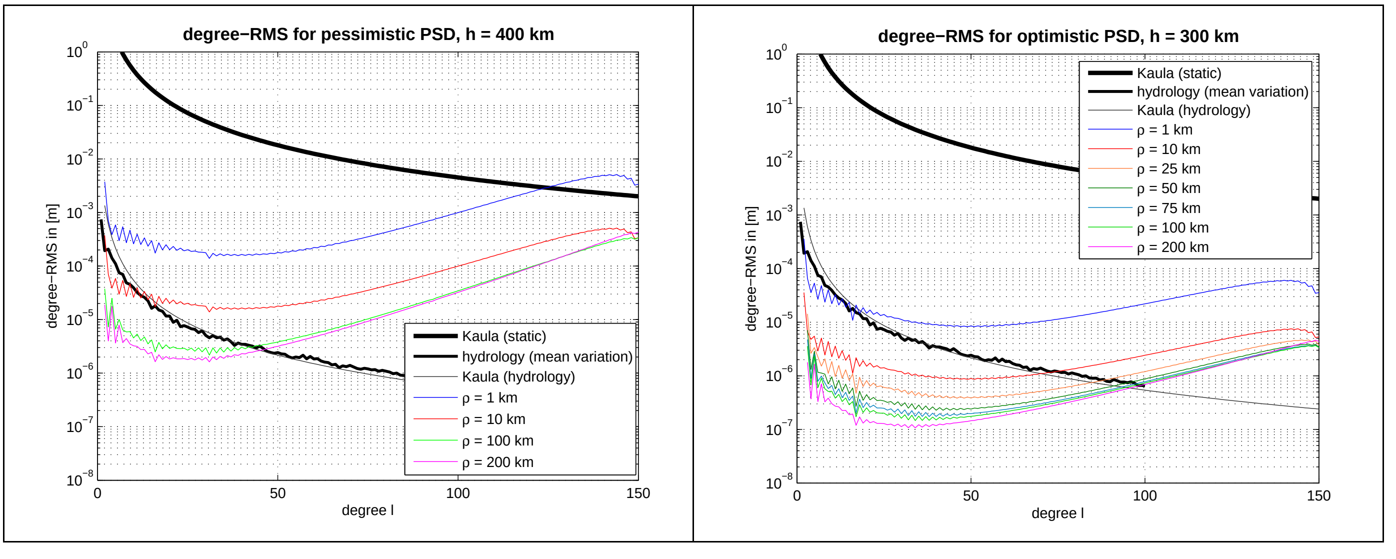

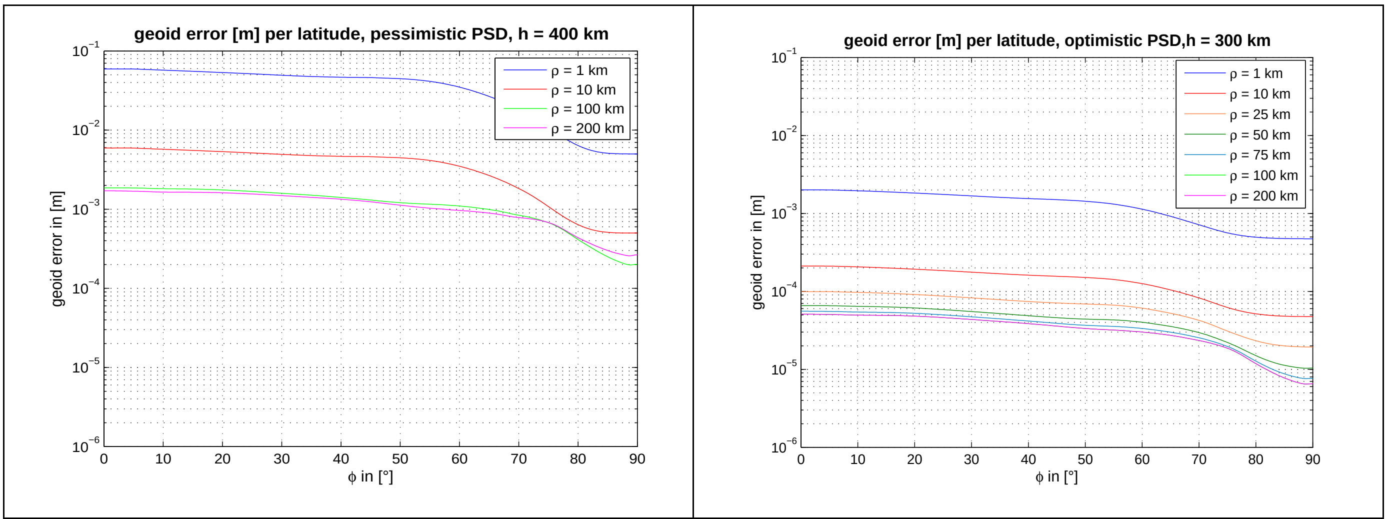

Figure 4-8: degree-RMS and geoid error per latitude (L_{max} = 100) for different intersatellite distances ρ (for a near polar orbit (I = 89°) and an time interval of T = 15 d); left: pessimistic case, right: optimistic case.

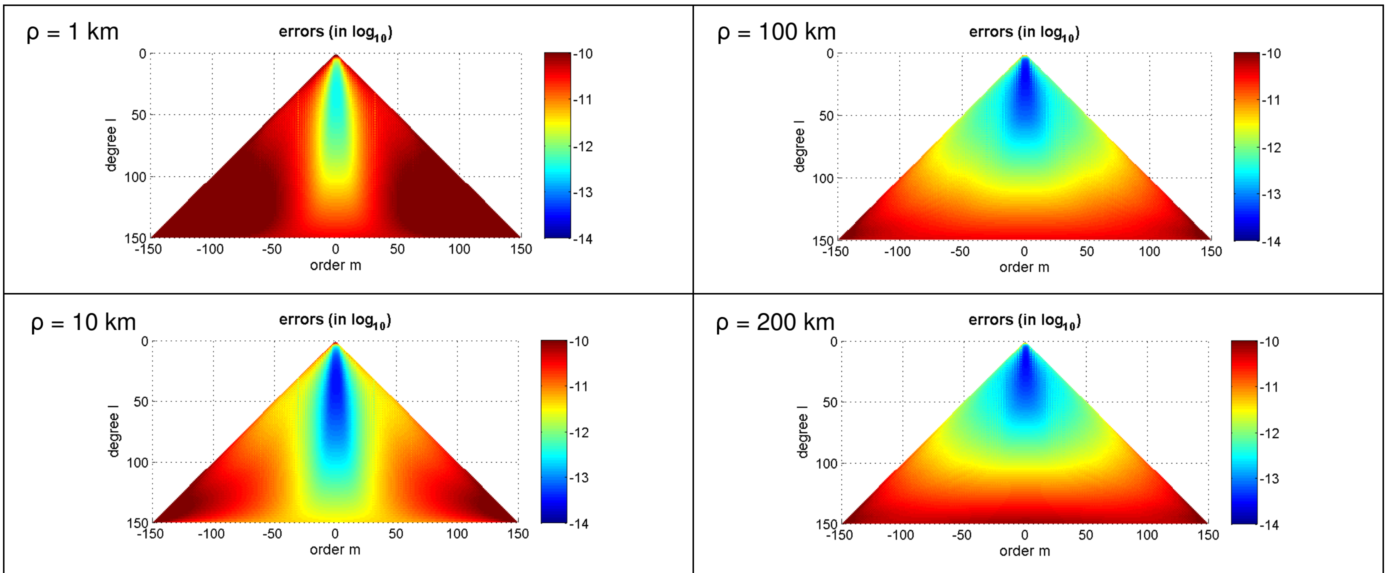

Figure 4-9: formal errors of different intersatellite distances ρ for pessimistic case (pessimistic PSD, h = 400 km); near polar orbit (I = 89°), T = 15 d

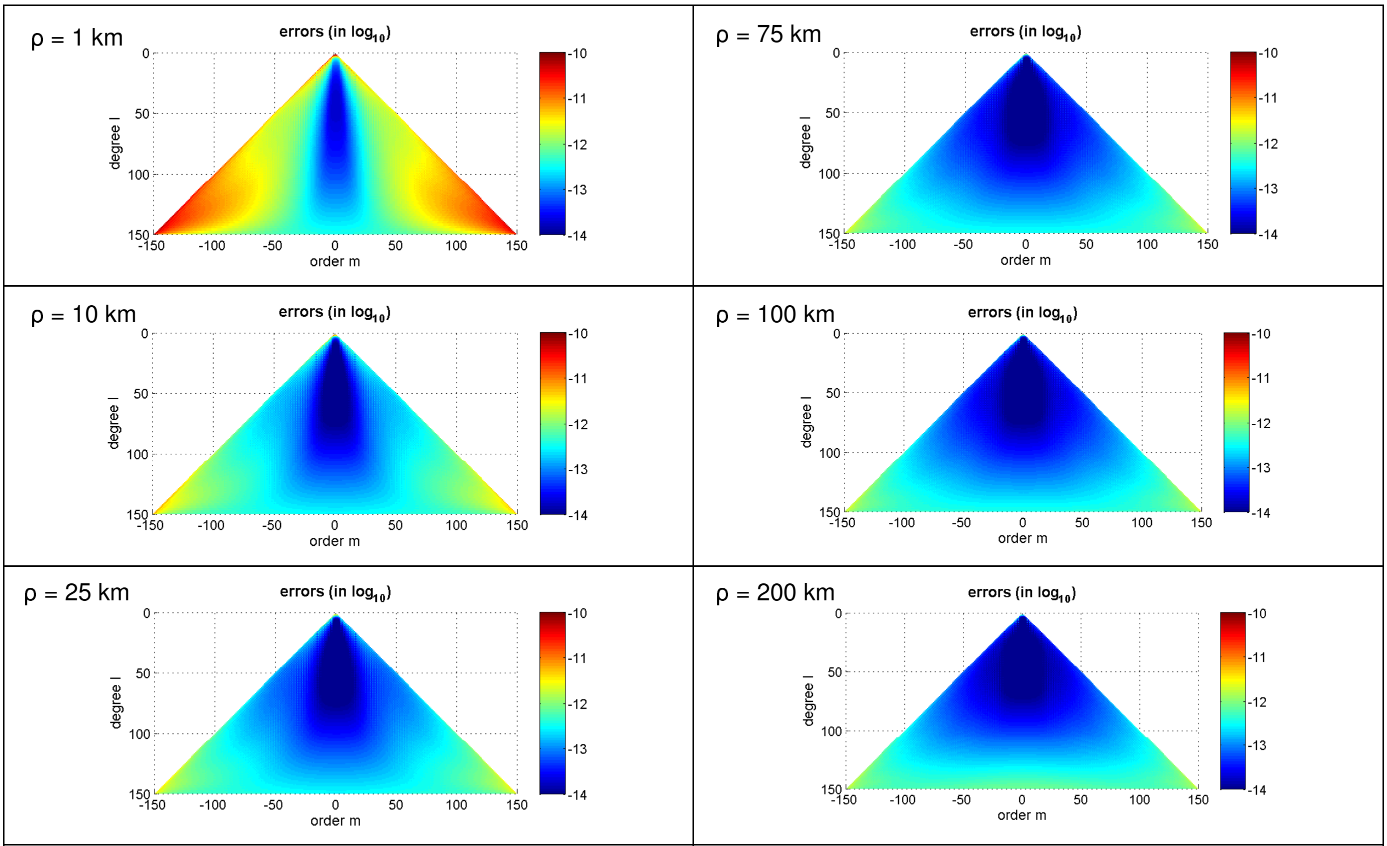

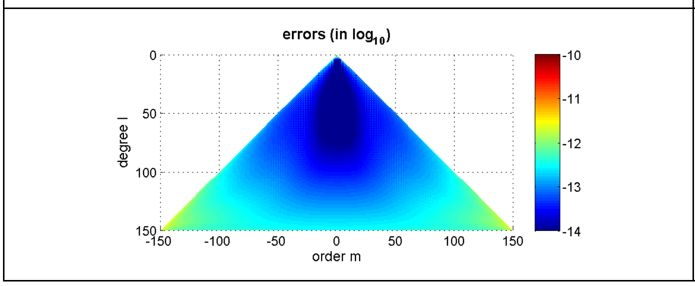

Figure 4-10: formal errors of different intersatellite distances ρ for optimistic case (optimistic PSD, h = 300 km); near polar orbit (I = 89°), T = 15 d

Figure 4-11 shows the covariance functions for points at latitude φ = 0°/45° for the intersatellite distances ρ = 1 km/100 km. In all cases, the typical anisotropic North-South striped errors for GRACE-like inline-formations is visible. The distance ρ has almost no influence on the isotropy.

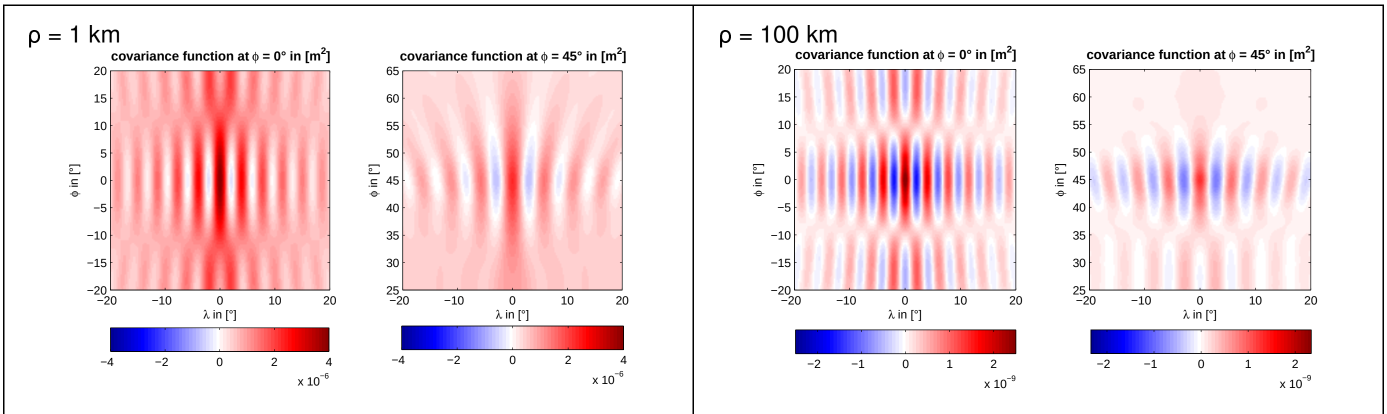

Figure 4-11: covariance functions of different distances (optimistic case); h = 300 km, I = 89°, T = 15 d

In summary the following conclusions can be drawn:

- the optimistic sensor noise case has a big impact, here a factor of 10 over all degrees compared to the pessimistic noise case.
- for the given noise cases, at least a satellite distance of ρ = 50 km should be applied. A distance of ρ = 75 km seems to be a good compromise between technological feasibility and geodetic sensitivity.
- the orbit height influences mainly higher degrees l, thus still promising results up to degree l = 50 can be obtained with the higher orbit (h = 400 km) compared to the lower orbit (h = 300 km). Thus the lower orbit height is desired, although the influence is less than from the discussed sensor noise levels. As a compromise between technical feasibility and geodetic sensitivity, a mean orbit height of h = 350 km should be aimed at.
- influence of observation interval T is $\sqrt{T}$ on all coefficients.
- inclined orbits (e.g. sunsynchronous) cause a polar gaps with the well known problems (large geoid errors over polar gaps, low order coefficients not well determined). But in combination with polar formations positive effects might be obtained (denser groudtrack coverage over equator, improved accuracy of coefficients of higher order), see also section 4-6.

4.2 New test cases for laser/accelerometer noise

Based on the investigations of the previous section, the parameters ρ = 75 km, h = 350 km, I = 90°, T = 15 d were defined as basic mission parameters. In this section the influence of different sensor noise parameters and characteristics is studied. These studies include variations of the flat white noise levels n_{rel}, n_{floor} of the laser and accelerometer and different exponents η of the 1/f-noise behaviour of the accelerometer at lower frequencies. The formulas for laser and accelerometer noise used in this section are the same as for the previous section with the only difference of the variable exponent η:

PSD of laser range error

$$\delta\tilde{d}(f, L_0, \mathrm{n_{rel}}) = L_0 \times \begin{cases} \mathrm{n_{rel}} & \text{for } f \geq 0.01\,\mathrm{Hz} \\ \mathrm{n_{rel}} \cdot \left(\dfrac{0.01}{f}\right) & \text{for } f < 0.01\,\mathrm{Hz} \end{cases} \quad \frac{\mathrm{m}}{\sqrt{\mathrm{Hz}}}$$

PSD of accelerometer error

$$\delta\tilde{\ddot{d}}_D(f, \mathrm{n_{floor}}, \eta) = \begin{cases} \mathrm{n_{floor}} & \text{for } f \geq 0.001 \text{ and } f \leq 0.01\,\mathrm{Hz} \\ \mathrm{n_{floor}} \cdot \left(\dfrac{0.001}{f}\right)^{\eta} & \text{for } f < 0.001\,\mathrm{Hz} \\ \mathrm{n_{floor}} \cdot \left(\dfrac{f}{0.01}\right)^{2} & \text{for } f > 0.01\,\mathrm{Hz} \end{cases} \quad \frac{\mathrm{m}}{\mathrm{s}^2\sqrt{\mathrm{Hz}}}$$

The parameters of the 7 noise test cases are displayed in **Figure 4-12** as well as their PSD-curves (laser, accelerometer and combined) and the estimated formal SH coefficient errors. **Figure 4-13** shows the degree-RMS-curves and geoid errors per latitude obtained from the different noise cases. Case 1 is the reference case and corresponds to the optimistic noise level defined in the previous section. In cases 2 and 3 the noise level n_{floor} of the accelerometer is increased. This has mainly an influence on the lower frequencies f < 10^{-3} Hz or f < $5\cdot10^{-3}$ Hz of the total noise level depending on the level of n_{floor}. As a result the accuracy of the higher order coefficients is decreased and the degree-RMS and geoid errors per latitude are increased over the whole range. In test case 4 the relative white noise level of the laser is reduced, which affects mainly the noise in the higher frequencies $f > 10^{-3}$ Hz of the total noise. As a result, mainly (but not only) the higher degree coefficients are improved, which is reflected in the formal errors, the degree-RMS curve and the geoid errors per latitude. In test cases 5 and 6 the exponent η of the low frequency 1/f accelerometer noise is reduced. As a result, mainly the higher order coefficients of degrees $l < 100$ (especially $l < 50$) are improved, as visible in the formal errors and the degree-RMS curve (also the geoid errors per latitude are reduced significantly). Test case 7 is a combination of test case 3 and test case 5, which means an increased relative noise level of the accelerometer but a decreased exponent η for the 1/f noise on the lower frequencies. As visible, the negative effect of the increase of n_{floor} is much worse as the benefit of a decreased η. In comparison to case 3 only the noise of the lower degree ($l < 50$) coefficients is reduced.

The main results of the investigations of this section are:

- a large improvement can be obtained if the white noise level n_{rel} of the laser can be reduced
- a reduction of the exponent η of the (1/f) noise part in the low frequency range of the accelerometer from $\eta = 3$ to $\eta = 1$ or at least to $\eta = 2$ will also improve the gravity field sensitivity
- the optimistic relative white noise level n_{floor} of the accelerometer should be kept, otherwise the gravity field sensitivity will be reduced
- instead of reducing the exponent η a shift of the accelerometers lower corner frequency towards lower frequencies will also be helpful
- in general it is advantageous to improve the total noise over the whole bandwidth of interest. This is achieved by the reduction of n_{rel} and η.

case 1 $n_{rel} = 5 \cdot 10^{-13}\ [1/\sqrt{\mathrm{Hz}}]$ $n_{floor} = 1 \cdot 10^{-11} [\mathrm{m/s^2}/\sqrt{\mathrm{Hz}}]$ $\eta = 3$	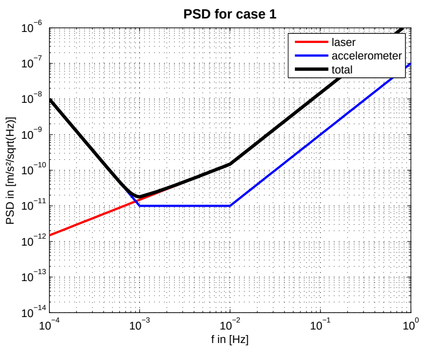	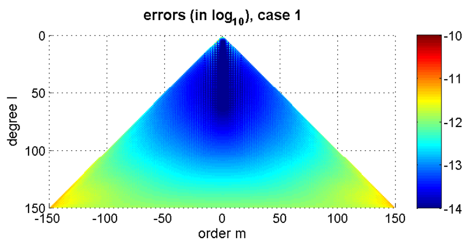
case 2 $n_{rel} = 5 \cdot 10^{-13}\ [1/\sqrt{\mathrm{Hz}}]$ $n_{floor} = 2 \cdot 10^{-11} [\mathrm{m/s^2}/\sqrt{\mathrm{Hz}}]$ $\eta = 3$	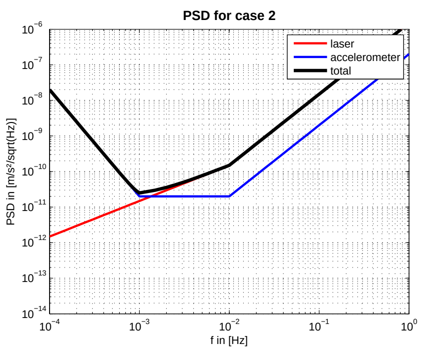	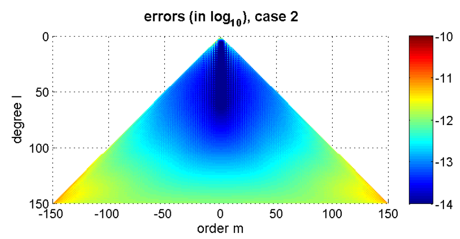

<table>
<tr>
<td>case 3

$n_{rel} = 5\cdot 10^{-13}\ [1/\sqrt{\text{Hz}}]$

$n_{floor} = 5\cdot 10^{-11} [\text{m/s}^2/\sqrt{\text{Hz}}]$

$\eta = 3$</td>
<td>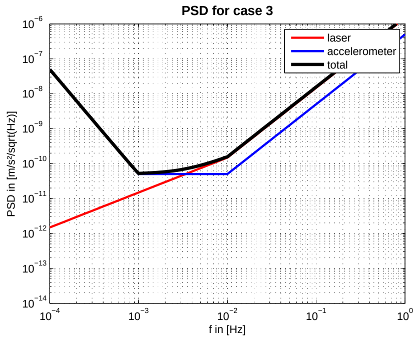
</td>
<td>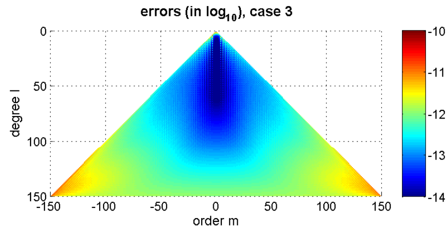
</td>
</tr>
<tr>
<td>case 4

$n_{rel} = (5/4)\cdot 10^{-13}\ [1/\sqrt{\text{Hz}}]$

$n_{floor} = 1\cdot 10^{-11} [\text{m/s}^2/\sqrt{\text{Hz}}]$

$\eta = 3$</td>
<td>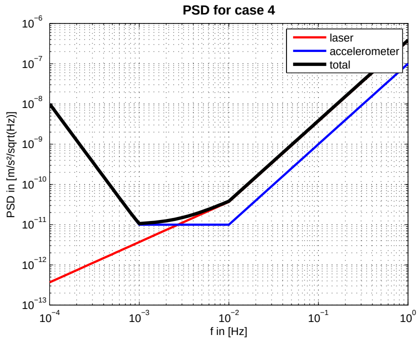
</td>
<td>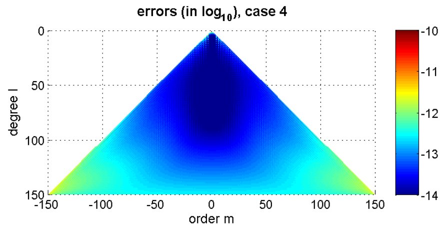
</td>
</tr>
<tr>
<td>case 5

$n_{rel} = 5\cdot 10^{-13}\ [1/\sqrt{\text{Hz}}]$

$n_{floor} = 1\cdot 10^{-11} [\text{m/s}^2/\sqrt{\text{Hz}}]$

$\eta = 2$</td>
<td>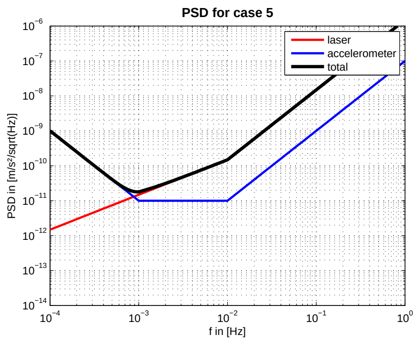
</td>
<td>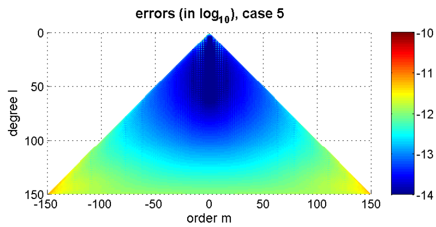
</td>
</tr>
<tr>
<td>case 6

$n_{rel} = 5\cdot 10^{-13}\ [1/\sqrt{\text{Hz}}]$

$n_{floor} = 1\cdot 10^{-11} [\text{m/s}^2/\sqrt{\text{Hz}}]$

$\eta = 1$</td>
<td>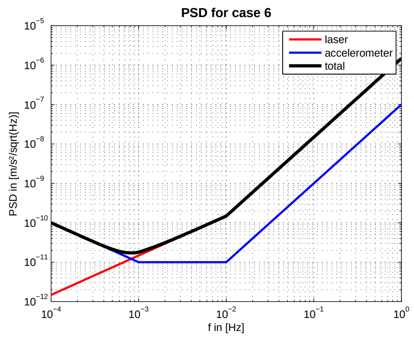
</td>
<td>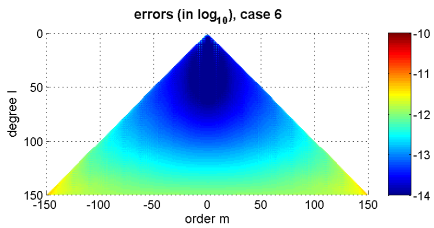
</td>
</tr>
</table>

case 7

$n_{rel} = 5 \cdot 10^{-13}\ [1/\sqrt{\text{Hz}}]$

$n_{floor} = 5 \cdot 10^{-11} [\text{m/s}^2/\sqrt{\text{Hz}}]$

$\eta = 2$

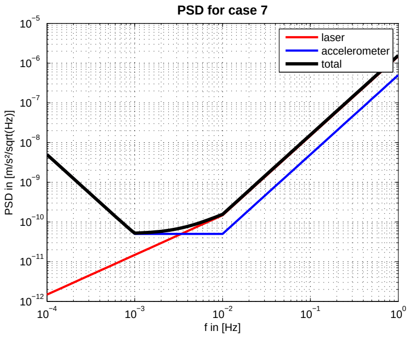

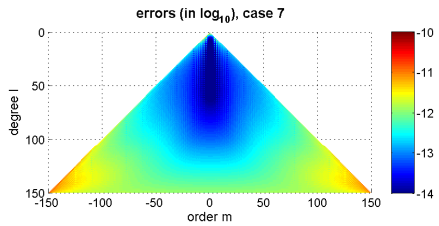

Figure 4-12: PSD and formal errors for new test cases

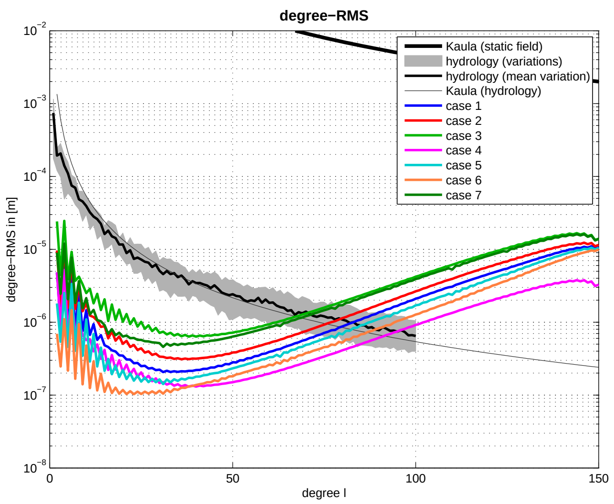

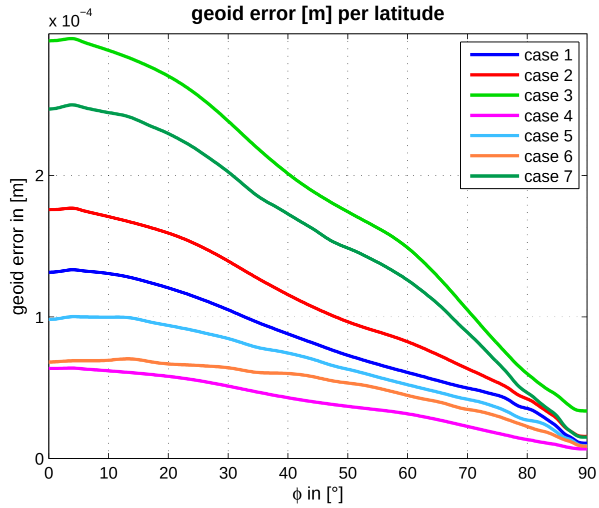

Figure 4-13: degree-RMS and geoid error per latitude for the new test cases

4.3 New reference for noise

Based on the investigations from last section, a new reference for noise was defined. Both values, the relative white noise level n_{rel} of the laser and the exponent η of the 1/f low frequency accelerometer noise were reduced within a level which seems technically feasible. These values and those of the (old) optimistic noise level are displayed in **Table 1**. **Figure 4-14** shows the PSD curves for both noise cases and the estimated formal errors and **Figure 4-15** the results in terms of degree-RMS and geoid errors per latitude. As it can be seen, an improvement over all degrees of about a factor of 2 is obtained with the new reference noise compared to the (old) optimistic noise.

(old) optimistic PSD	new reference
$n_{rel} = 5 \cdot 10^{-13}\ [1/\sqrt{\text{Hz}}]$	$n_{rel} = 2.67 \cdot 10^{-13}\ [1/\sqrt{\text{Hz}}]$
$n_{floor} = 1 \cdot 10^{-11}\ [\text{m/s}^2/\sqrt{\text{Hz}}]$	$n_{floor} = 1 \cdot 10^{-11}\ [\text{m/s}^2/\sqrt{\text{Hz}}]$
$\eta = 3$	$\eta = 2$

Table 1: new reference vs. the old optimistic instrument noise (for ρ = 75 km, h = 350 km, I = 90°, T = 15d)

(old) optimistic PSD	new reference
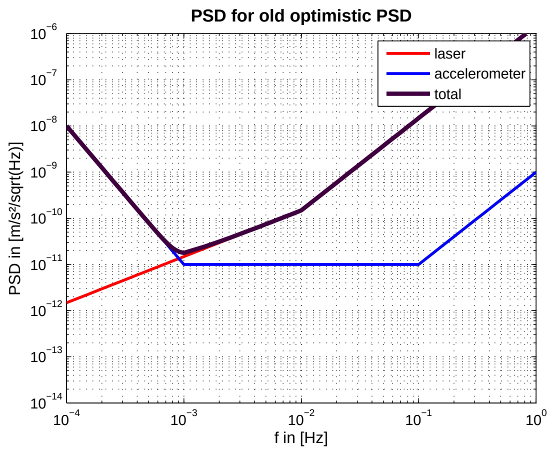	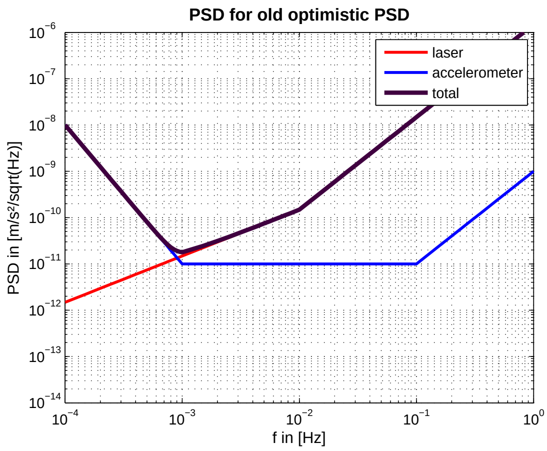
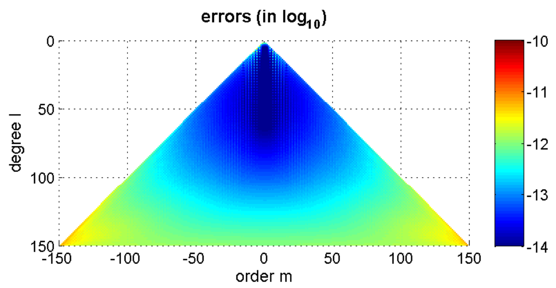	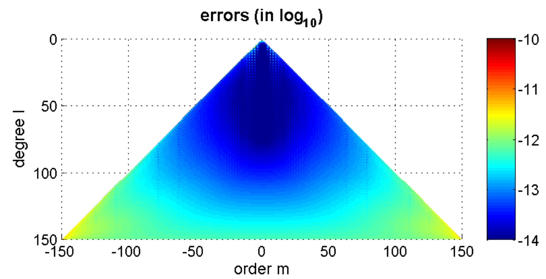

Figure 4-14: PSDs and formal errors for the former optimistic noise and the new reference for noise

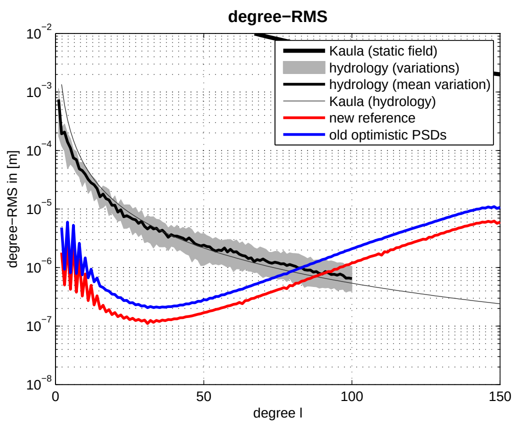	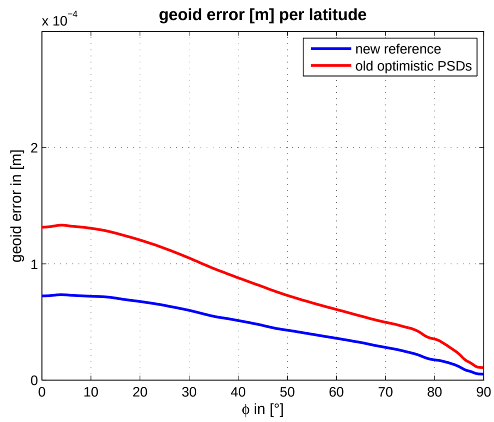

Figure 4-15: degree-RMS and geoid errors per latitude for the former optimistic noise and the new reference for noise

4.4 Laser noise only for different orbit heights

The idea of this section is to investigate a satellite mission which is flying in a higher orbit, e.g. 500 km – 600 km, where possibly the air drag is very low so that an accelerometer can be avoided or at least produces only a very small error level. Then the main error source is the laser and the accelerometer might be neglected in the error budget. To investigate the possible benefit of such a higher orbit, the degree-RMS curves and the geoid error per latitude are estimated in **Figure 4-16** for the laser-noise-only cases for orbit heights of h = 300 km/400 km/500 km/600 km in comparison with the total noise case with h = 350 km (to see the difference of the effects between total and laser noise both cases are investigated for h = 300 km). The following conclusions can be drawn from the figure:

- for the same orbit height it has a significant influence if the accelerometer noise can be neglected. Compared to the total noise the laser-noise only case leads to an improvement over all degrees, especially for the degrees l < 50 up to one order of magnitude
- however, accelerometer noise can only kept low or ignored for high orbits (h > 500 km/600 km). This means that the SH errors rise rapidly for higher degrees, e.g. 1 order of magnitude for degree l = 50 and 2 orders of magnitude for l = 100if h = 600 km is compared to h = 300 km for the laser-noise only case.
- the comparison of the total noise case for h = 350 km and the laser-noise-only case for h = 600 km shows that an improvement of the latter might only be gained for degrees l < 25 while the errors rise rapidly for higher degrees. Thus a higher orbit laser-noise-only mission seems not to be advantageous.

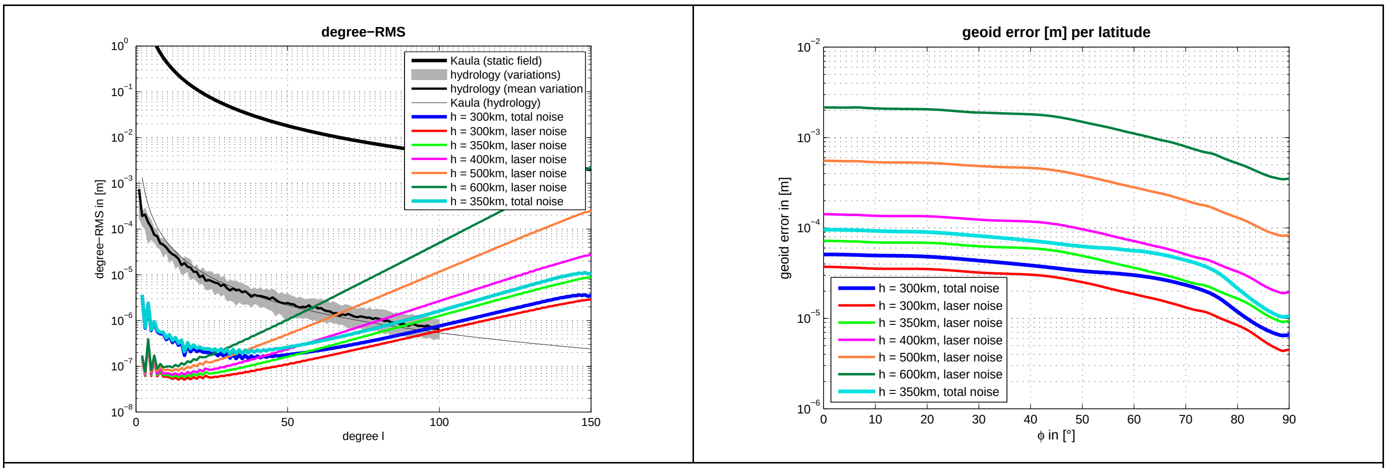

Figure 4-16: degree-RMS and geoid-error per latitude for only-laser-noise case for different orbit heights (optimistic laser PSD, ρ = 100 km, I = 89°, T = 15 d)

4.5 Sensitivity of formations

In this section the sensitivity of the different formations (inline (GRACE-like), Pendulum, Cartwheel) discussed within this project is investigated. Since the original QLT is in its present state not able to simulate formations, the new (pseudo) formation-QLT is used. A white noise level of $10^{-10}[\mathrm{m/s^2}/\sqrt{\mathrm{Hz}}]$, which fits the coloured new reference noise level quite well within the measurement bandwidth, is used within the simulations. As basic parameters an average intersatellite distance of ρ = 75 km, an orbit height and investigation time of h = 335 km and T = 32 d (corresponding to the selected repeat mode β/α = 503/32) and I = 90° have been assumed. Subsection 4.5.1 shows the results of the different basic formations, subsection 4.5.2 deals with different versions of Pendulums and in subsection 4.5.3 different orientations of Cartwheels are investigated.

4.5.1 Comparison of basic formations

The results for the three basic formations are displayed in **Figure 4-17** in terms of formal errors and covariance functions (for a point at the equator) and in **Figure 4-18** as degree-RMS and geoid errors per latitude. For the Pendulum and Cartwheel the best versions from subsections 4.5.2 and 4.5.3 have been chosen for the comparison.
Concerning sensitivity and isotropy a big gain can be expected from the Pendulum and Cartwheel compared to an inline-formation. Both advanced formation types, the Pendulum and the Cartwheel, lead to a similar accuracy. In terms of degree-RMS an improvement over all degrees can be expected from the Cartwheel and Pendulum, especially for the higher degrees an improvement of about one order of magnitude is obtained. The lower latitude regions benefit most from the advanced formations Pendulum/Cartwheel, as the geoid error per latitude shows. Here an improvement of approximately one order of magnitude can be achieved, while at near-polar regions all geoid errors per latitude are similar (the reason is the mainly along-track oriented tracking of all three formations over the poles). For the Pendulum/Cartwheel the geoid error per latitude now is in a similar level over all latitudes. The formal error plots show that the Pendulum and Cartwheel mainly improve the coefficients of higher order compared to the inline-formation. Here a similar error level over all orders of one degree is reached with the Pendulum. As the covariance functions illustrate both advanced formations, the Pendulum and the Cartwheel lead to an almost isotropic signal (here for a point on the equator), which means that the well known North-South striations from GRACE can be avoided. For the Cartwheel the signal is almost perfectly isotropic.
Both advanced formations, the Cartwheel and the Pendulum, lead to a big improvement and show results of almost the same quality. The Cartwheel shows a slightly worse performance in the degree-RMS-curve but higher isotropy. However it has to be taken into account that the orientation of the Cartwheel is not stable for a near-polar (or sun-synchronous orbit) due to the perigee drift (see subsection 4.5.3).

<table>
<tr><td>GRACE
(ρ = 75 km)</td><td>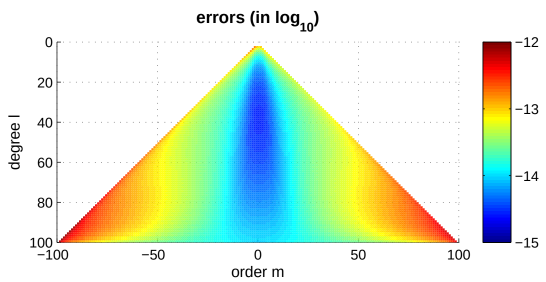</td><td>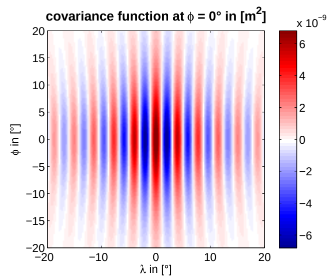</td></tr>
<tr><td>PENDULUM
($\rho_x = \rho_y$ = 62 km)</td><td>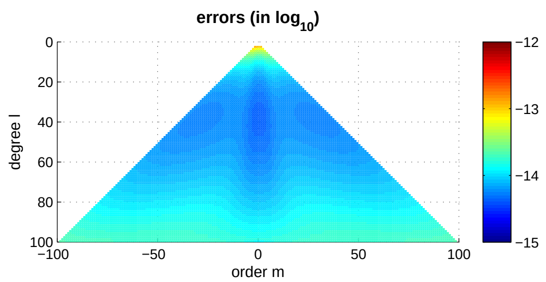</td><td>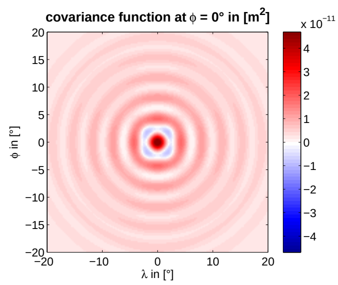</td></tr>
</table>

CARTWHEEL

(ρ_r = 50 km, ρ_x = 100 km, equatorial radial)

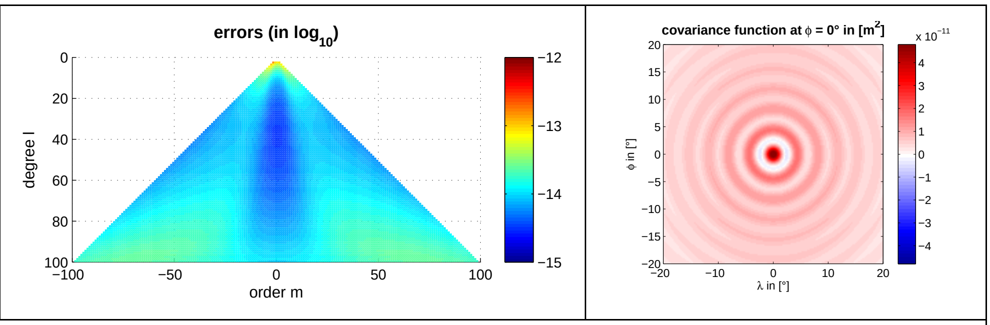

Figure 4-17: comparison of formations in terms of formal errors and covariance functions (I = 90°, $PSD = 1^{-10}\ [m/s^2/\sqrt{Hz}]$, T = 32 d, h = 335 km)

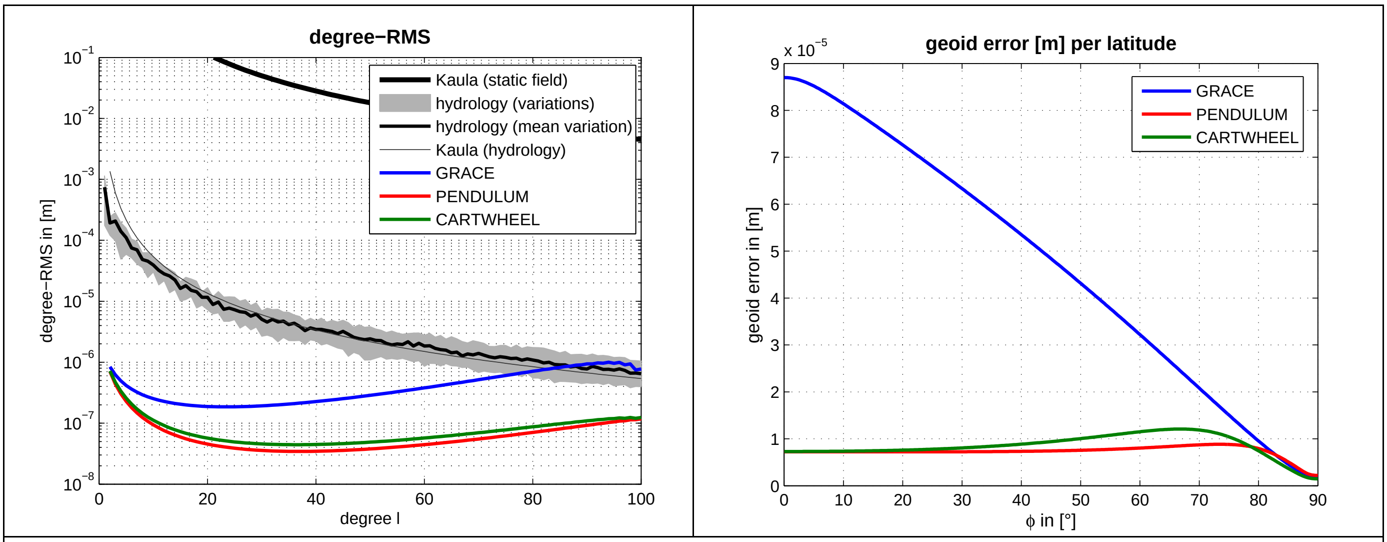

Figure 4-18: comparison of formations in terms of degree-RMS and geoid-error per latitude

4.5.2 Comparison of PENDULUMS

Different options of Pendulums are possible leading to the same average intersatellite distance of ρ = 75 km. Depending on the choice of the constant along-track component ρ_x and the maximum cross-track distance ρ_y over the equator different (maximum) yaw angles α between the line-of sight and the groundtracks over the equator can be achieved (Pendulums with maximum cross-track component outside the equator are neglected, since a different inclination of both satellites causes technical problems due to a different nodal drift rate of both satellites). Corresponding to the yaw angle α or the relation between the components ρ_x,ρ_y the signals contains more along-track or cross-track information. The highest isotropy is obtained if the along-track and cross-track components are the same. But it has to be taken care that the cross-track component is maximal over the equator and disappears over the poles. Thus a Pendulum with $\rho_x = \rho_y$ has maximum isotropy over the equator but reduced isotropy for higher latitudes while a Pendulum with $\rho_y > \rho_x$ has maximum isotropy over mid-latitude regions and reduced isotropy over the equator. The influence of the yaw angle α on the sensitivity is investigated in this section.
Figure 4-19 and **Figure 4-20** show the results for the three types of Pendulums with yaw angles α = 23°/45°/67° investigated in this section. From the degree-RMS and geoid errors per latitude it is clearly visible that the Pendulum with the yaw angle below 45° shows the worst performance while the performance of the other two Pendulums with $\alpha \geq 45°$ is similar. The reason is that the Pendulum with α = 23° never reaches nowhere full isotropy while the others do. This can also be seen in the covariance functions, where the North-South-direction is more pronounced and in the

formal error plots, where the typical characteristic of an inline GRACE-like formation (higher accuracy at lower orders) is present. But still a Pendulum with a lower yaw angle α leads to a significant improvement compared to an inline-formation.
The comparison of the results of the Pendulums with α = 45° and α = 67° yields that the performance in terms of degree-RMS is almost similar. While the geoid errors per latitude for the pendulum with α = 45° are more accurate over the equator and low latitude regions the Pendulum with α = 67° is more accurate over mid-latitude regions. The reason is the place where the isotropy is maximal. This can be seen in the covariance functions. While the covariance function at φ = 0° is quite isotropic for the pendulum with α = 45° it shows an East-West emphasis for the Pendulum with α = 67° (which will become more isotropic for mid-latitudes). From the formal error plots it can be gathered that a larger yaw-angle α leads to a higher accuracy of the coefficients of higher orders due to a stronger appearance of cross-track signals and vice versa. A yaw angle of α = 45° leads to a similar accuracy over all orders of one degree (largest homogeneity). In general a yaw angle α between of 45° and 67° can be suggested, but since a larger yaw angle means larger technological efforts (pointing/tracing) a Pendulum with α = 45° is suggested.

PENDULUM ($\rho_x = \rho_y$ = 62 km, → α = 45°)	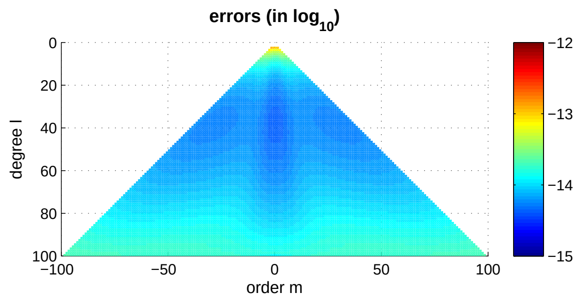	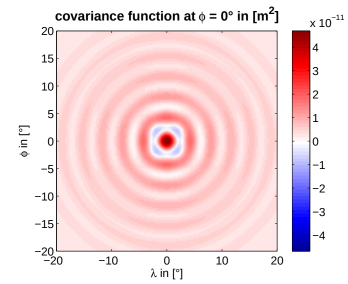
PENDULUM (ρ_x = 71 km, ρ_y = 35,5 km, → α = 23°)	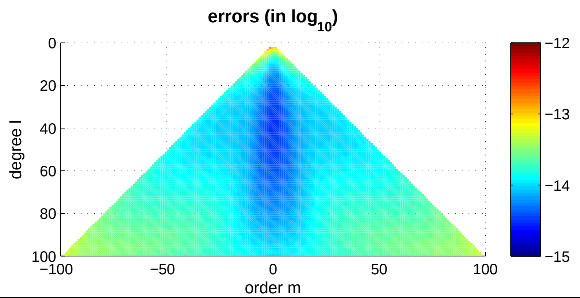	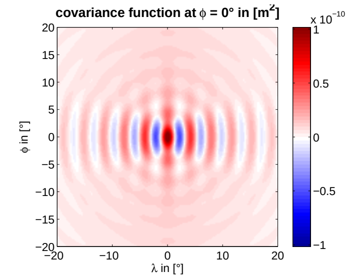
PENDULUM (ρ_x = 46 km, ρ_y = 92 km, → α = 67°)	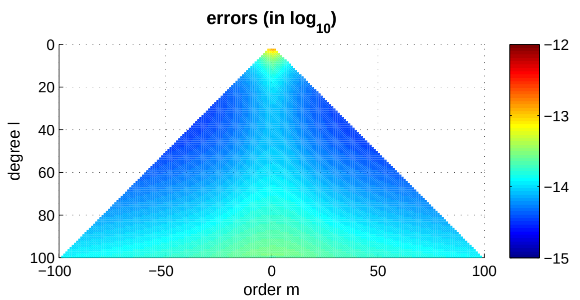	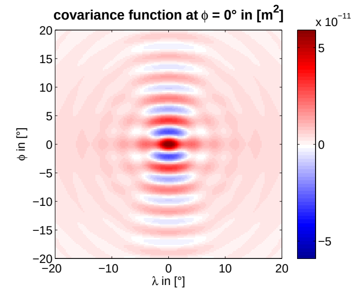

Figure 4-19: comparison of PENDULUMs with different maximum yaw angles α (ρ_{avg} = 75 km, I = 90°, $PSD = 1^{-10}\ [m/s^2/\sqrt{Hz}]$, T = 32 d, h = 335 km).

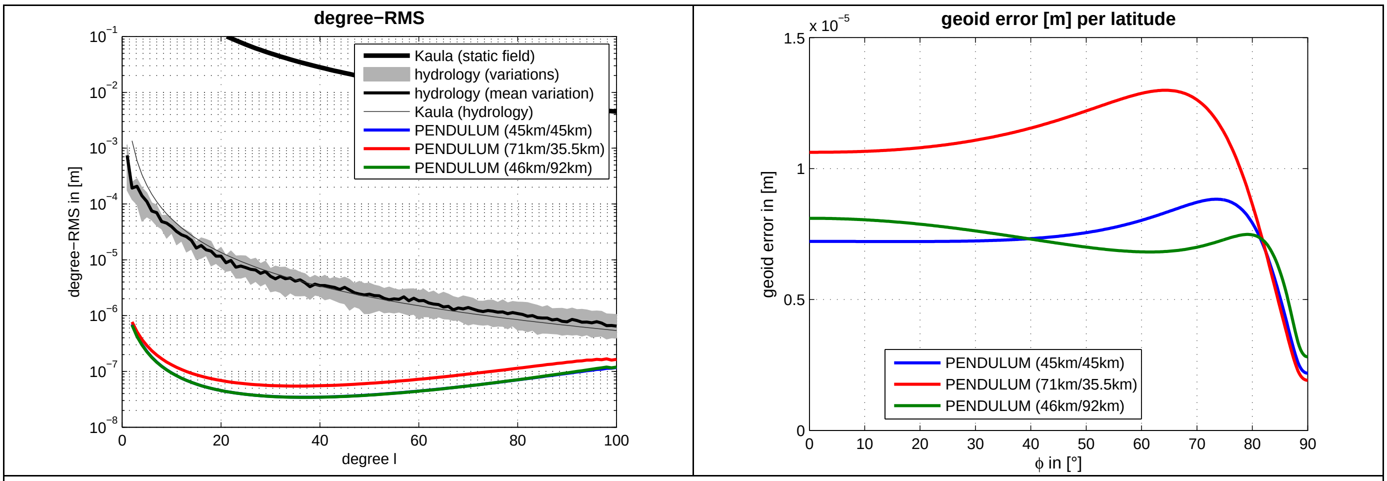

Figure 4-20: comparison of different PENDULUMs in terms of degree-RMS and geoid errors per latitude

4.5.3 Comparison of CARTWHEELs

The shape of a Cartwheel formation is fixed as a 2:1 along-/cross-track ellipse within the Hill-frame with the given value for the maximum along-track component ρ_x and the maximum radial component ρ_r respectively. Although the shape is fixed the orientation of the Cartwheel w.r.t. the Earth can be different. For instance the Cartwheel can be established such that the maximum radial component appears over the equator and the maximum along-track-component appears over the poles and vice versa. In principle the Cartwheel can be implemented such that the maximum radial component emerges over any latitude and the maximum along-track component appears a quarter of a revolution later. Strictly speaking a Cartwheel captures all orientations during a mission lifetime if the orbit inclination deviates from I = 63°, because the orientation starts to turn due to the perigee drift, if no compensation is foreseen. For instance for a near polar orbit the perigee drift is 4° so that after 90 days the orientation corresponds to the original one again. In this section three orientations are investigated, the first one has the maximum radial component over the equator (equatorial radial), the second one shows it over the pole (polar radial) and the third one has it over mid latitudes of φ = ±45° (of course also the maximum along-track component appears over mid latitudes of φ = ±45°).
The results are displayed in **Figure 4-21** and **Figure 4-22**. From the degree-RMS it can be seen that the polar radial Cartwheel shows clearly the worst performance while the other two orientations show a similar accuracy. The explanation of the reduced sensitivity of the polar radial orientation can be found in the covariance function, which shows the well-known anisotropic North-South stripes. The reason is that the signal over the equator and the low latitudes contains almost only along-track-information, which leads to a reduced geoid accuracy for lower latitudes. Only for higher latitudes φ > 45° the geoid error is reduced significantly since over these regions the signal now only contains radial information (less anisotropy). The results for the lower latitudes are quite similar as for an inline-formation, and this can be seen also in the formal error plots, where the lower order coefficients show the highest accuracy. However the radial information over the higher latitudes adds some valuable information for coefficients of higher orders.
Regarding the formal error plots and the degree-RMS the Cartwheels with 'equatorial radial' and 'radial over φ = ±45°' orientation show very similar results with slight advantages of the 'radial over φ = ±45°' Cartwheel. In contrast to the inline-formations also coefficients of medium orders show improved accuracy. Concerning the geoid errors per latitude the 'equatorial radial' Cartwheel is more accurate over low latitude regions and the 'radial over φ = ±45°' Cartwheel is more sensitive over medium and higher latitudes. This can also be seen in the covariance functions, where in principle full isotropy is reached for the 'equatorial radial' Cartwheel and a slight North-South structure is visible for the 'radial over φ = ±45°' Cartwheel.
The results show that the maximum radial component of a Cartwheel should be 0° ≤ φ ≤ 45°. Since an important topic of a future mission is hydrology, which has very strong signals over very low

latitudes an 'equatorial radial' orientation or 'very low latitude radial' Cartwheel might be desired. But anyway it has to be considered that the orientation of the Cartwheel is not fixed due to the perigee drift.

CARTWHEEL (ρ_r = 50 km, ρ_x = 100 km, equatorial radial)	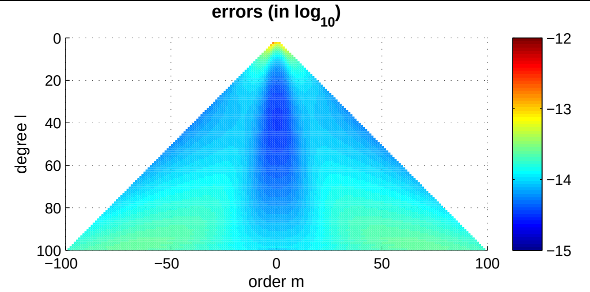	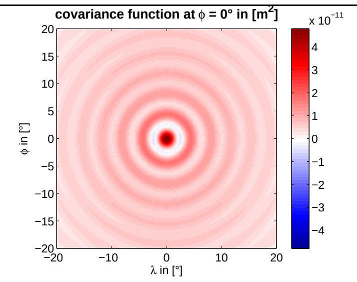
CARTWHEEL (ρ_r = 50 km, ρ_x = 100 km, polar radial)	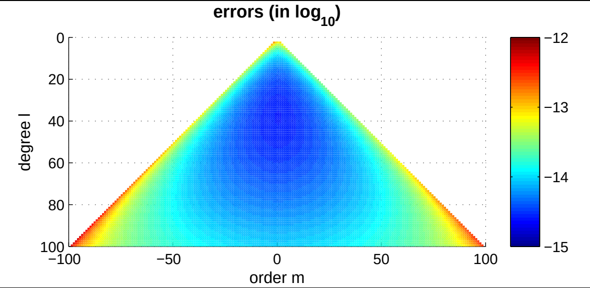	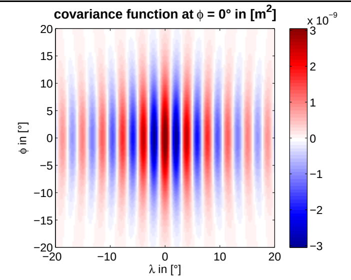
CARTWHEEL (ρ_r = 50 km, ρ_x = 100 km, radial at φ = 45°)	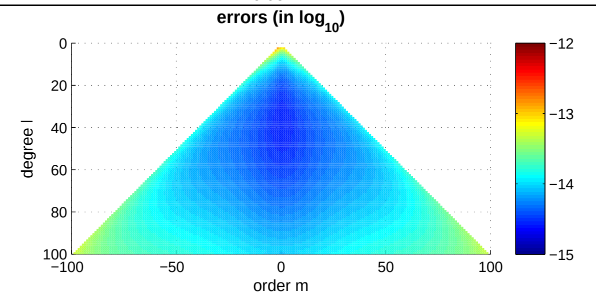	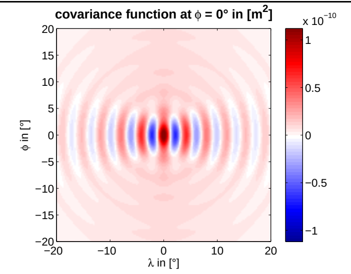

Figure 4-21: comparison of CARTWHEELs with different orientations (ρ_{avg} = 75 km, I = 90°, $PSD = 1^{-10}\ [m/s^2/\sqrt{Hz}]$, T = 32 d, h = 335 km).

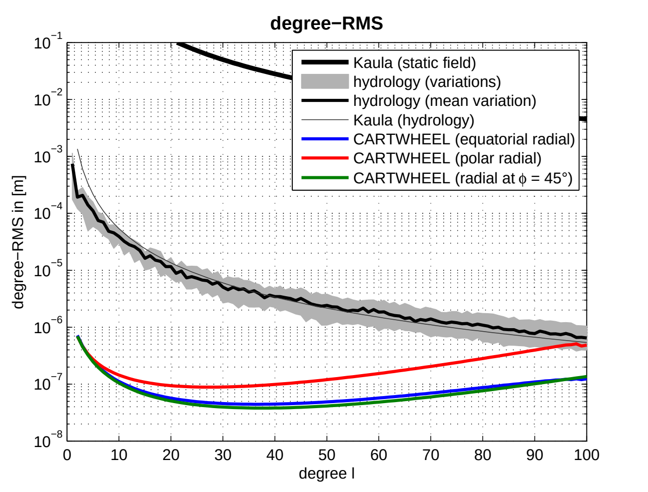

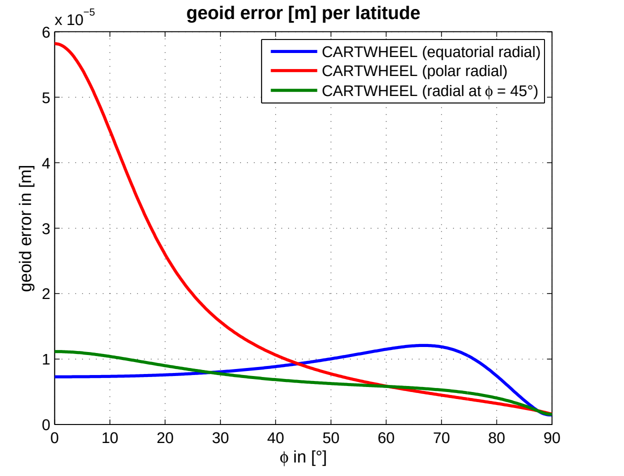

Figure 4-22: comparison of different CARTWHEELs in terms of degree-RMS and geoid errors per latitude

4.5.4 Results from investigations of formations

From the investigation of the different formations of the previous subsections the following conclusions can be drawn:

- Pendulum and Cartwheel formations are able to improve sensitivity and isotropy compared to GRACE formations. If a suited option for both formations is chosen, the accuracy is similar for both (with slight advantages for the Cartwheel).
- the most accurate, isotropic and homogeneous results for Pendulums are obtained for yaw angles of $\alpha \geq 45°$. A yaw angle of $\alpha = 45°$ seems to be a good compromise between sensitivity and technical feasibility.
- the most accurate, isotropic and homogeneous results for Cartwheels are obtained if the maximum radial component appears over regions $0° \leq \varphi \leq 45°$
- by means of the advanced formations and the assumed noise levels a resolution of the time variable hydrology up to degrees $l \geq 100$ should be possible (see **Figure 4-18**). (Of course this conclusion has to be taken with care since the degree-RMS is a global measure. Locally a higher resolution for hydrology should be possible.)

Note: The above conclusions are valid for the sensor noise. Concerning aliasing of time variable signals the results can be different.

4.6 Sensitivity of Bender-design

When designing a future satellite mission also the option of a multi-formation has to be studied. A multi-formation mission might be able to improve temporal and/or spatial sampling, dependent on the orbit-design (see [RD-1]). One promising option is the combination of formation on orbits with different repeat modes and inclination. Such an heterogeneous mission design, also known as Bender-design, might have a lot of benefits concerning the spatial and temporal sampling (see [RD-1]). For instance the groundtracks of a near polar orbit, which show large spacing at lower latitudes can be densified in this regions by means of inclined formations. Another aspect is the different (temporal) aliasing behaviour (e.g. for ocean tides) for different orbits, so that aliasing can be reduced or ocean tides can even be estimated. In this subsection the sensitivity of such Bender-formations is studied using always a polar satellite pair in combination with a sun-synchronous pair or a low inclined pair ($I = 63°$). The parameters used for this investigation are those used in the first full-scale simulation series (see TN from DEOS), applying always an intersatellite distance of $\rho = 75$ km. The orbit height and time interval are for the polar pair $h = 335$ km, $T = 32$ d ($\beta/\alpha = 503/32$), for the sun synchronous pair $h = 348$ km, $T = 32$ d ($\beta/\alpha = 503/32$) and for the low inclination pair $h = 352$ km, $T = 31$ d ($\beta/\alpha = 481/31$). In section 4.6.1 Bender-designs using only inline-formations are studied based on the new reference for noise. In section 4.6.2 Bender-options applying also the advanced formations (mixed Bender missions) are investigated for the mean noise level of $10^{-10}\,[\mathrm{m/s^2}/\sqrt{\mathrm{Hz}}]$. For the mixed Bender missions always a inline formation was set on the polar orbit.

4.6.1 Sensitivity for coloured noise (only GRACE-BENDER)

First the characteristics of inline-formations on different inclinations is investigated before they are combined to a Bender-mission. **Figure 4-23** displays the formal error plots and covariance functions for the three different inclinations investigated. As already known the accuracy of the low order coefficients is reduced dramatically for a sun-synchronous orbit due to polar data gap. This effect amplifies if the inclination deviates more from a polar orbit and the data gap grows larger. For the low inclination already coefficients of orders up to $m = 20$ or 30 can not be determined any more or have a bad accuracy. On the other hand the coefficients of higher orders are improved for inclined satellite pairs, as the formal error plots show. This is caused by the growing intersection angle of ascending and descending arcs which lead to a better isotropy since now also East-West-Signal-Information is added. This can be also seen in the geoid-error per latitude for an SSO, where the

error is reduced for lower latitudes compared to a polar orbit. Furthermore a slight circular structure seems to emerge in the covariance functions of the SSO (the covariance function for I = 63° is not meaningful because it is contaminated by the polar gap, which is a drawback of the software applied and should be ignored therefore).
It can be seen that by combining pairs on different inclinations (Bender-design) complementary information is merged, which might lead to a significant improvement. **Figure 4-24** and **Figure 4-25** show the results obtained for the two (GRACE-)Bender designs (polar pair + SSO pair, polar pair + I=63°pair) compared to the single polar pair. The degree-RMS, the geoid-errors per latitude and the formal errors show that already a Bender combination of a polar and sun-synchronous pair will lead to a significant improvement compared to a single polar pair. For the Bender-combination of a polar and a low inclined pair (I = 63°) the improvement is even larger. Especially for the latter combination the results seem to be quite homogeneous with a quite unique geoid error per latitude over all latitudes and a similar error level over all orders of one degree. The covariance functions show that the latter Bender-combination leads already to quite isotropic errors. In summary it can be concluded that a big benefit for the sensitivity can be expected for Bender-combinations, especially if one satellite-pair flies on an orbit with low inclination, but also a combination of polar and sun-synchronous orbit is valuable.

GRACE (polar)

(h = 335 km, T = 32 d)

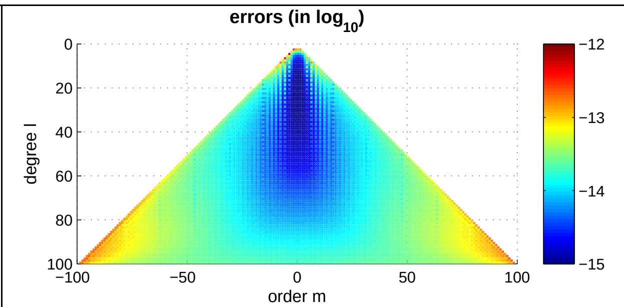

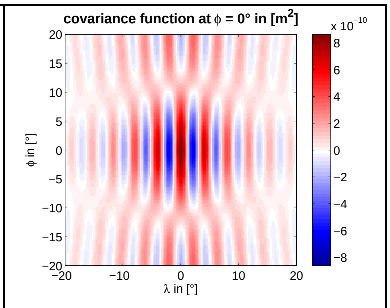

GRACE (SSO)

(h = 348 km, T = 32 d)

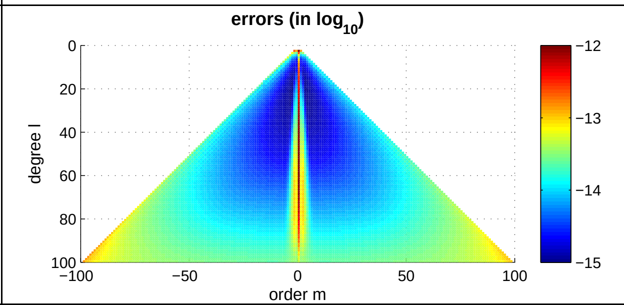

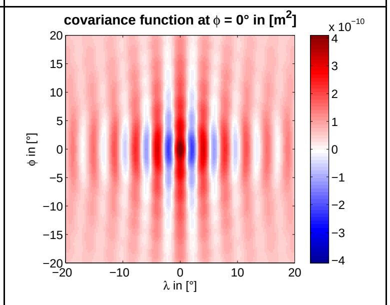

GRACE (I = 63°)

(h = 352 km, T = 31 d)

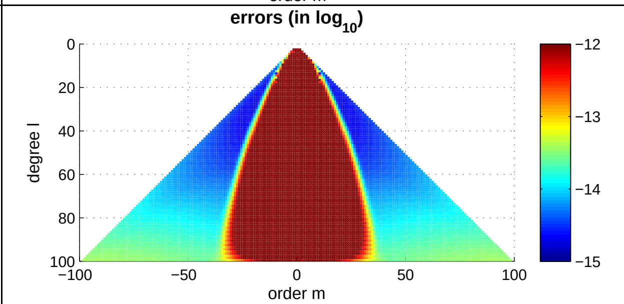

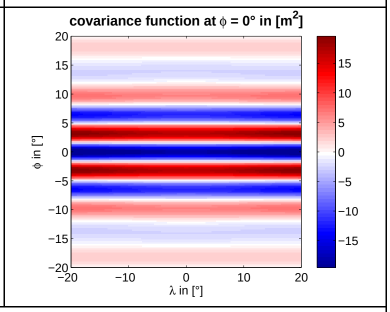

Figure 4-23: formal errors and covariance functions of inline-formations with different inclinations (ρ = 75 km, new reference for noise)

GRACE (polar) (h = 335 km, T = 32 d)	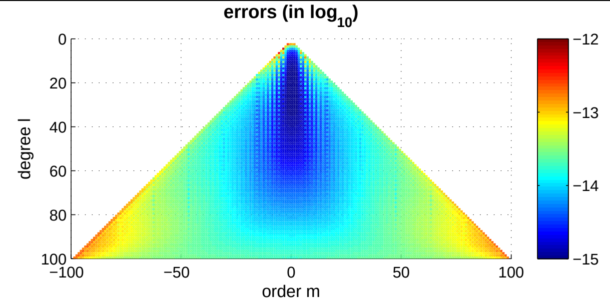	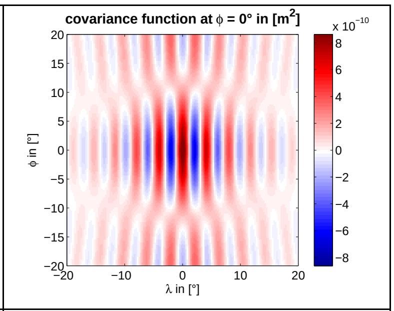
GRACE-BENDER (polar + SSO)	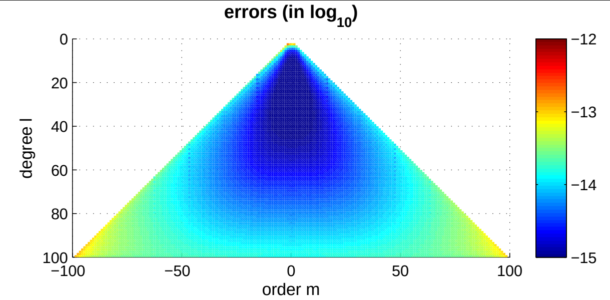	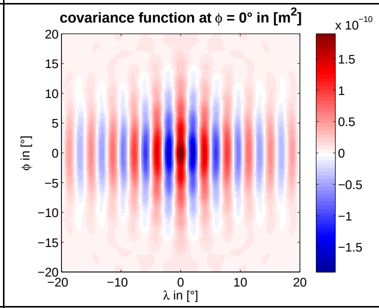
GRACE-BENDER (polar + I=63°)	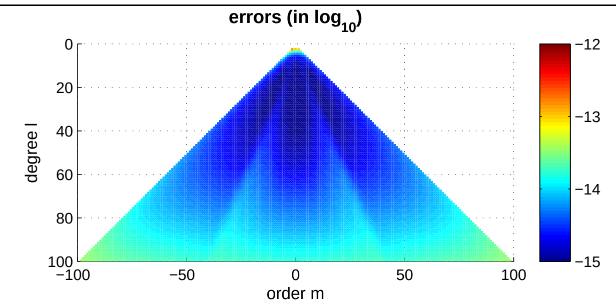	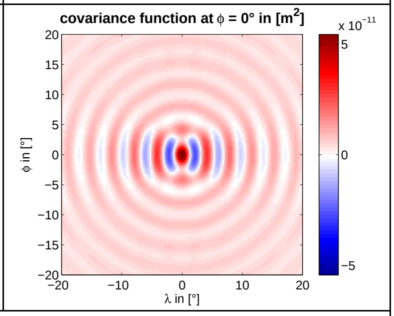

Figure 4-24: comparison of single polar inline-formation and combinations of inline-formations with different inclinations (BENDER-design); formal errors and covariance functions

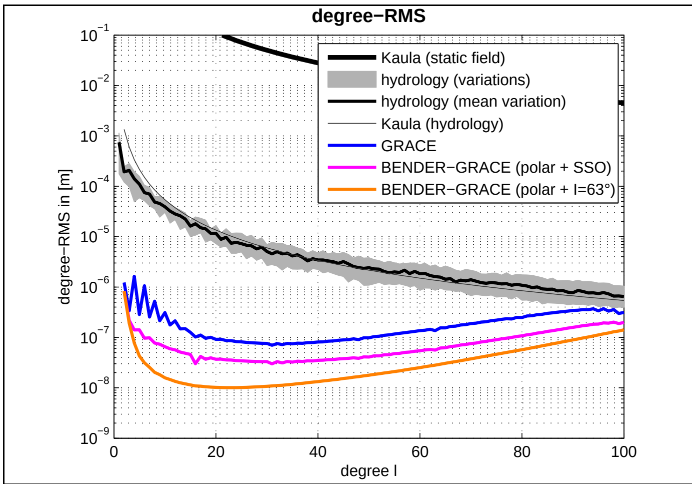

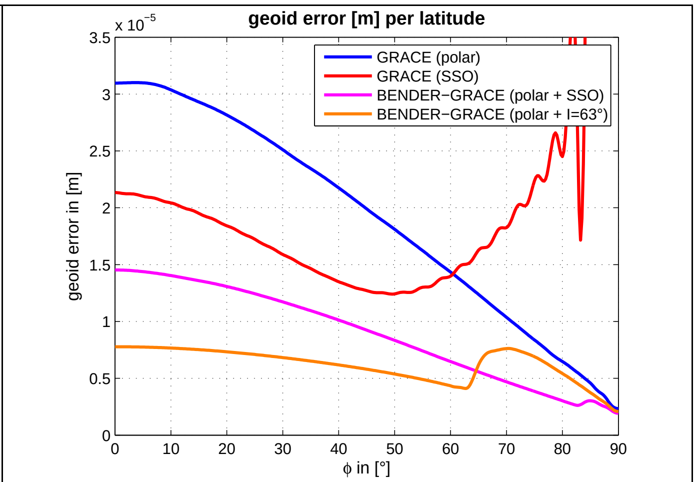

Figure 4-25: comparison of single polar inline-formation and combinations of inline-formations with different inclinations (BENDER-design); degree-RMS and geoid errors per latitude

4.6.2 Sensitivity for white noise

In this section mixed Bender combinations using a polar inline-formation and different formations (inline, Pendulum, Cartwheel) on an inclined orbit (SSO, I = 63°). First the sensitivity of the three types of formations for the different inclinations (polar, sun-synchronous, I = 63°) is investigated in terms of formal error plots in **Figure 4-26**. As mentioned in the previous subsection the low order coefficients again are very in accurate or can not be determined for inclined orbit, and depending on the inclination this effect grows. For the inline- and Cartwheel-formations a similar effect can be observed. For both the error spectrum is shifted to higher orders if the inclinations deviates more from a polar orbit. This is due to fact that East-West information is added when the intersection angle between ascending and descending orbits grows, which adds more isotropy and thus effects the higher orders in a positive way. Again, as mentioned in the previous section, a combination of such pairs in different inclinations might be very valuable due to the combination of complementary information.
For the Pendulums the behaviour for different inclinations is different dependent on which satellite (left or right) is the leader. This is visualised in **Figure 4-29**. In case of a polar formation there is no dependence on the leading satellite since the useful cross-track-information gathered is the same for both types (see also results in **Figure 4-26**). In contrast for an inclined orbit there is a dependence on the inclination. If the inclination is I < 90° there seems to be an advantage if the right satellite is the leader. As visible in **Figure 4-29** the signal contains a large East-West component over the equator while it only contains a small East-West component in case the left satellite is leading. For the case of inclinations I > 90°, e.g. a sun-synchronous orbit, there seems to be a benefit if the left satellite is the leader. This is displayed in **Figure 4-29** where the Pendulum with the left satellite as a leader now senses more East-West signal over the equator while a Pendulum with a right leading satellite gathers less East-West information. The presumptions drawn from **Figure 4-29** are proved by the formal error plots in **Figure 4-26**. Here the Pendulum formations with a left leader for the SSO and a right leader for I = 63° show a good performance with an improvement of the higher orders compared to the polar Pendulum, which is due to the enhanced isotropy (and sensitivity). In contrast a left leader for I = 63° and a right leader for an SSO diminish the accuracy of the higher orders compared to a polar Pendulum due to reduced isotropy (and sensitivity) and thus should not be applied in a Bender-combination.

The results for the mixed Bender-missions are shown in **Figure 4-27** in terms of degree-RMS and covariance-functions and in **Figure 4-28** for selected cases in terms of degree-RMS and geoid errors per latitude. As illustrated by the degree-RMS curves the Bender-combinations lead to an improvement of approximately one order of magnitude compared to the single polar inline-formation. Here the Bender-mission composed of two inline-formations (polar + I=63°) already shows a good performance which can be exceeded by the mixed combinations only by a factor of 2. But in contrast to the pure inline Bender combination the mixed Bender missions show a higher isotropy (see covariance functions). For all mixed cases the covariance functions are almost perfectly circular except for those applying the problematic Pendulum configurations (left leading satellite for I = 63°, right leading satellite for SSO) mentioned before. For instance the Bender mission composed of the polar inline formation and a Pendulum with a left leader at I = 63° shows a worse accuracy (sensitivity + isotropy) as the pure inline Bender mission. The most homogeneous formal error plots are obtained for the mixed cases (inline + Pendulum/Cartwheel) combining a polar orbit and a SSO, where the mixed combination of a polar inline formation and a SSO Pendulum (left leader) is outperforming the mixed Bender mission with the SSO-Cartwheel. For the mixed combinations of a polar orbit and a low inclination orbit (I = 63°) structures with reduced accuracy at low/medium orders are visible which originate from the huge polar data gap of the inclined orbit. Both combinations lead to a similar accuracy regarding the different types of error plots shown. Concerning the geoid errors per latitude similar conclusions can be drawn. While the combinations of polar and low inclination orbits (I = 63°) are very accurate in mid latitude regions due to the dense groundtrack coverage and less accurate over higher latitude regions due to the polar data gap of the inclined formations the geoid errors per latitude are more homogeneous for the combinations of polar orbits and SSO since the effects mentioned afore are less pronounced. The geoid errors per latitude for all combinations of the polar inline-formation and a low inclined formation (inline, Pendulum, Cartwheel) are quite similar except for the lower latitude where the pure inline Bender mission is worse by factor of 2. The best and most homogeneous behaviour concerning the geoid errors per latitude seems to be obtained by the mixed Bender combination of the polar inline formation and a SSO Pendulum with a left leader.

From the investigations in subsection 4.6 the following conclusions can be drawn concerning the Bender-design:

- combination of satellite formations with different inclinations with lead to complementary information seems to be most promising
- it has to be taken care of which satellite is the leader at inclined Pendulums
- promising results are obtained by the combination of a polar inline-formation with inclined inline/Pendulum/Cartwheel formations, especially for the combination with an SSO Pendulum/Cartwheel.
- Most promising seems to be the combination of a polar inline-formation with a SSO Pendulum

	polar	SSO	I = 63°
GRACE	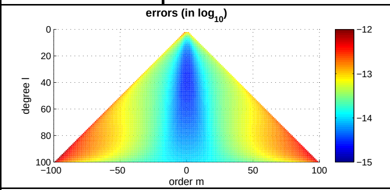	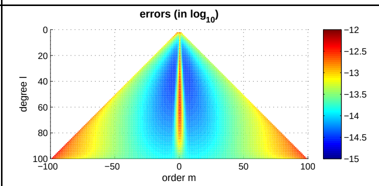	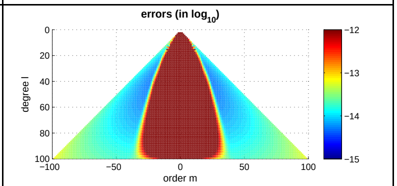
PENDULUM (left satellite is leading)	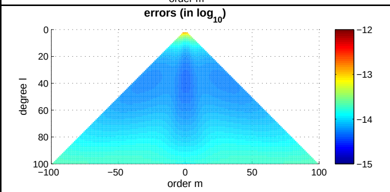	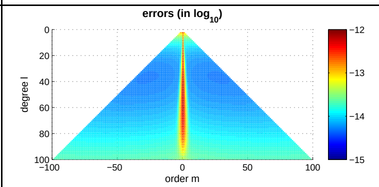	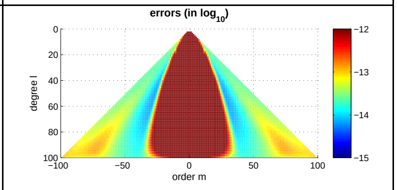
PENDULUM (right satellite is leading)	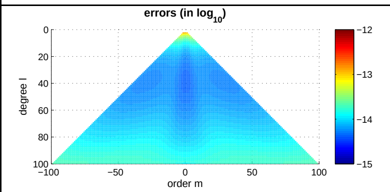	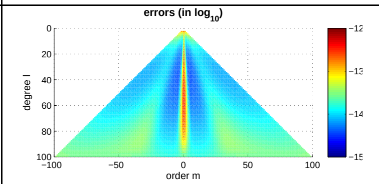	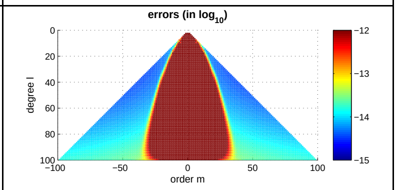
CARTWHEEL	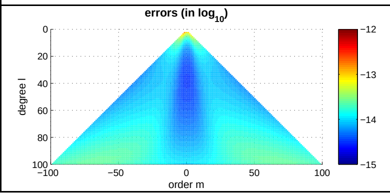	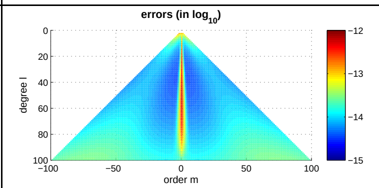	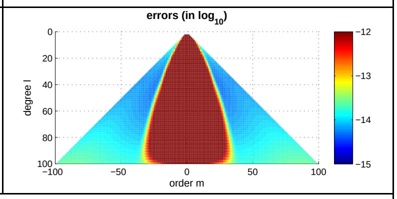

Figure 4-26: formal errors of different single formations on different inclinations

	polar + SSO		polar + I=63°	
polar GRACE + GRACE	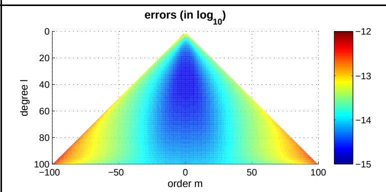	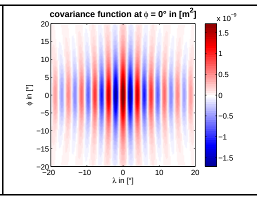	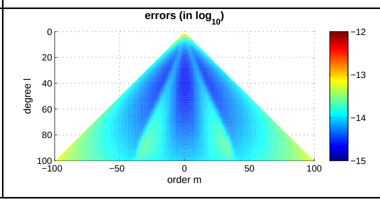	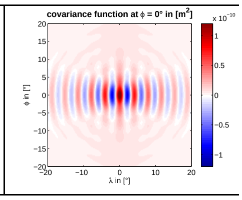

polar GRACE + PENDULUM (left satellite is leading)	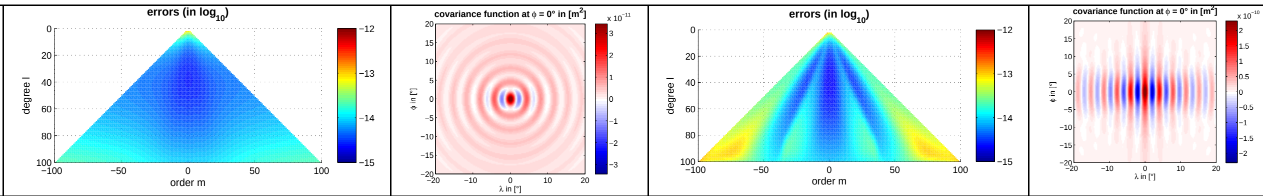
polar GRACE + PENDULUM (right satellite is leading)	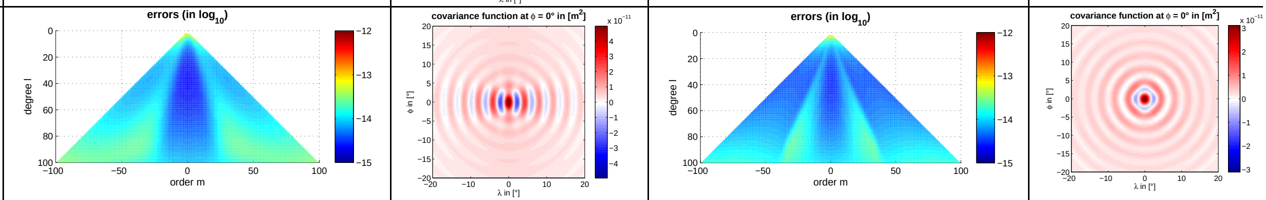
polar GRACE + CARTWHEEL	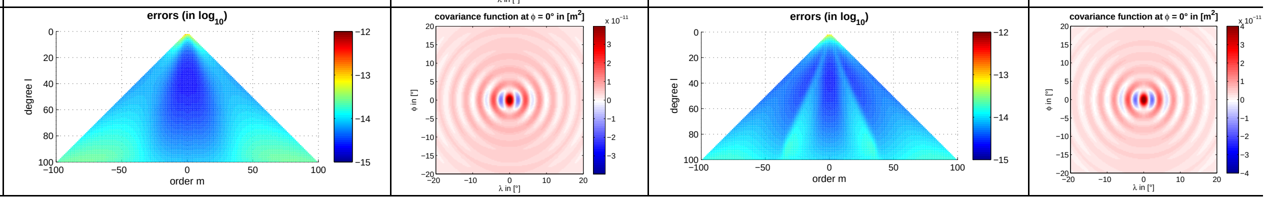

Figure 4-27: comparison of different mixed BENDER-constellations (polar GRACE + formation on SSO/I=63°)

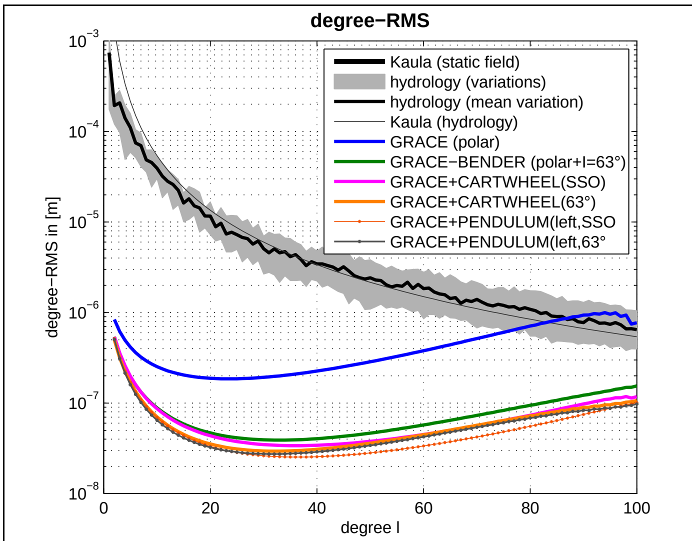

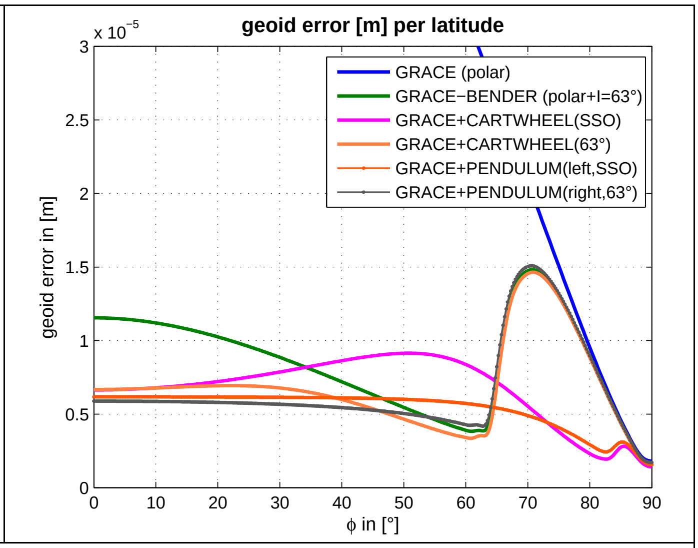

Figure 4-28: comparison of different mixed BENDER-constellations in terms of degree-RMS and geoid errors per latitude.

PENDULUM, polar orbit:

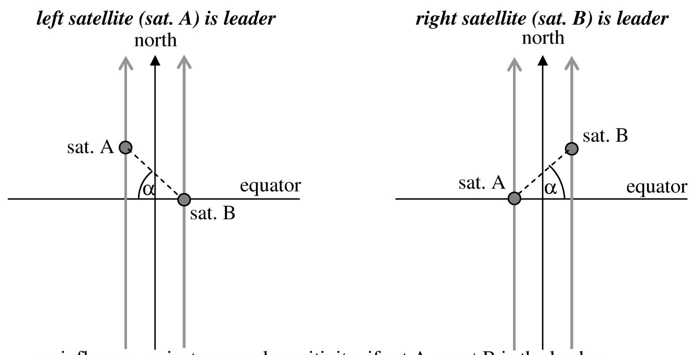

→ no influence on isotropy and sensitivity, if sat A or sat B is the leader.

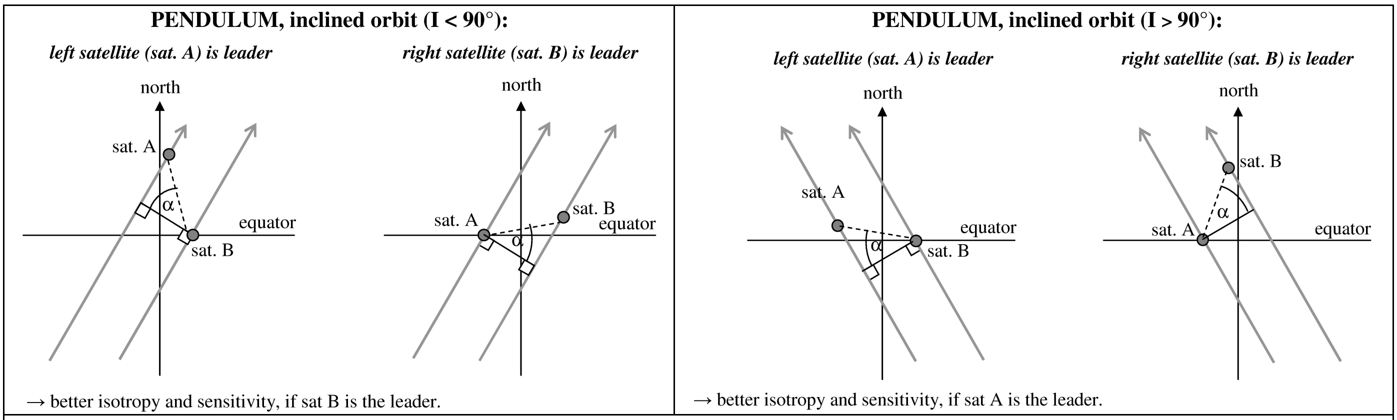

Figure 4-29: explanation for the dependance of the sensitivity on the leading satellite in case of inclined orbits

5. COMPARISON OF POLAR AND SSO INLINE- AND PENDULUM-FORMATIONS AND THEIR COMBINATIONS (BENDER-DESIGN)

It was shown in section 4.6 that the sensitivity can be increased by combining (different) formations on different orbits. The largest improvement can be achieved if formation flights with complementary information are combined. In section 4.6 only combinations of inline-formations and combinations of polar inline-formations and SSO-pendulums/cartwheels are investigated. In this section further combinations of polar and SSO inline- and pendulum-formations are investigated (except the combination of polar pendulum and SSO-inline due to the relatively low accuracy of higher orders for the inline-formations). Cartwheel-formations are not considered since they can not be implemented with sufficient accuracy at present state, as showed in [RD-2] and [RD-3], and also their realisation at low orbit height, e.g. h ≈ 350 km, seems to be problematic due to high power consumption. For simulations including a polar pendulum a repeat mode of $(\beta/\alpha) = 463/30$ with an orbit height oh h ≈ 417 km was assumed since a lower orbit height also seems to be not feasible due to an enhanced propulsion consumption [RD-2]. For all the other formations the repeat modes and orbit heights (@ h ≈ 335-350 km) originally suggested for the simulations were used. **Figure 5-1** and **Figure 5-2** show the results for various combinations of polar and SSO inline-/pendulum-formations as well as of the basic single formations. The formations and formation-combinations tested are:

- polar inline ($(\beta/\alpha) = 503/32$, h ≈ 335 km)
- polar pendulum ($(\beta/\alpha) = 463/30$, h ≈ 417 km)
- SSO-pendulum ($(\beta/\alpha) = 503/32$, h ≈ 348 km, $\alpha = 45°$)
- inline-Bender (polar inline + SSO-inline)
- inline-Bender (polar inline + (I = 63°)-inline)
- polar inline + SSO-pendulum ($\alpha = 67°$)
- polar inline + polar pendulum ($\alpha = 67°$)
- polar pendulum ($\alpha = 23°$) + SSO-pendulum ($\alpha = 45°$)

For all formations an average intersatellite distance of $\rho = 75$ km and white range-acceleration noise of psd = 10^{-10} [m/s²/sqrt(Hz)] is used. For the SSO-pendulums the constellation with the left satellite as a leader was used since the constellation with a right leader is less sensitive, as showed in section 4.6.

As it can be seen in **Figure 5-1** and **Figure 5-2** the best results for the formation combinations concerning accuracy and isotropy can be obtained for the combinations using the SSO-pendulum. This is because the SSO-pendulum offers both, a large isotropy compared to inline formations and an improved accuracy for higher degrees compared to the polar pendulum due to the lower orbit. Here the combination of polar inline + SSO-pendulum (mixed-Bender) outperforms the combination of polar pendulum + SSO-pendulum (pendulum-Bender) since the polar inline shows higher accuracy for the low order coefficients than the polar pendulum.
Concerning the single formations, the best performance is achieved by the SSO-pendulum, if the polar data-gap is disregarded. But even the polar pendulum, which is flying in a higher orbit is able to improve the accuracy compared to the inline-formation (see **Figure 5-2**).
The degree-RMS-curve in **Figure 5-2** shows that the SSO-pendulum, inline-Bender (inline, polar + (I = 63°)), pendulum-Bender (pendulum, polar + SSO) and the combination polar-inline + polar-pendulum lead to similar results. In this case the mission options with lower cost/risk/complexity levels should be favoured, i.e. inline-Bender or the SSO-pendulum.

The most promising option seems to be the mixed Bender-combination of a polar-inline-formation and a SSO-pendulum. Such a constellation has the advantage that each of the formations forming this combination is a valuable mission on its own. This means that such a constellation can be realized by two independent agencies, e.g. ESA and NASA, where each agency is responsible for one formation.

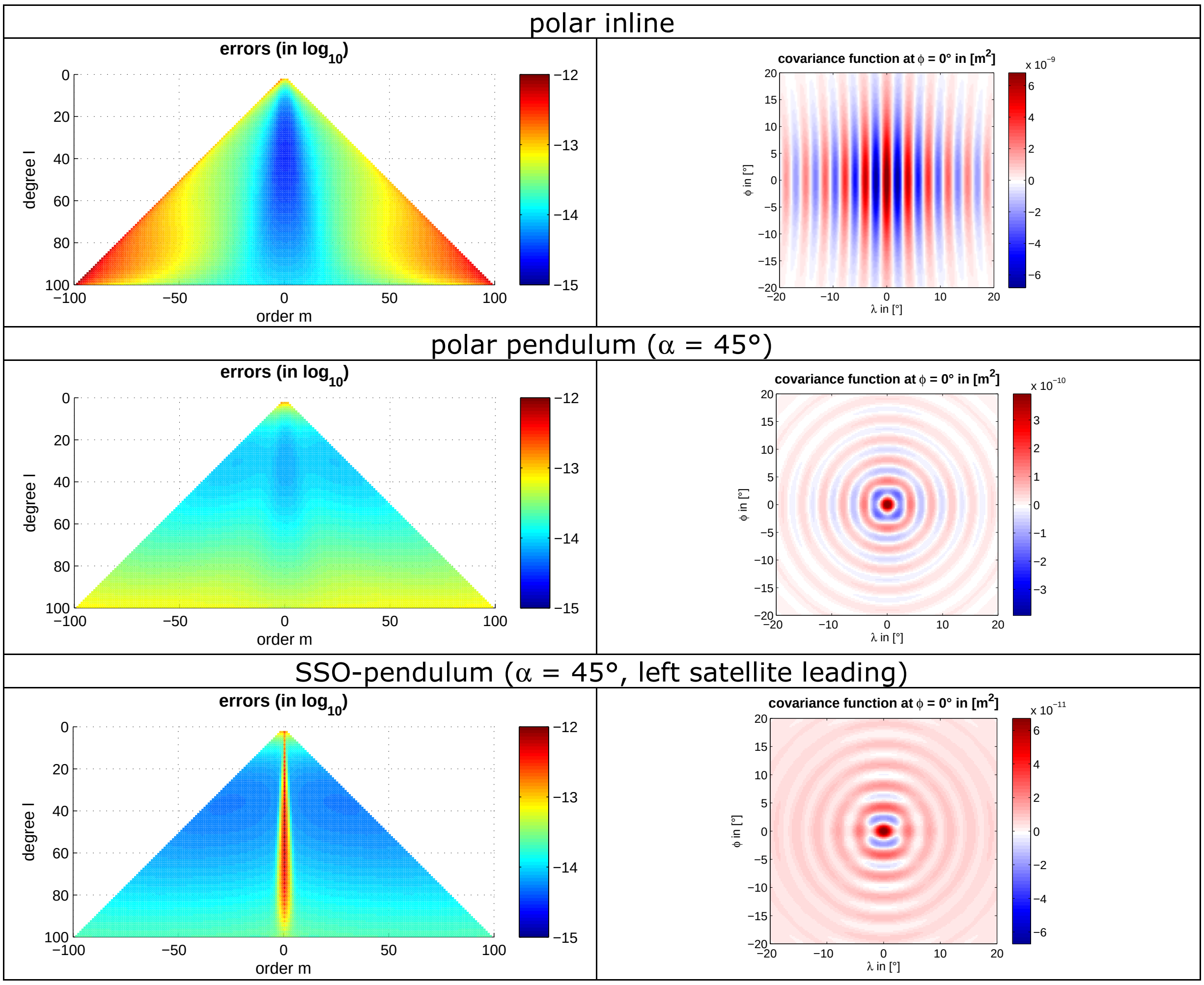

inline-Bender (polar + I=63°)

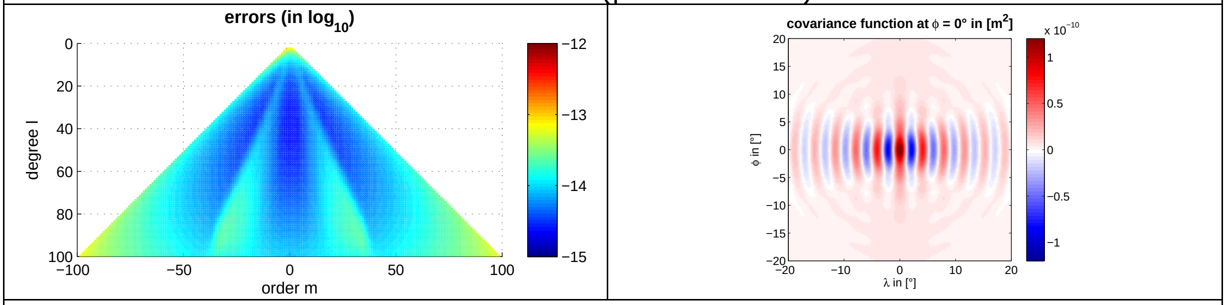

inline-Bender (polar + SSO)

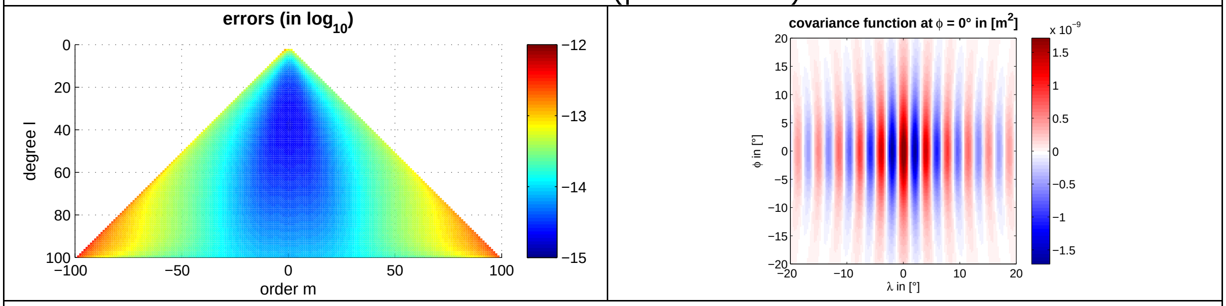

mixed Bender: polar inline + SSO-Pendulum (α = 67°, left satellite leading)

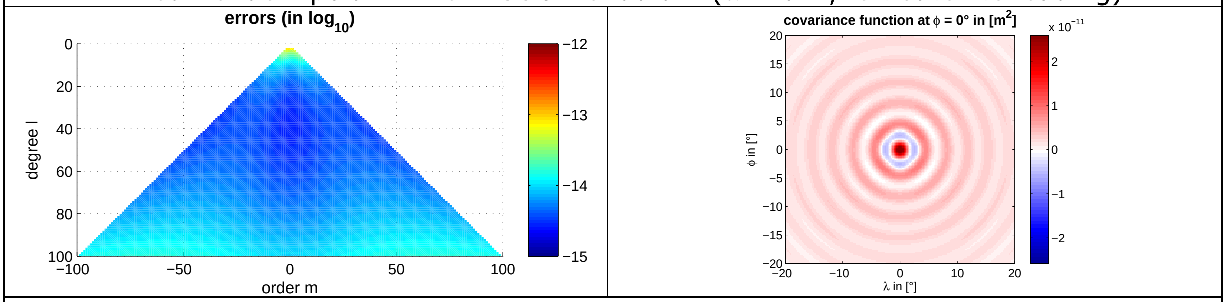

polar inline + polar pendulum (α = 67°)

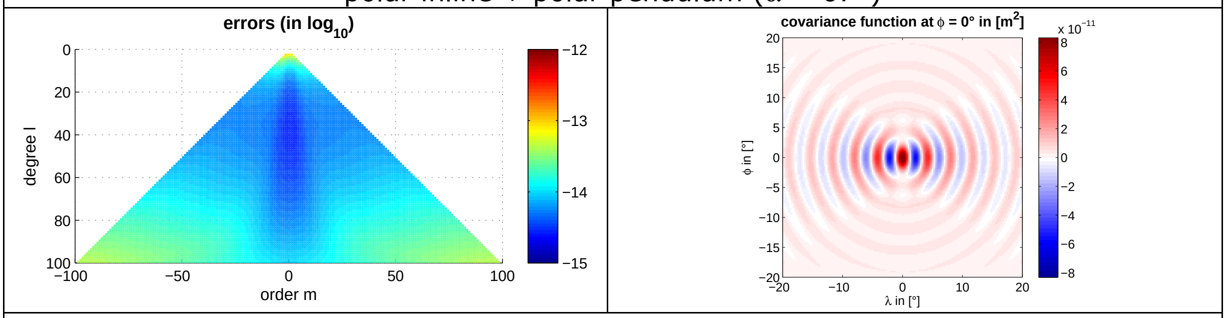

polar pendulum (α = 23°) + SSO-pendulum (α = 45°, left satellite leading)

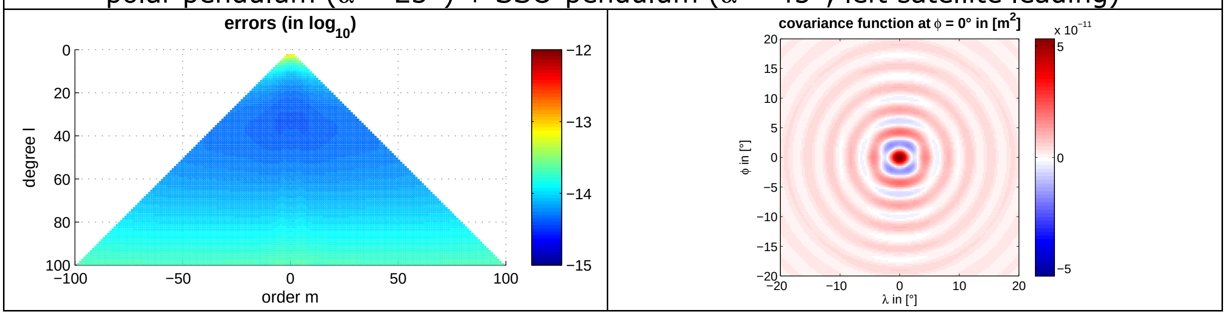

Figure 5-1 : comparison of polar and SSO inline-formations and pendulums and combinations of them (Bender-design) in terms of formal coefficient errors and covariance functions. The orbits used are: polar inline: $(\beta/\alpha) = 503/32$, $h \approx 335$ km; polar pendulum: $(\beta/\alpha) = 463/30$, $h \approx 417$ km; SSO-orbits: $(\beta/\alpha) = 503/32$, $h \approx 348$ km.

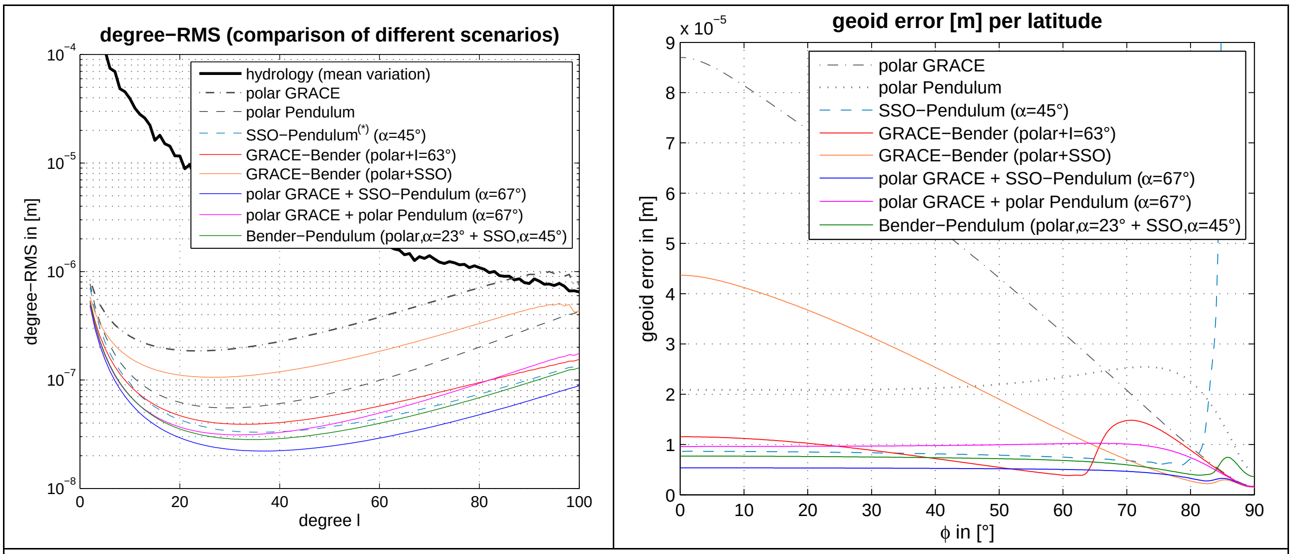

Figure 5-2: comparison of polar and SSO inline-formations and pendulums and combinations of them (Bender-design) in terms of degree-RMS and geoid errors per latitude.

In the previous comparisons in **Figure 5-1** and **Figure 5-2** the best formations and combinations of formations of each type of formation/combination have been compared. **Figure 5-3** to **Figure 5-7** shows the results of different designs of each type of formation/combination.
In **Figure 5-3** the various designs of SSO-pendulums using different line-of-sight angles α are compared. It can be seen that the SSO-pendulum with $\alpha = 45°$ seems to be the most promising option.
In **Figure 5-4** different designs of the combination polar inline + SSO-pendulum using different line-of-sight angles α are tested. The most promising option is the combination with a pendulum with $\alpha = 67°$. However, the improvement in contrast to a single SSO-pendulum is only a factor of 1.5-2, if the polar data-gap is disregarded.
In **Figure 5-5** different designs of the combination polar inline + polar pendulum with different line-of-sight angles α are investigated. The most promising option seems to be the combination with a pendulum with $\alpha = 67°$.
In **Figure 5-6** different implementations of pendulum-Bender missions (polar pendulum + SSO-pendulum) with different line-of-sight angles α are investigated. In the first row the combinations with a polar pendulum with $\alpha = 23°$ are tested. The best options seems to be the combination of a polar pendulum ($\alpha = 23°$) + SSO-pendulum ($\alpha = 45°$). In the second row the combinations with a polar pendulum with $\alpha = 45°$ are investigated. The best option seems to be the combination of a polar pendulum ($\alpha = 45°$) + SSO-pendulum ($\alpha = 45°$). In the third row the combinations with a polar pendulum with $\alpha = 67°$ are analyzed. The best option seems to be the combination of a polar pendulum ($\alpha = 67°$) + SSO-pendulum ($\alpha = 45°$). These best three options are compared in **Figure 5-7**. It shows that in principle all three options with a SSO-pendulum with $\alpha = 45°$ are quite similar, with only slight advantages of the combination polar pendulum ($\alpha = 23°$) + SSO-pendulum ($\alpha = 45°$) at near-polar areas.

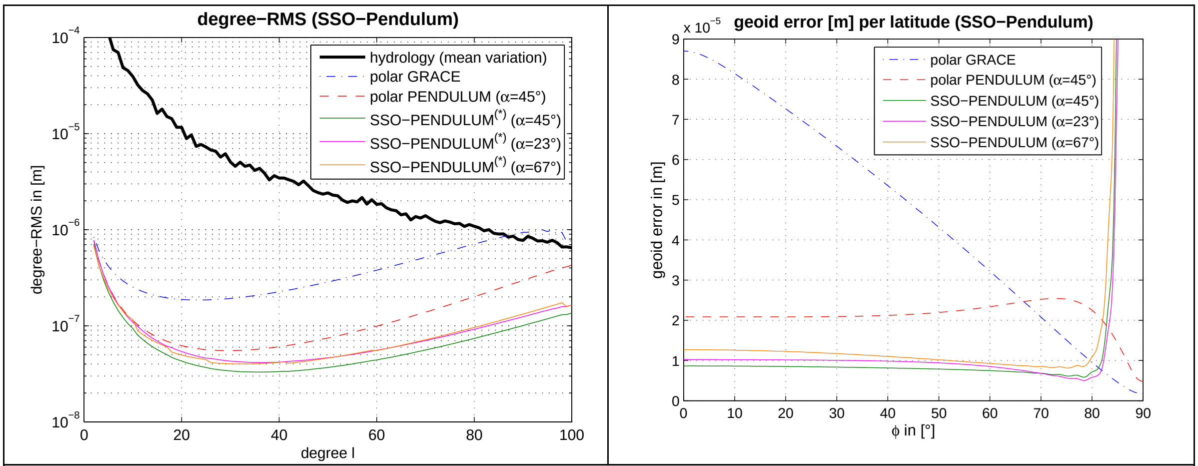

Figure 5-3: comparison of single formations: polar inline/pendulum and SSO-pendulums with different yaw angles α.

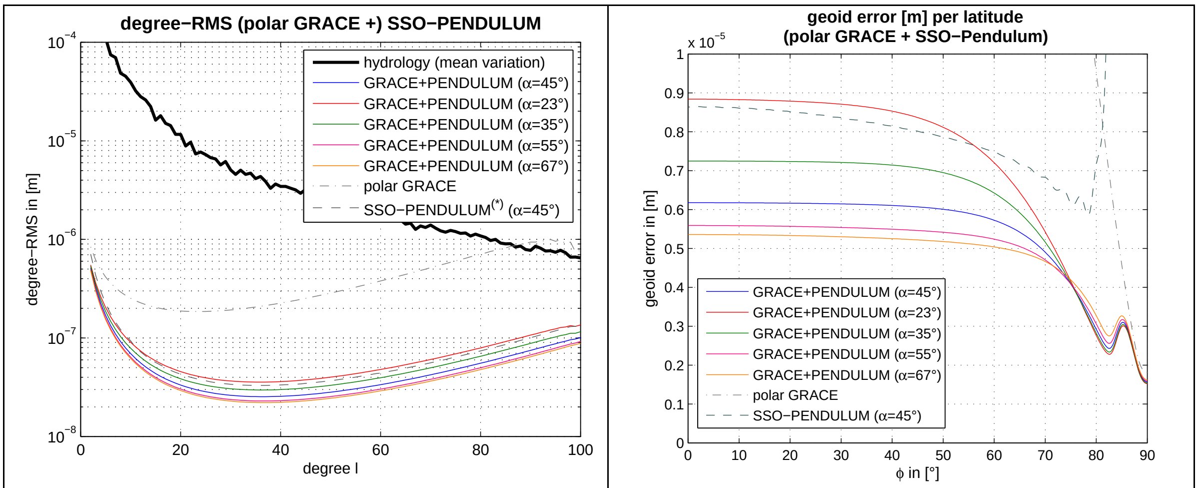

Figure 5-4: comparison of combinations of polar inline formation with SSO-pendulums with different yaw angles α.

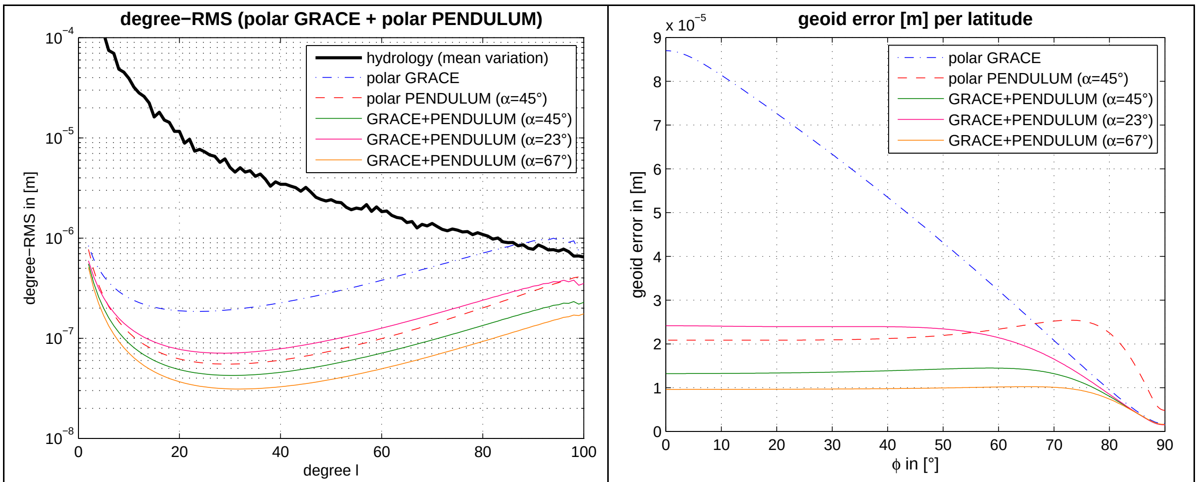

Figure 5-5: comparison of combinations of polar inline formation with polar pendulums with different yaw angles α.

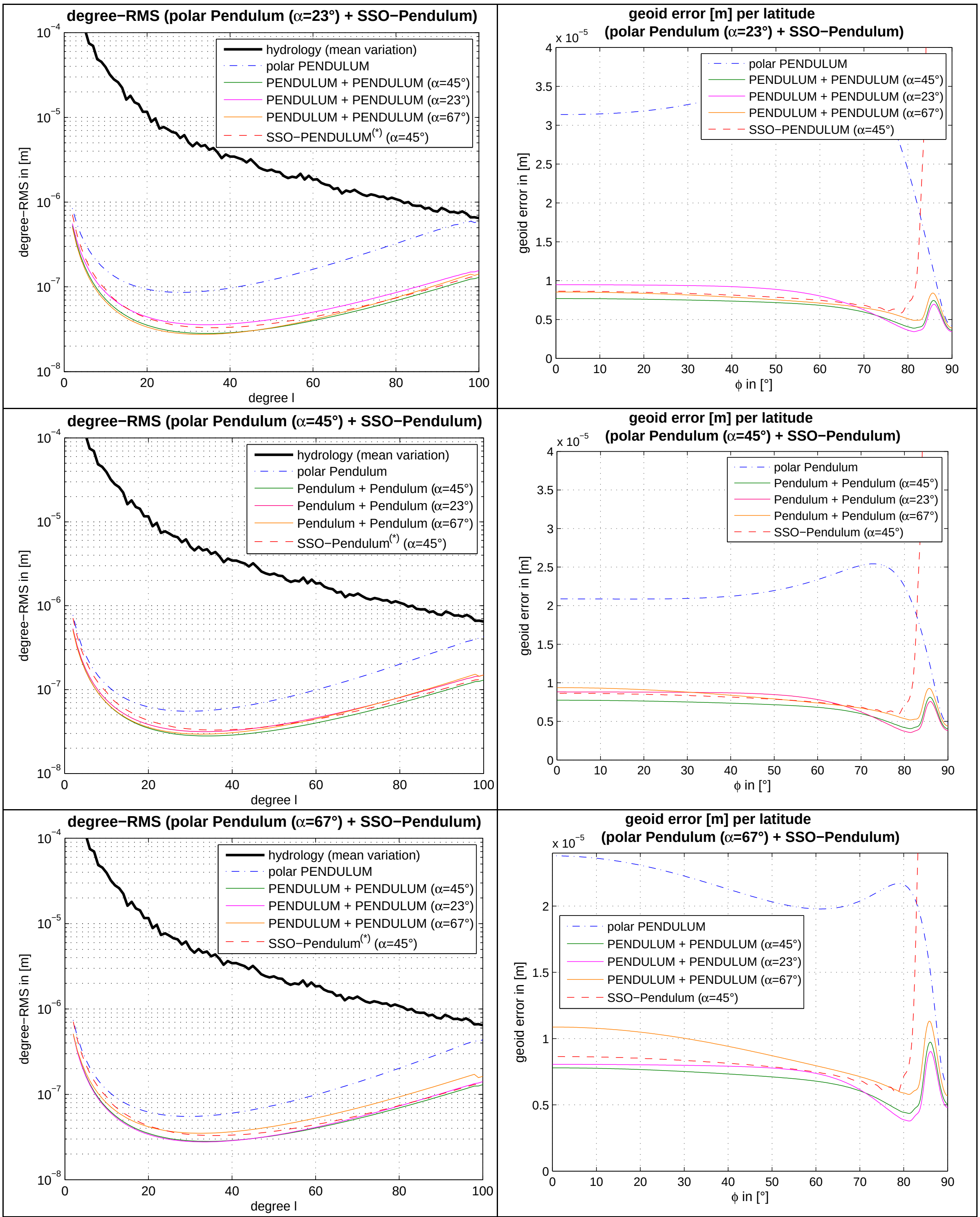

Figure 5-6: comparison of combinations of polar pendulums and SSO-pendulums with different yaw angles α); first row: combinations of polar pendulum with α = 23°, second row: combinations of polar pendulum with α = 45°; third row: combinations of polar pendulum with α = 67°.

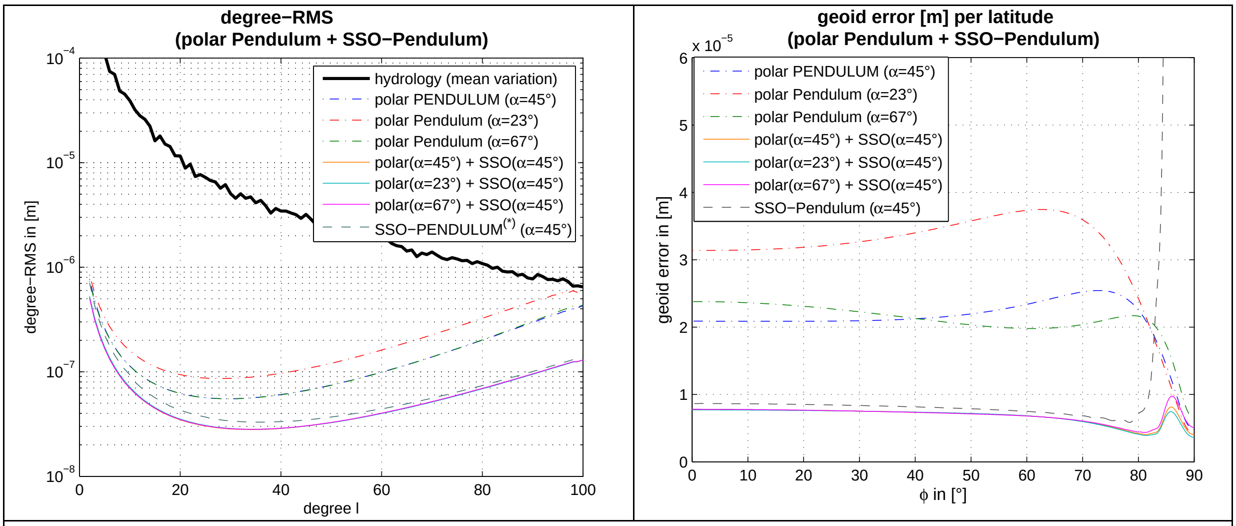

Figure 5-7: comparison of combinations of polar pendulums with different yaw angles α and SSO-pendulums with a yaw angle of α = 45° (best of each row of **Figure 5-6**).

6. COMPARISON OF THE RESULTS FROM THE FULL-SCALE RETRIEVALS WITH THE QUICK-LOOK SIMULATIONS

In this section a comparison between the results from the Quick-look tools (QLF) and the full-scale retrievals (FS) of [RD-3] has been done. However, the comparison is difficult due to:

- the QLT are only able to propagate sensor noise in terms of PSD, temporal and spatial aliasing cannot be studied with it. In contrast the FS (case 2 retrievals of [RD-3]) also contain the aliasing errors generated by the hydrology and 10% of atmosphere+ocean. Thus a 1:1 comparison is not possible
- the simulations of the advanced formations of cartwheels and pendulum are only possible with the pseudo-QLT which means that only white noise on the level of range-accelerations can be used. The realistic sensor noise used in the FS in contrast is coloured and shows besides the a-priori PSD (e.g. the realistic PSD used in this TN) typical features of the individual formations (see [RD-2] and [RD-4]), e.g. severe peaks on the orbit frequency and its multiples for the cartwheel which lead to strong distortions in the gravity field retrievals ([RD-3]). This means also that a 1:1 comparison between QLT and FS is not possible. However, missions using the inline-formation can also be investigated with the semi-analytic QLT which allows the simulation of coloured noise (as PSD).

Despite these problems the idea is to derive scaling factors which can be used for propagation of the FS-performance to higher degrees L with the QLT and a comparison of the propagation with the science requirements in the Final Report. The following scenarios have been analysed:

- scen 1: polar inline (ρ = 75 km, (β/α) = (503/32), h ≈ 335 km)
- scen 2: SSO inline ρ = 75 km, (β/α) = (503/32), h ≈ 348 km); for the degree-RMS the influence of the polar gap is neglected (denoted by $^{(*)}$)
- scen 4: polar pendulum ($\rho_x = \rho_y$ = 62 km, (β/α) = (503/32), h ≈ 335 km)
- scen 5: polar cartwheel (ρ_r = 50 km, (β/α) = (503/32), h ≈ 335 km)
- scen 6: polar pendulum ($\rho_x = \rho_y$ = 62 km, (β/α) = (463/30), h ≈ 417 km)
- scen 1 + scen 3: inline-Bender (polar inline ((β/α) = (503/32)) + (I = 63°)-inline ((β/α) = (481/31)))
- scen 1 + scen 4: polar inline + polar pendulum
- scen 1 + scen 5: polar inline + polar cartwheel

- scen 3 + scen 4: mixed-Bender (polar pendulum + (I=63°)-inline)
- scen 3 + scen 5: mixed-Bender (polar cartwheel + (I=63°)-inline)

For both, the simulations with the QLT and the full-scale retrievals always the time span of a full repeat cycle has been used, in order to have the best comparability and to reduce spatial aliasing effects in the FS. The noise applied is 10^{-10} m/s²/sqrt(Hz) for the QLT and additionally the constellations based on the inline-formations have been simulated with the model for the realistic PSD for the coloured noise.
The scaling factors k between the degree-RMS of FS and QLT have been derived on the logarithmic scale by means of least-squares adjustment from the equation

$$\log_{10}(\mathrm{FS}) = \log_{10}(\mathrm{QLT}) \cdot k$$

Figure 6-1 shows the results of the QLT and FS for the above scenarios in terms of degree-RMS and geoid-errors per latitude. In the first line the results of the QLT for white noise assumptions are shown, in the second line a comparison of the QLT for white and coloured noise for the constellations based on inline-formations is displayed and in the third line the FS results are shown.
The QLT results in first line show that by the assumption of identical (white) noise for all scenarios the single formations of pendulum (scen 4) and cartwheel (scen 6) show a similar performance as all 2-fomation missions, which is almost up to one order of magnitude better than for the single-inline formations. The pendulum on the higher orbit (scen 6) shows similar errors as the lower pendulum (scen 4) for the lower degrees and rising errors for higher degrees due to stronger signal attenuation of higher orbits. But still the errors of the lower pendulum are half an order of magnitude less than for the single-inline-formations, which means that it is a valuable formation. The best performance is achieved by the constellations combining the low inclined inline-formation (scen 3) and the polar pendulums/cartwheels (scen 4/scen 5), followed by the single polar pendulum (scen 4). However the difference between these three missions and the other three 2-formation missions applying the polar inline formation is quite small (less than factor 2) so that the mission-selection should depend mostly on driving factors as cost, complexity, risk and feasibility (e.g. the pendulum on the lower orbit (scen 4) seems to be unrealistic, see [RD-2]). For comparison, also the best formation-combination identified in section 5 is displayed. This constellation also outperformed the scenarios investigated by the FS, which shows again that this might be a valuable mission.
The comparison between the QLT results for white noise and coloured noise for the missions based on the inline-formation in the second line of **Figure 6-1** shows that the results in terms of degree-RMS for the coloured noise are approximately half an order smaller than for the white noise. This is caused by the general noise level, which is less for the realistic sensor PSD. Apart from such a simple shift or scaling between them, also other features are visible, which are caused by the different shape of white and coloured noise. For instance the results for the coloured noise are worse than for white noise for the lower degrees for the single polar inline-formation. Furthermore the single inline-formations show larger errors for white noise over areas of lower latitude. In contrast to the single inline–formations the inline-Bender shows a different slope of the degree-RMS for white and coloured noise. For this mission-type the lower slope of the white noise assumption might underestimate the real errors of higher degrees. The comparisons show that apart from the aliasing contained in the FS also differences between FS and QLT occur for the advanced formations due to the different noise assumptions.
The FS results show except for the constellations containing the cartwheel a similar behaviour as the results from the QLT, but shifted about one order of magnitude (one order of magnitude worse). The bad results for the cartwheel originate from the strong noise on the orbit frequency and multiples of it for this formation. Furthermore the inline-Bender also shows a slightly reduced performance between degrees 30 and 40.
Due to the low performance of the cartwheels the constellations containing this formation are excluded from the comparison. For the other formations a comparison of FS and QLT seems reasonable due to the similar, but shifted performance. But it has to be considered that despite the

derived scaling factors stronger differences might appear due to aliasing effects in the FS and the fact that only white noise is used in the QLT.

results for scenarios, quick-look-tool, white noise (10^{-10} m/s²/sqrt(Hz))

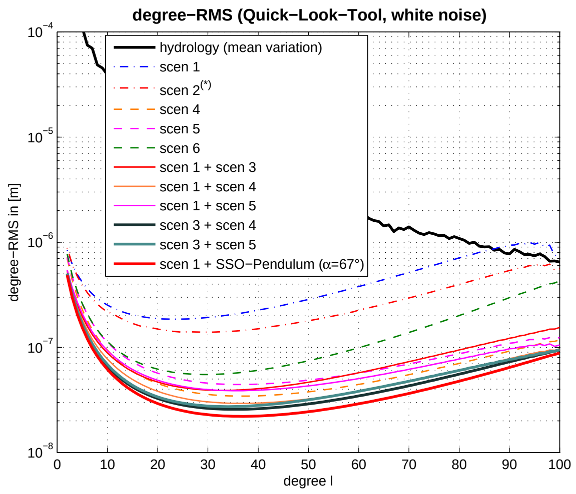

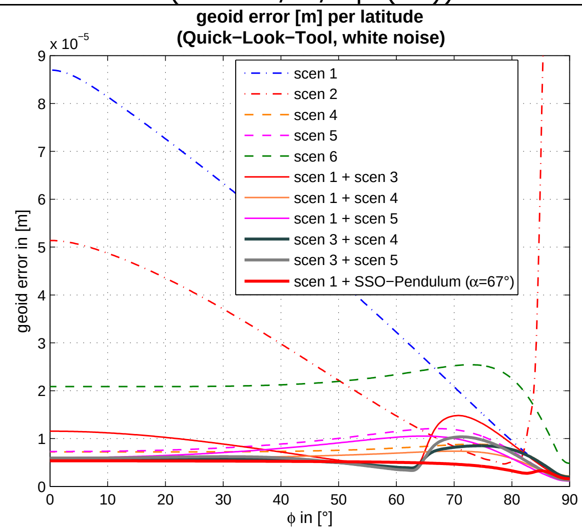

comparison of inline-scenarios, quick-look-tool: white noise (10^{-10} m/s²/sqrt(Hz)) vs. coloured noise

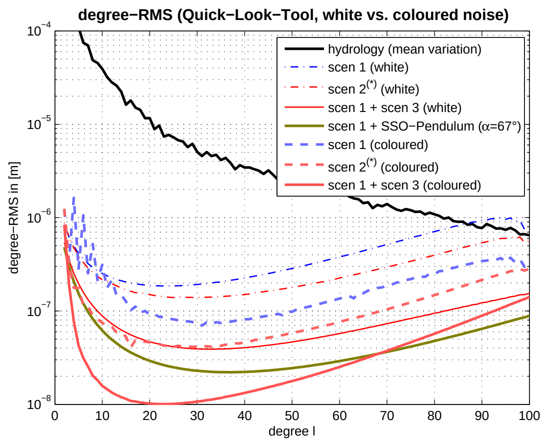

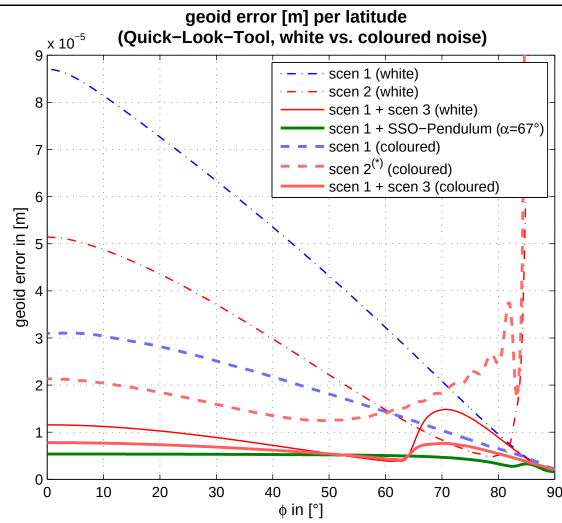

results for scenarios, full-scale retrieval (case 2)

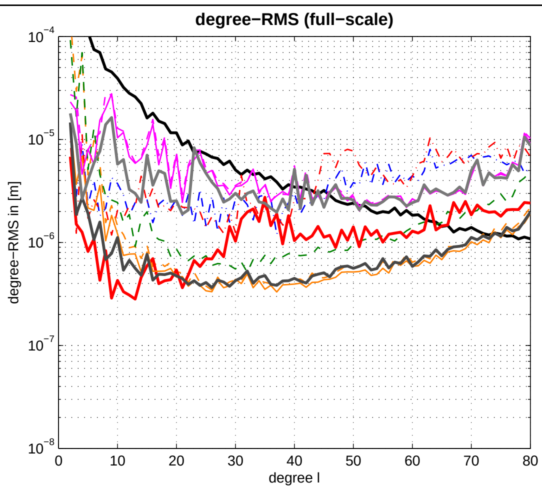

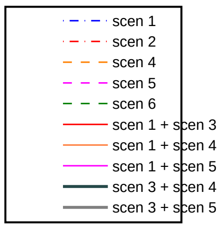

Figure 6-1: comparison of results from Quick-look tool and full-scale retrievals; (*) means that the near zonal coefficients of reduced accuracy due to the polar gap are neglected.

In **Figure 6-2** to **Figure 6-15** comparisons for the scenarios without cartwheels have been made between full-scale retrievals, the formal errors of the full-scale retrievals and the Quick-Look tool results for white noise. For the scenarios based on inline-formations additionally comparisons for the coloured noise case have been made. From the comparisons scale factors between FS and QLT are estimated, which have been used for a prediction of the FS performance up to degree L = 250. As assumed from **Figure 6-1** the scaling factors are quite similar in a range of about 0.9 (the scaling factors for the white noise are a little bit larger than 0.9 while those for the correlated noise are a little bit smaller) corresponding to a difference of about one order of magnitude.

The triangle plots of the missions based on inline-formations (scen1, scen2, scen1-scen3) show that the scaled QLT results for coloured noise fit better to the formal errors of the FS than the scaled QLT results for the white noise do. The reason for this is that the formal FS errors were propagated by white noise assumptions on the range-rate level, while the white noise QLT results were estimated from white noise on the level of range accelerations. However, compared with the true FS error triangle plots those of the scaled white noise QLT results seem still quite reasonable. This is confirmed by the degree-RMS curves for the single polar inline formation, where the scaled curves for white and coloured noise are quite similar. For the inline-Bender constellation (scen1-scen3) and the SSO-inline formation (scen2) however a difference in the slope of the degree-RMS curve for the scaled white and coloured noise QLT results exists, which produces a difference of almost one order of magnitude for degree l = 250 for scen1-scen3 and half an order of magnitude for scen2. The comparison wit the degree-RMS of the FS (true and formal) shows that the coloured noise QLT seems to be more realistic. This means on the other hand that at least for constellations containing inclined formations the predicted degree-RMS based on the white noise QLT results might be to optimistic A possible solution might be the estimation of degree-dependent scaling factors, e.g. the estimation of a linear trend of the scaling factor.
As the triangle plots for all investigated scenarios show, the white noise QLT simulations underestimate the accuracy of the coefficients of higher order. Furthermore, as recognized above for scenarios scen1-scen3 and scen2, the slope of the degree-RMS curves is underestimated by the white-noise QLT simulations, as the comparisons between the FS and QLT show. Thus the prediction of the FS up to degree L = 250 has to be judged with care.

The predictions for all investigated missions are displayed in **Figure 6-16** for scaled and unscaled QLT-simulations up to degree L = 250. Concerning the scaled predictions the best performance is obtained for the formations and combinations containing the pendulum, which are scen4, scen1-scen4 and scen3-scen4. The single inline formations (scen1, scen2) show the worst performance, which is about one order of magnitude less than for the combinations containing the pendulum. Scenario scen1-scen3 performs about a factor of 2 worse than the constellations containing the pendulum. The pendulum on the lower orbit height (scen 6) is in between the single-inline formations and the other missions, but it intersects the degree-RMS of the inline-formations around degree l = 200, which is caused by the larger slope due to the higher orbit. The single inline-formations intersect the hydrology-signal-RMS around degree l = 45 and the static gravity signal-RMS around degree l = 210, while the missions with the best performance intersect the hydrology signal-RMS at degree 80 and the static gravity signal-RMS at degrees l > 250.
The comparison of the scaled QLT results with the science requirements is outside the scope of this section, it is displayed and discussed in [RD-5] and in the Final Report [RD-6].

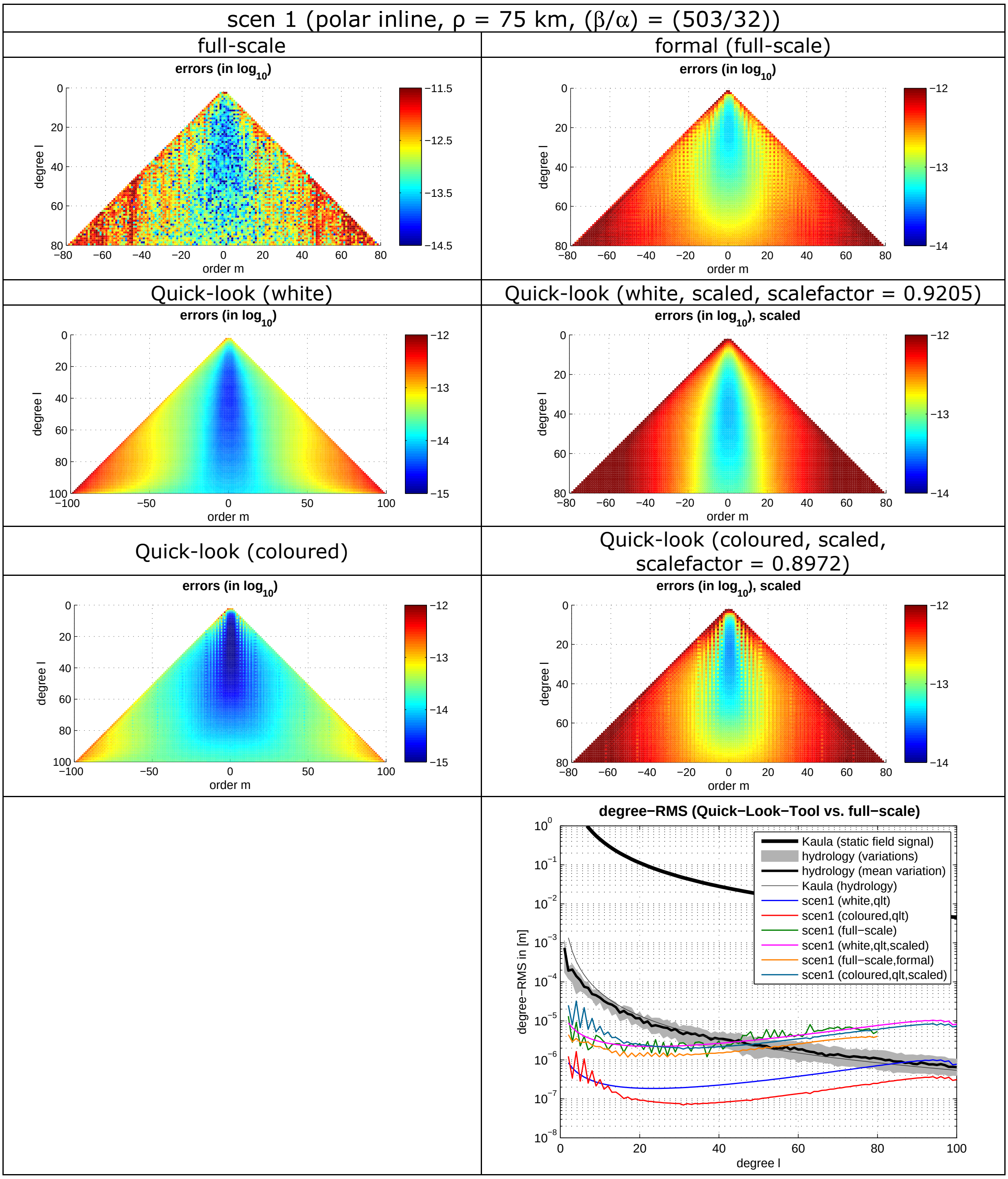

Figure 6-2: comparison of the results from Quick-look tool and full-scale retrievals for scenario 1 (polar inline, (β/α) = 503/32).

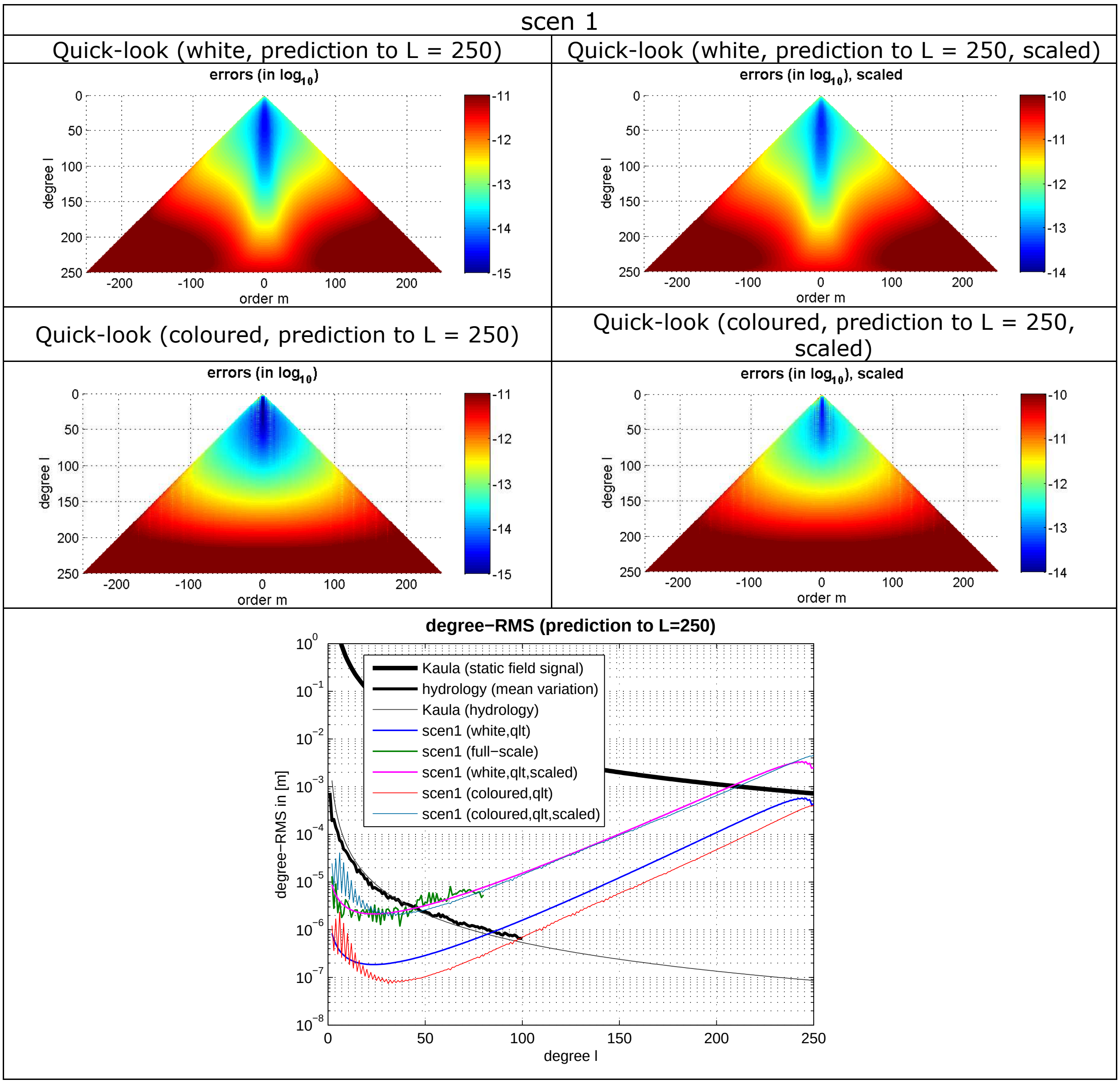

Figure 6-3: predictions of the performance of scenario 1 up to degree L = 250 (unscaled and scaled results of the Quick-look tool).

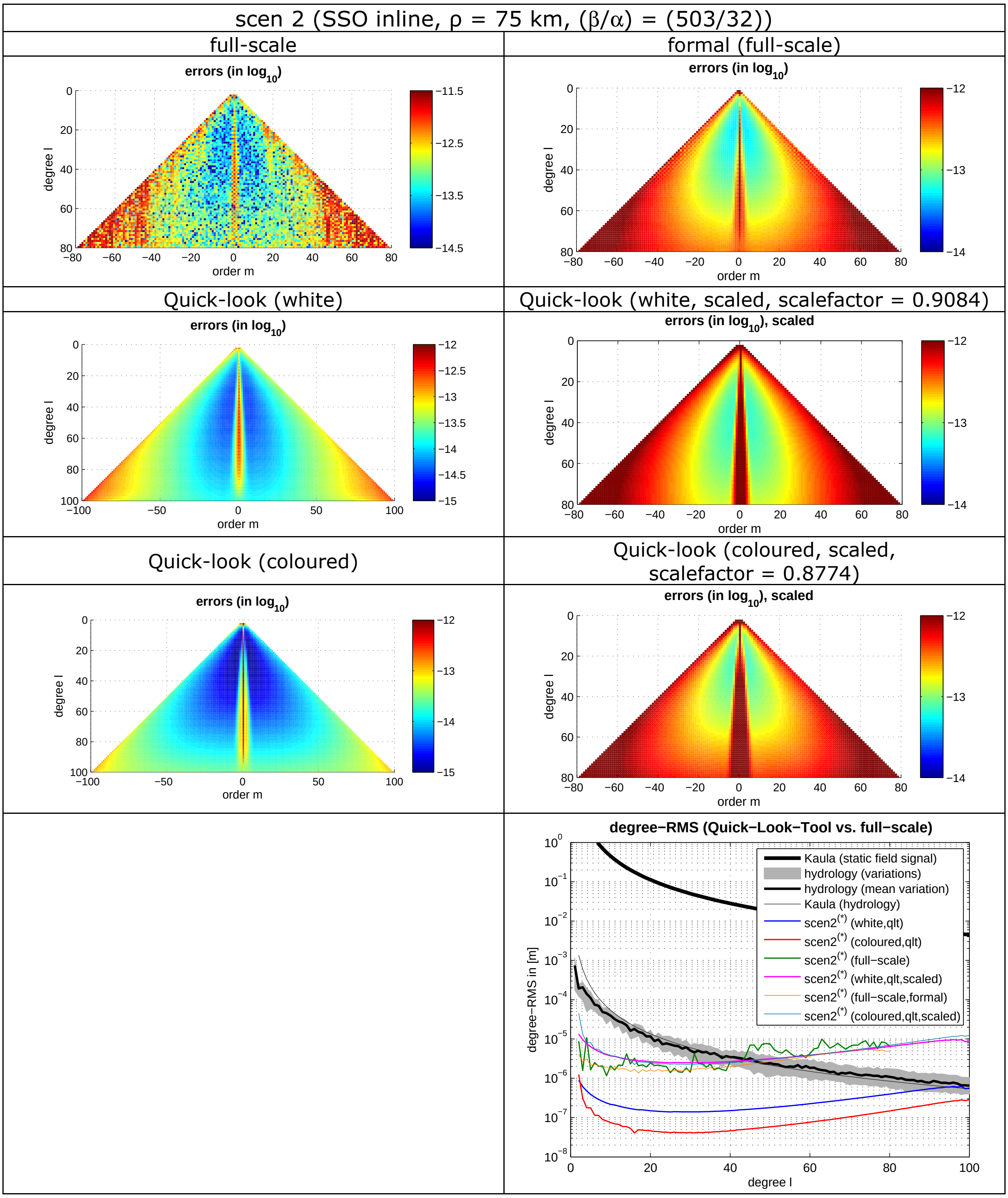

Figure 6-4: comparison of the results from Quick-look tool and full-scale retrievals for scenario 2 (SSO-inline, (β/α) = 503/32).

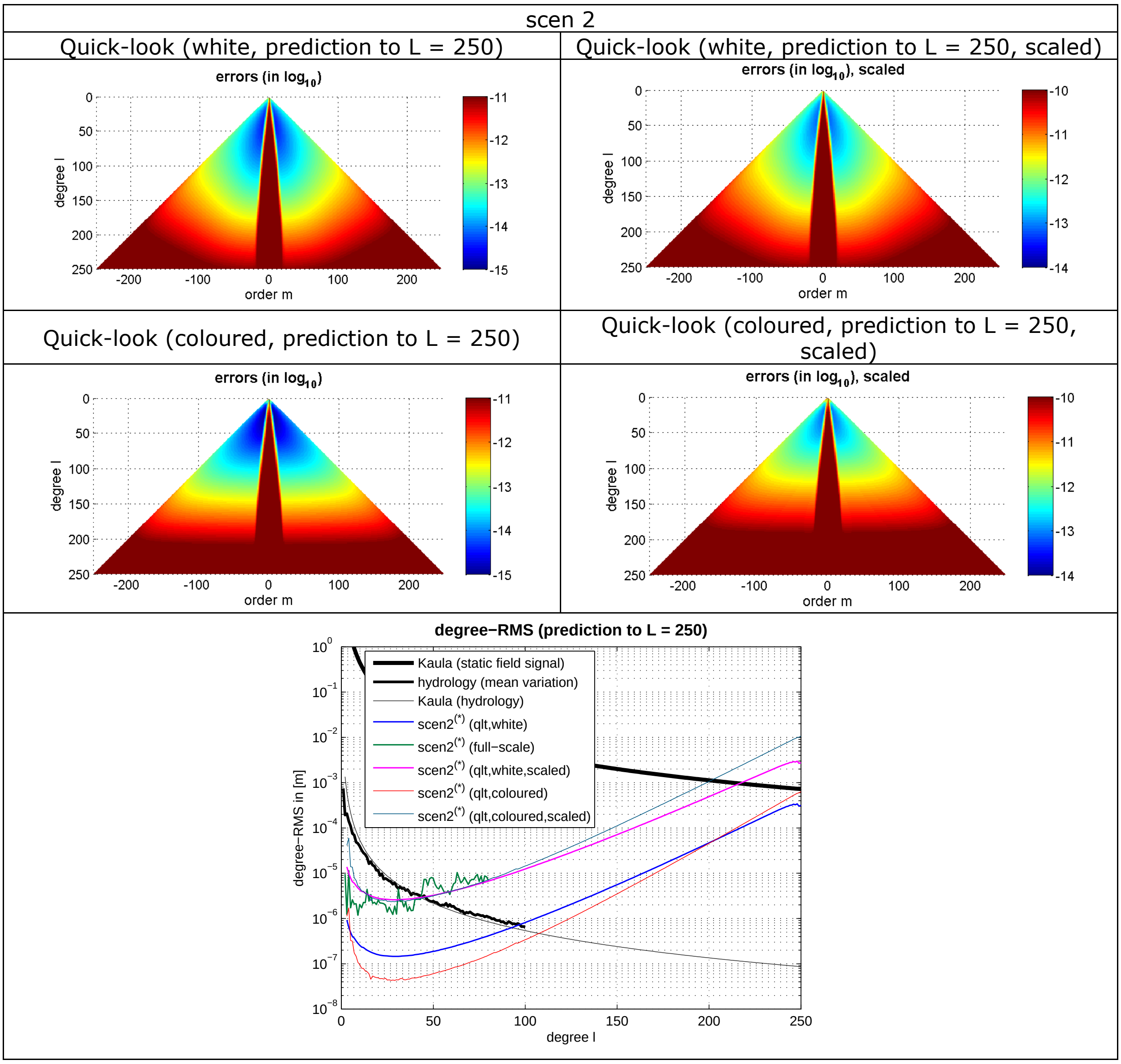

Figure 6-5: predictions of the performance of scenario 2 up to degree L = 250 (unscaled and scaled results of the Quick-look tool).

scen 4 (polar pendulum, (ρ_x/ρ_y) = (62/62 km), (β/α) = (503/32))

full-scale

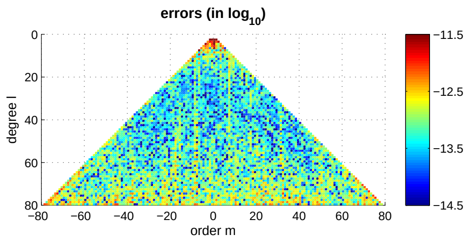

formal (full-scale)

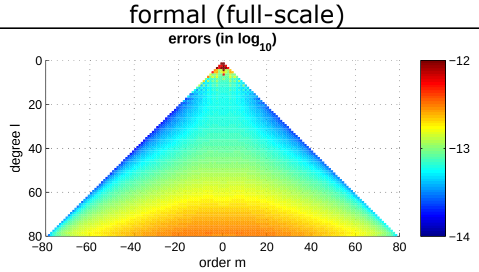

Quick-look

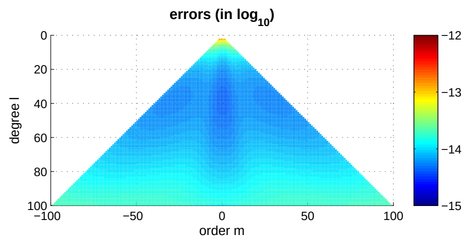

Quick-look (scaled, scalefactor = 0.9143)

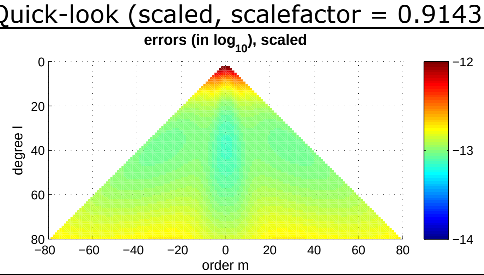

Figure 6-6: comparison of the results from Quick-look tool and full-scale retrievals for scenario 4 (polar pendulum, (β/α) = 503/32).

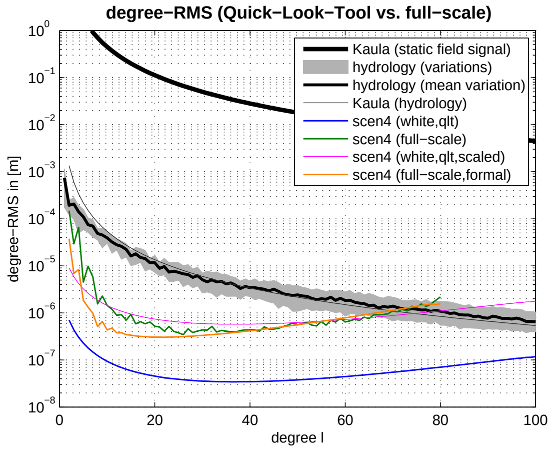

scen 4

Quick-look (prediction to L = 250)

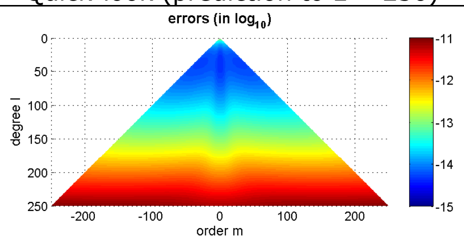

Quick-look (prediction to L = 250, scaled)

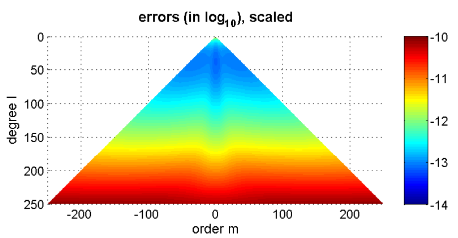

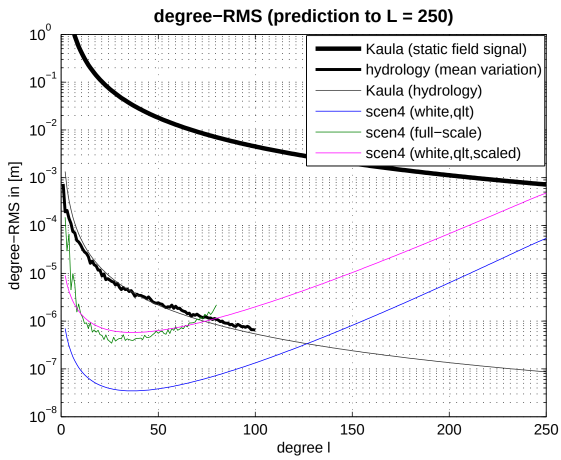

Figure 6-7: predictions of the performance of scenario 4 up to degree L = 250 (unscaled and scaled results of the Quick-look tool).

scen 6 (polar pendulum, (ρ_x/ρ_y) = (62/62 km), (β/α) = (463/30))

full-scale

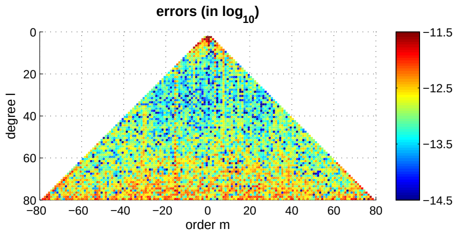

formal (full-scale)

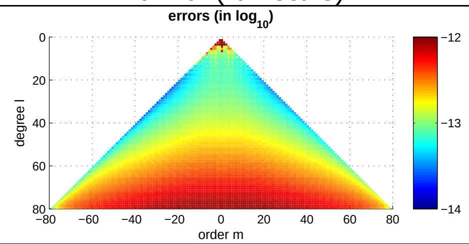

Quick-look

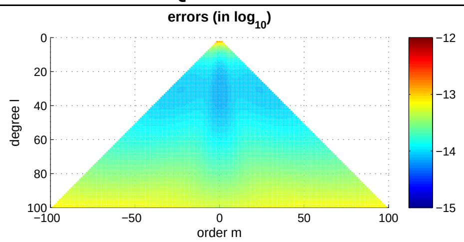

Quick-look (scaled, scalefactor = 0.9143)

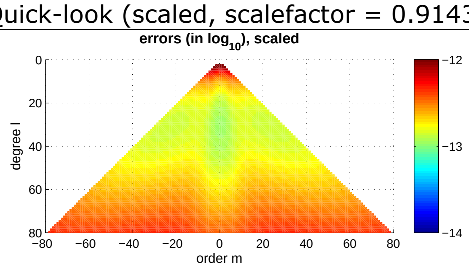

Figure 6-8: comparison of the results from Quick-look tool and full-scale retrievals for scenario 4 (polar pendulum, (β/α) = 463/30).

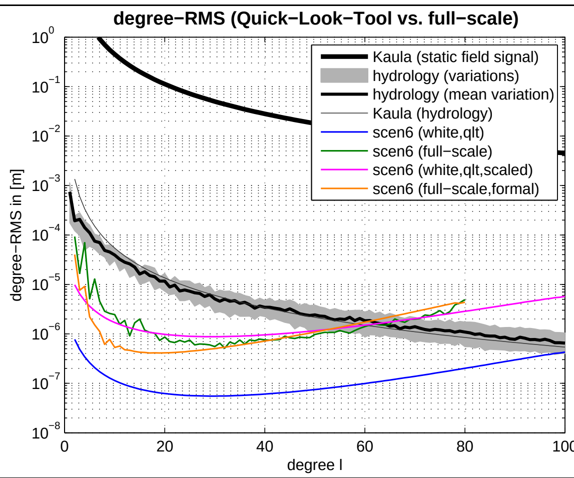

scen 6

Quick-look (prediction to L = 250)

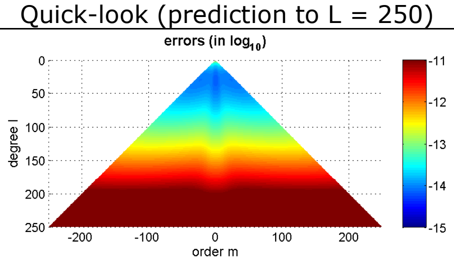

Quick-look (prediction to L = 250, scaled)

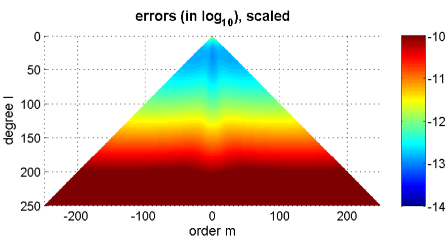

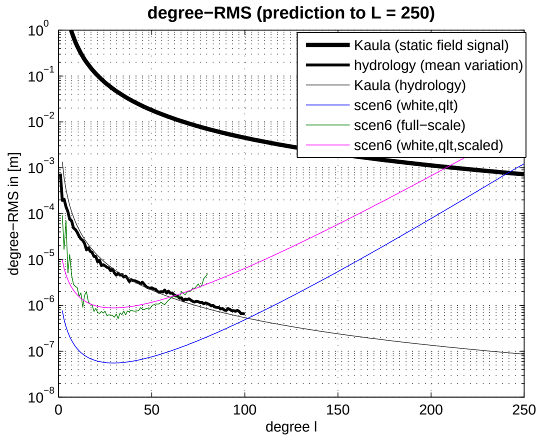

Figure 6-9: predictions of the performance of scenario 6 up to degree L = 250 (unscaled and scaled results of the Quick-look tool).

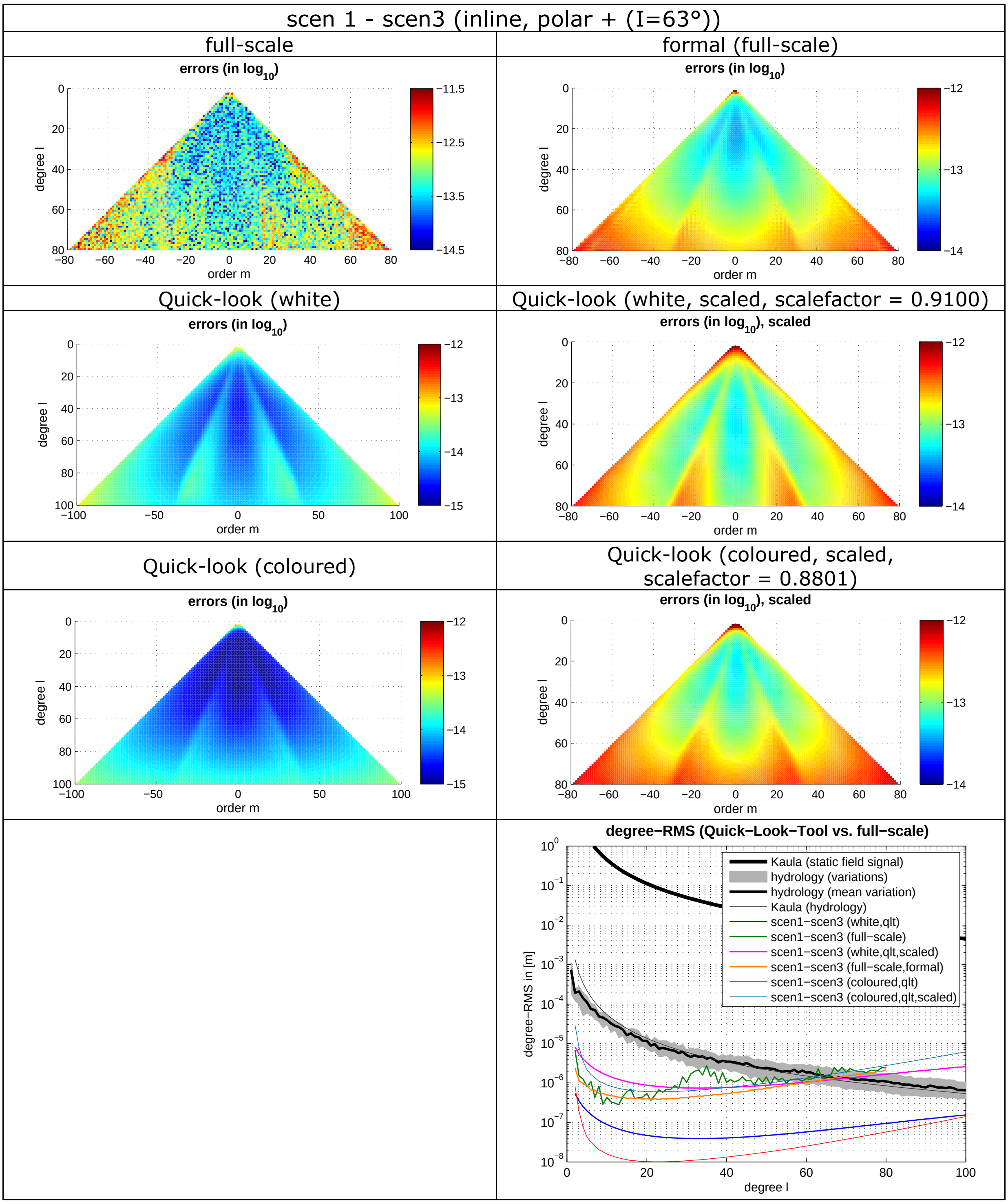

Figure 6-10: comparison of the results from Quick-look tool and full-scale retrievals for scen1-scen3 (polar inline + SSO inline, $(\beta/\alpha) = 463/30$).

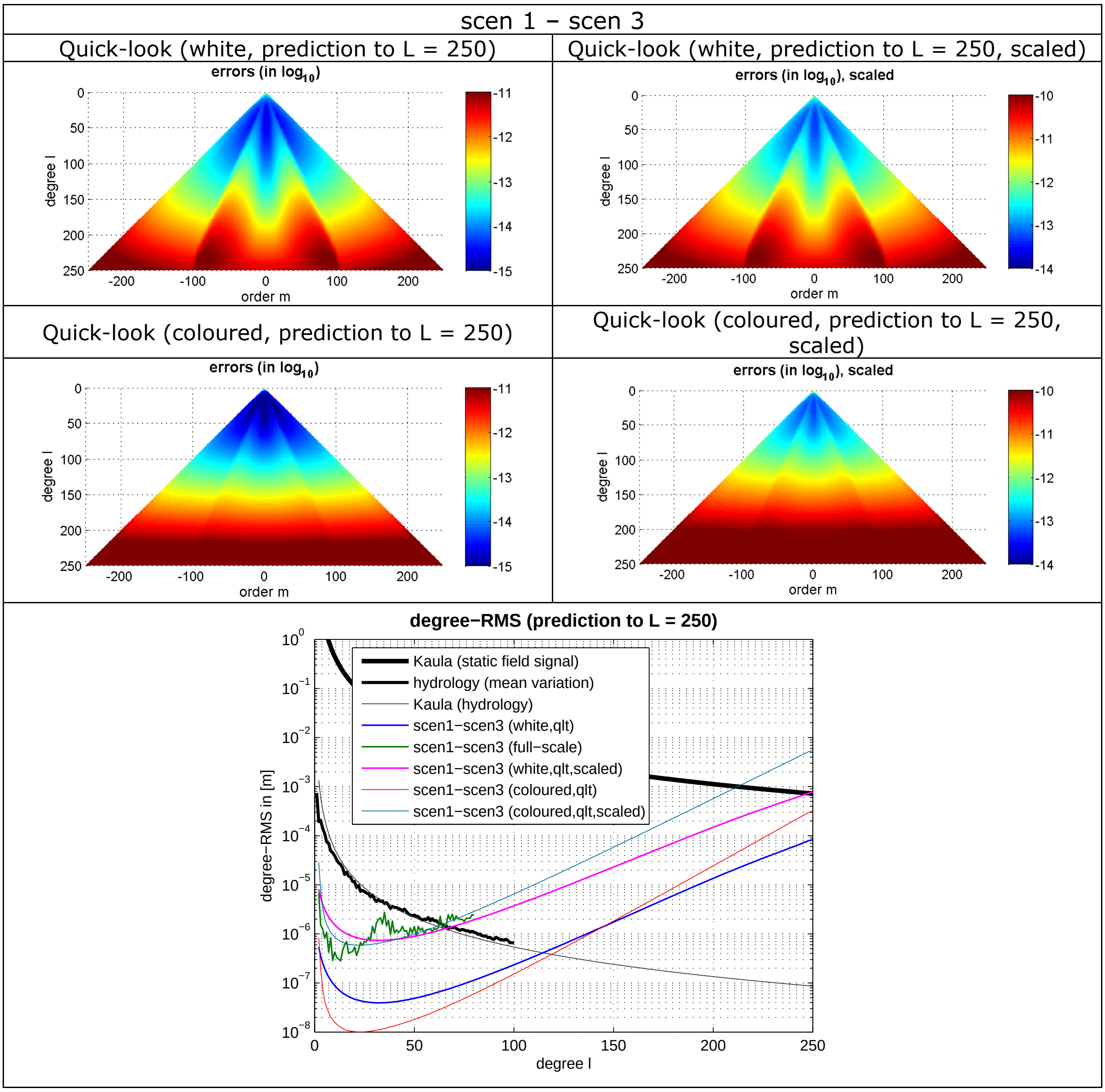

Figure 6-11: predictions of the performance of scen1-scen3 up to degree L = 250 (unscaled and scaled results of the Quick-look tool).

scen 1 – scen 4 (polar inline + polar pendulum)

full-scale

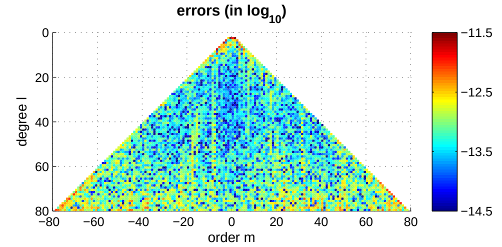

formal (full-scale)

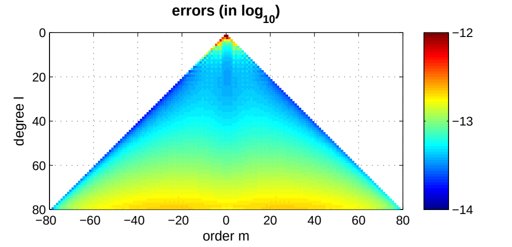

Quick-look

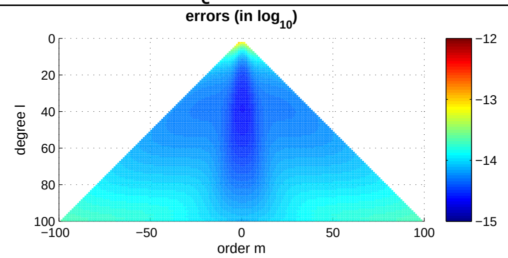

Quick-look (scaled, scalefactor = 0.9165)

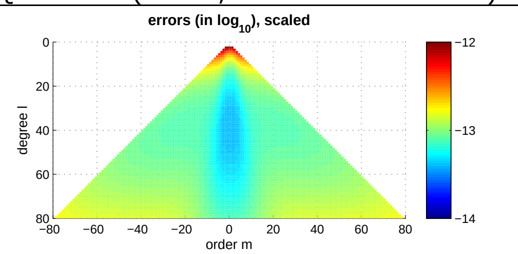

Figure 6-12: comparison of the results from Quick-look tool and full-scale retrievals for scen1-scen4 (polar inline + polar pendulum, (β/α) = 463/30).

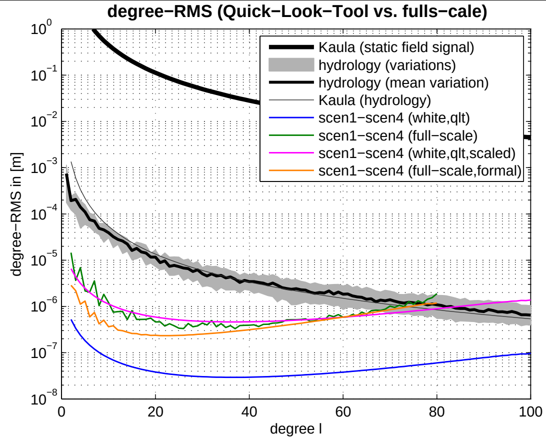

scen 1 – scen 4

Quick-look (prediction to L = 250)

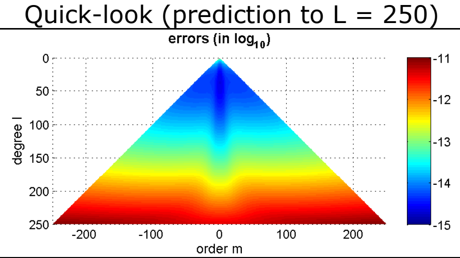

Quick-look (prediction to L = 250, scaled)

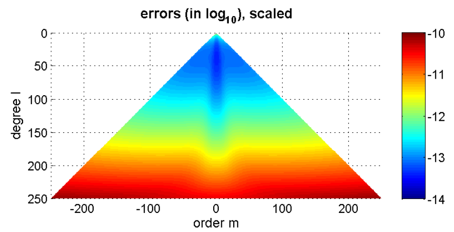

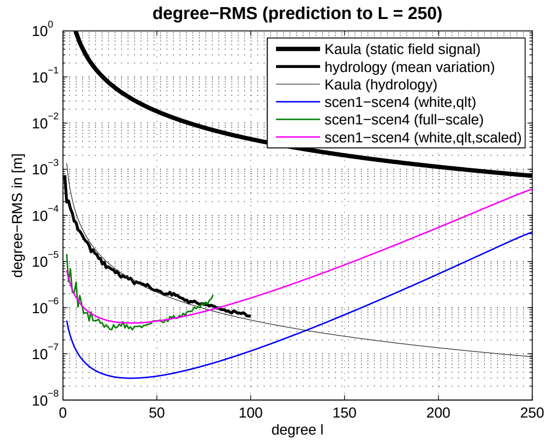

Figure 6-13: predictions of the performance of scen1-scen4 up to degree L = 250 (unscaled and scaled results of the Quick-look tool).

scen 3 – scen 4 (inline (I = 63°) + polar pendulum)

full-scale

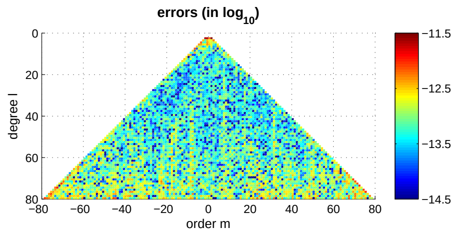

formal (full-scale)

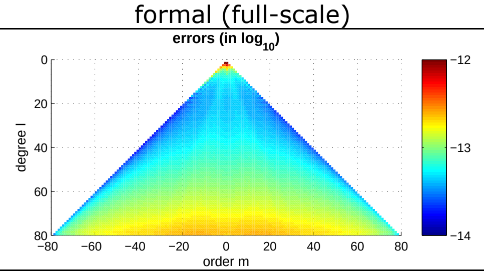

Quick-look

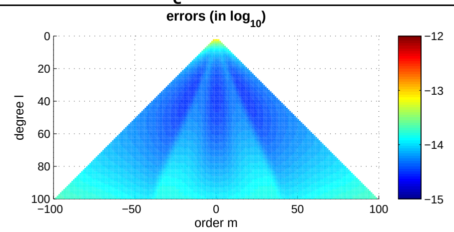

Quick-look (scaled, scalefactor = 0.9133)

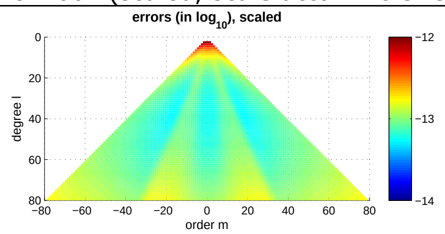

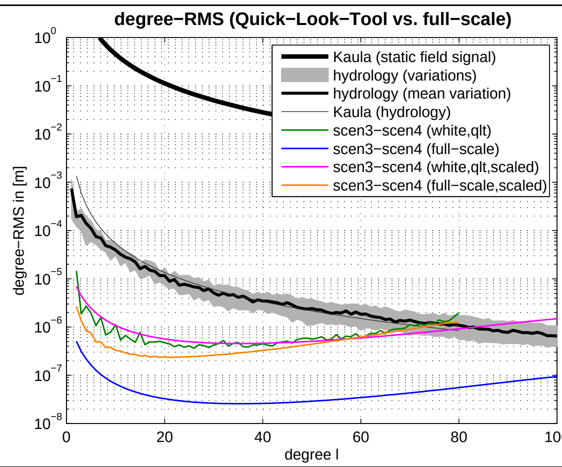

Figure 6-14: comparison of the results from Quick-look tool and full-scale retrievals for scen3-scen4 (inline (I=63°, (β/α)=481/31) + polar pendulum ((β/α)=463/30)).

scen 3 – scen 4

Quick-look (prediction to L = 250)

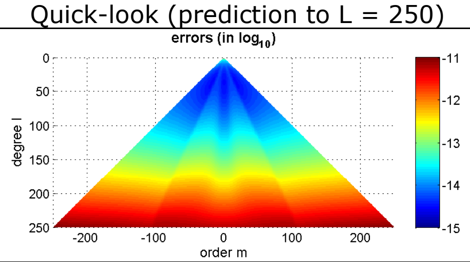

Quick-look (prediction to L = 250, scaled)

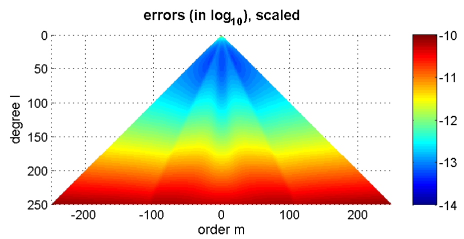

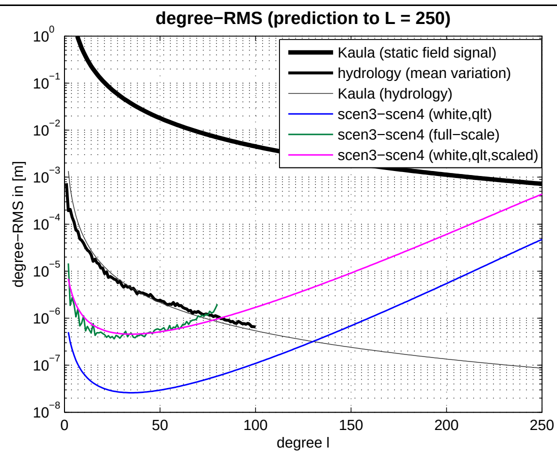

Figure 6-15: predictions of the performance of scen3-scen4 up to degree L = 250 (unscaled and scaled results of the Quick-look tool).

comparison between predictions to L = 250:
Quick-look-tool (white noise, psd = 10^{-10} m/s²/sqrt(Hz)): unscaled vs. scaled

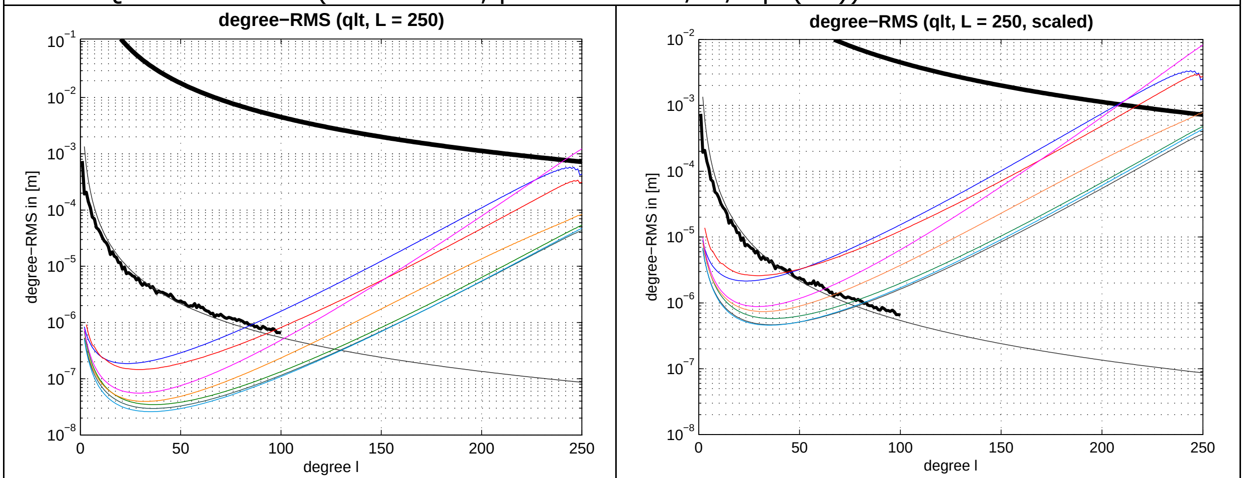

Figure 6-16: comparison of unscaled and scaled predictions with the Quick-look-tool up to degree L = 250

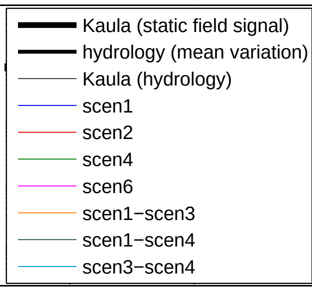

ACRONYMS

DEOS	Delft-Institute for Earth Oriented Space Research
FS	Full-scale retrieval
GIS	Geodetic Institute, University of Stuttgart
GRACE	Gravity Recovery And Climate Experiment
LEO	Low Earth Orbit
ll-SST	low-low Satellite to Satellite Tracking
PSD	Power Spectral Density
QLT	Quick Look Tool
RD	Reference Document
RMS	Root Mean Square
RRM	Requirements Review Meeting
SGG	Satellite Gradiometry
SH	Spherical Harmonics
SSO	Sun Synchronous Orbit
SST	Satellite to Satellite Tracking
TN	Technical Note
TU	Technical University

END OF DOCUMENT